Sliding Wear of PVD Hard Coatings: Fatigue and Measurement Aspects

ALINA SIVITSKI

TUT
PRESS

TALLINN UNIVERSITY OF TECHNOLOGY
Faculty of Mechanical Engineering
Department of Mechatronics
Department of Materials Engineering

Dissertation was accepted for the defence of the degree of Doctor of Philosophy in Engineering on September 30, 2010

Supervisors: Prof. Priit Kulu, Faculty of Mechanical Engineering, Department of Materials Engineering, Tallinn University of Technology

Prof. Maido Ajaots, Faculty of Mechanical Engineering, Department of Mechatronics, Tallinn University of Technology

Opponents: Prof. Michal Besterci, Institute of Materials Research of Slovak Academy of Sciences

Senior Researcher PhD Maksim Antonov, Faculty of Mechanical Engineering, Department of Materials Engineering, Tallinn University of Technology

Defence of the thesis: November 1, 2010, at 14.00
Room No.: V-215
Tallinn University of Technology
Ehitajate tee 5, Tallinn

Declaration:
Hereby I declare that this doctoral thesis, my original investigation and achievement, submitted for the doctoral degree at Tallinn University of Technology has not been submitted for any academic degree.

/Alina Sivitski/

European Union
European Social Fund

Investing in your future

Õhukeste kõvapinnete liugekulumine: väsimuse ja mõõtmise aspektid

ALINA SIVITSKI

CONTENTS

LIST OF ABBREVIATIONS AND SYMBOLS

ABBREVIATIONS

AFM – Atomic Force Microscope
ASTM – American Standards for Materials Testing
BoD – Ball-on-Disk
CoF – Coefficent of Friction
CoW – Coefficent of Wear
CWTS – Cold Work Tool Steel
FEM – Finite Element Method
HDF – Height Distribution Function
HM – Hard Metal
HV – Vickers Hardness (followed by load)
HSS – High Speed Steel
NS – Nitrided Steel
PM – Powder Metallurgy
PoD – Pin-on-Disk
RT – Rototribometer
PVD – Physical Vapor Deposition
SEM – Scanning Electron Microscope
SF – Spray Forming
STS – Stainless Steel
XRD – X-ray Diffraction

SYMBOLS

a – wear scar radius (mm)
b – wear track width (mm)
d – diameter of sample (mm)
E – modulus of elasticity (E_1 – of coating, E_2 – of substrate) (GPa)
F_N – normal load (N)
H – hardness (Pa)
H_1 – nanohardness of coating (GPa)
H_2 – hardness of substrate (HV)
h – wear depth (m, mm)
h_1 – coating thickness (mm)
h_2 – substrate thickness (mm)
K – coefficient of wear
k – dimensional coefficient of wear (mm^3/ N·m)
L_c – critical contact load in adhesion scratch testing (N)
l – length of the substrate (mm)
n – frequency of rotation (rpm)
p – normal contact pressure over that particular discrete region (Pa)

R – stress ratio in the indentation testing

R_a – arithmetic average of the absolute values of the roughness profile ordinates (μm; nm)

r_{ball} – radius of pin or ball (mm)

r_{track} – radius of wear track on disk (mm)

S – wear scar area in RT test (mm)

S_a – arithmetic mean or average of the absolute distances of the surface points from the mean plane (μm^2)

s – sliding distance (m)

V – volume wear (mm^3)

V_{ball} – ball volume wear (mm^3)

V_{disk} – disk wear volume (mm^3)

w – measured deflection in the middle of the plate

$wt\ \%$ – content percent by weight

Greek symbols

δ – deflection of the free end of the strip substrate (mm)

μ_2 – Poisson's ratio of substrate

$\sigma_{residual}$ – residual stress in the coating after deposition process (MPa)

υ – linear velocity of rotation (m/s)

PREFACE

PVD coatings are widely used for lifetime extension of cutting, sheet metal forming tools, dies and special machine parts that require high wear resistance. The selection of the appropriate coating for specific application depends on the coating functional properties such as fatigue, cracking, wear and frictional resistance. The coating characteristics are formed under the influence of substrate structure, chemical and physical properties (E – modulus of elasticity, H – hardness) as well as surface roughness and residual stress in the coating. The great number of coating, substrate parameters and their interaction make the problem of coatings properties estimation more complicated. In this thesis the experimental results of new dry sliding wear testing method and device along with theories describing the coating and substrate properties influence on coatings sliding wear and fatigue parameters are offered. The new ways of coating performance prediction are stated for their successful long-term applications.

Acknowledgements

Alina Sivitski

LIST OF PUBLICATIONS

The present PhD thesis is based on the following papers, which are referred in the text by their Roman numerals I – IV.

I. <u>Sivitski, A.</u>; Ajaots, M.; Põdra, P. Wear of PVD hard coatings in sliding contacts (review). Küttner, R. (Eds.). *Proceedings of the 6th international conference of DAAAM Baltic Industrial Engineering*, 24 – 26th April 2008, TUT Press, Tallinn, Estonia, 2008, p. 549 – 554.

II. <u>Sivitski, A.</u>; Gregor, A.; Saarna, M.; Kulu, P.; Sergejev, F. Application of the indentation method for cracking resistance evaluation of hard coatings on tool steels. *Estonian Journal of Engineering*, 2009, 15, 4, p. 309 – 317.

III. <u>Sivitski, A.</u>; Gregor, A.; Saarna, M.; Kulu, P.; Sergejev, F. Properties and performance of hard coatings on tool steels under cyclic indentation. *Acta Mechanica Slovaca*, 2009, 13, 4, p. 84 – 94.

IV. Podgursky, V.; Nisumaa, R.; Adoberg, E.; Surzhenkov, A.; <u>Sivitski, A.</u>; Kulu, P. Comparative study of surface roughness and tribological behavior during running-in period of hard coatings deposited by lateral rotating cathode arc. *Wear*, 2010, 268, 5 – 6, p. 751 – 755.

Authors contribution

The author of this thesis was responsible for collecting, processing and further analysis of experimental data (Paper II, III). In Paper I the whole analysis was made by author consulting with other authors. The author also took part in discussion on the content (Paper IV). The list of publications that are not included into present work is added above. However the intellectual merit which is the result of the framework where the contribution of every author should not be underestimated.

Approbation at international conferences

1. 18th International Baltic Conference Engineering Materials & Tribology, BALTTMATRIB 2009, Tallinn, Estonia, October 22 – 23, 2009.

2. European Congress on Advanced Materials and Processes, EUROMAT 2009, Glasgow, Great Britain, October 7 – 10, 2009.

3. 6th international conference of DAAAM Baltic industrial engineering, Tallinn, Estonia, April 24 – 26, 2008.

4. 10th International Symposium on Machine Design, OST – 07, Tallinn, Estonia, September 27 – 29, 2007.

1 INTRODUCTION

1.1 Background

The functional properties of PVD hard coatings are influenced by many parameters [1 – 4]. The list of the main parameters is presented below.

List of parameters which influence the coating functional properties:

1. Hardness and modulus of elasticity
2. Chemical composition
3. Crystal structure defects
4. Coating thickness
5. Coating adhesion
6. Substrate material and its microstructure
7. CoF and CoW in sliding wear test
8. Resistance to indentation fatigue
9. Surface roughness
10. Residual stress

More detailed overview of effect of the parameters on hard coatings wear has been offered.

1. Although hardness has long been regarded as a primary material property which affects the wear resistance, there is strong evidence to suggest that the modulus of elasticity have an important influence on sliding wear behavior. The last fact demands to take into account both parameters at ones in the form of modulus of elasticity/hardness ratio E/H ratio or H/E ratio (i.e. a description in terms of 'elastic strain to failure') [1]. The ratio between H and E is widely quoted as a valuable measure in determining the limit of elastic behavior in a surface contact, which is crucial for the avoidance of wear [1, 5].

Previous research [6 – 8] shows that cracking resistance and cracks types of ceramics are strongly dependant on the values of E/H ratio. For materials with higher hardness ($E/H < 40$), the elastic deformations under the indenter are not negligible compared to the plastic ones [9, 10]. Both plastic and elastic deformation of coated sample influence the final depth of the contact impression after loading and unloading process during fatigue indentation test (see Fig. 50). The E/H ratio determines the spatial extent of the elastic deformation that may be present under loading before permanent yielding occurs.
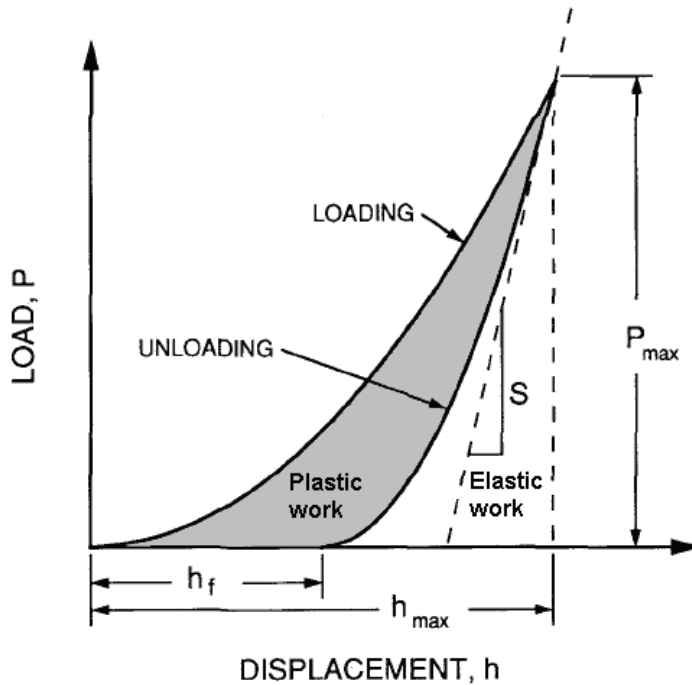
Fig. 1. A schematic representation of load versus indenter displacement data for an indentation experiment. The quantities shown are P_{max} – the peak indentation load; h_{max} – the indenter displacement at peak load; h_f – the final depth of the contact impression after unloading; and S – the initial unloading stiffness [11].

2. Chemical composition of the coating also influences the sliding wear process. Previous research [2] has shown that wear rate of TiAlN coatings decreases with increasing Al content because of protective layers of amorphous aluminium oxides, which are formed on the top of TiAlN coating at high temperatures. Last fact explains a much improved oxidation resistance at elevated temperatures of TiAlN coatings compared to TiN. However room temperatures have been investigated in this work. It is known that CrN coatings as well as AlCrN have much slower oxidation in air in contact with copper [1]. The reason of TiN oxidation is the catalytic effect of copper. TiN oxidation leads to the formation of titanium oxide that is rapidly worn away. The better corrosion resistance of AlCrN leads to the lower friction coefficient and wear rates as has been revealed in AlCrN and TiAlN studies [3].

3. Crystal structure defects affect the wear characteristics. The presence of pores, scratches or other defects in the coatings' structure decreases the wear resistance because they play the role of stress concentrators. It has been shown [4]

that even if the two coatings' has the same hardness, the wear coefficient can vary due to structural defects.

4. Coatings thickness is a critical factor that affects the hard coatings wear rates. It has been shown [12] that mechanical properties and the hardness of thin TiAlN coatings with thickness in range of $(3 - 8)$ μm for cemented carbides as substrates, significantly affect the wear rates. On the contrary, thick $(8 - 10)$ μm coatings' wear depends mainly on the thickness of coating itself. Coating thickness is effected by deposition time. According to coating growth mechanism the thicker is coating the greater is superficial grain size that leads to hardness and wear resistance reduction [12]. This explains why thin coatings have superior mechanical strength.

5. The coating adhesion proved to have an effect on coating wear rate and thus, on lifetime [13]. The stronger is the coating/substrate interface the longer is the coating lifetime. Lately multilayered coatings are developed to guarantee a strong adhesion between coating and the substrate and to obtain wear-protective coatings with low chemical reactivity and low friction, as well as to increase the hardness and toughness of the coating [12, 14].

6. Another aspect that has an effect on coated system cracking and fatigue is the substrate material and its microstructure. Hard coatings are generally applicable to protect wear of softer material. The substrate material choice depends on the fact that deposition temperature must be lower than material critical temperature. (Ti,Al)N based coatings are deposited at $T = 500$ ºC and therefore is not suitable for alloys which are not thermostable.

Different crystal structures of the substrate and the coating can cause poor adhesion between them. Additionally, cyclic indentation tests on ceramics reveal that fine and homogeneous material structures are preferable as they are characterized by slow crack growth [15].

7. One of the most important engineering tasks is the prediction of the coated systems coefficient of friction (CoF) and coefficient of wear (CoW) along with their minimization in particular contact. The sliding wear rates and CoW of PVD hard coatings are influenced by many parameters. Wear mechanism has an effect on the evolution of the PVD hard coatings' wear process. Adhesion, two-body and three-body abrasive, tribo-oxidation and surface fatigue wear mechanisms can occur. Different types of hard coatings can be applied as solid lubricants to suppress the adhesive wear in poorly lubricated and high stress contacts. For example, TiN coatings prevent the adhesion and seizure between the cutting tool and metal chip [16]. The same coating has been successfully used for increasing the wear resistance in gearing.

8. The resistance to indentation fatigue should be taken into account when considering the coating application for sheet metal cutting tools lifetime extension. Investigations of coatings indentation fatigue parameters such as cracking resistance and crack types are commonly carried out using Vickers indentation method for its ability of measuring mechanical properties in a microscopic range [17 – 19] and suitability for thin coatings (coatings with a few microns thickness).

Most of available published works [17, 20] on the cracking resistance of hard coatings explain the morphology of a coating crack under static indentation, although cyclic indentation gives more precise estimates for long-term damage mechanisms. For contact fatigue under cyclic indentation investigation spherical and conical indenters are widely used [15]. However, Vickers pyramid indentation has an advantage over spherical and conical ones. A far more accurate measurement of the length of radial crack propagating from square indentation imprint corners can be obtained as compared to the circle impression. As hard coatings are brittle films, the publications focused on indentation cracking [6, 19] and fatigue [19, 21 – 23] of brittle materials can be used as a base for coatings fatigue properties determination.

The fatigue indentation testing begins with single loading test. Three types of deformation models were observed during the single indentation cycle in previous research [17]: 1 – elastic deformation of the coating and plastic deformation of the substrate without cracking (plastic zone model), 2 – cracking of the layer directly beneath the indenter (contact region model) and 3 – cracking of the layer beneath the indenter and the uplift of the substrate near the indenter causing elastic bending of the coating (uplift model). However, under cyclic indentation, elastic brittle hard coatings do not show plastic deformation up to tensile fracture (normal stress) and may not suffer fatigue damage and the fracture criterion obeys static strength. Thus, the propagation of the crack of the coated system may be attributed to the ratcheting deformation of the substrate under cyclic indentation.

The damage mode of a single and cyclical loaded coated system is determined by five major crack types observed in brittle materials during single indentation tests [19, 22]: cone, radial, median, half-penny, and lateral (circumferential) cracks. Previous observations [19, 24, 25] of mechanical sectioning of brittle materials indentation tests revealed that the cracks emanating from the corners of indent impressions are mostly radials cracks (Palmqvist cracks). In addition to the damage mode determination the contact damage models in cyclic loading for brittle materials are described [19]. The tensile-driven cone cracking ("brittle" mode) and shear-driven microdamage accumulation ("quasi-plastic" mode) were determined [19].

9. Surface roughness of the coating proved to be the important factor in sliding wear and fatigue under cyclic indentation process [26, 27]. Previous studies [27 – 29] have shown that the relatively high friction during dry machining of (Ti,Al)N coatings is caused by the macroparticles on the coating surface, e.g. CoF of AlTiN is 0.3 in contrast to 0.7 for AlTiN [29]. The only difference between AlTiN and AlTiN is that AlTiN is smoother than AlTiN because of the arc process optimisation and surface post-treatment [29].

Generally, the smoother surface proves the lower wear rates. However, extra smooth surfaces may result in the increase of contact bodies' atoms attraction. Coating roughness influence on coefficient of friction and sliding wear research [30] reveal the increment of friction coefficient with surface roughness (in the range of tens of nanometers) decrease.

10. Residual stress in coatings arises due to mismatch of lattice during coating epitaxial growth, phase transformations and thermal stress caused by coating and substrate different thermal contractions in deposition process [31 – 34]. Compressive stresses are commonly present in hard PVD coated surfaces and they are in the range of (0.5 – 10 GPa) for coating with thickness of 1 – 10 μm [35 – 37]. Suitable high compressive residual stress is tribologically beneficial for PVD coatings [35 – 37]. The cracking resistance of coated systems increases with coatings higher elastic modulus and compressive stress [35]. Surface roughness and residual stress combinations is crucial in manufacturing PVD coatings. Surface with optimal roughness/residual stress resulted in better surface fatigue [38].

1.2 Main objectives of the doctoral thesis

The aim of presented work is to offer the ways of hard coatings functional properties improvements, to give an overview of coatings selection rules depending on application and to prognose the hard coating behavior in concrete working conditions. The main objectives of this doctoral thesis are:

1.   To implement a new sliding wear test method and to develop the equipment (rototribometer) for coatings sliding wear characterization along with comparative pin-on-disk and ball-on-disk wear studies.
2.   To investigate coatings fatigue wear mechanisms in dry sliding and cyclic indentation.
3.   To determine the dependence between coatings physico-mechanical properties, dry sliding and indentation fatigue wear parameters.

2   EXPERIMENTAL AND METHODOLOGY

2.1 Substrate and coatings materials

Four different materials mostly used for metal cutting or sheet metal forming tools applications were used as substrates for coatings in this work. Three coated systems with the substrates of cold work tool steels (CWTS) – spray formed (SF) Weartec and powder metallurgical (PM) Vanadis 6 and nitrided steel (NS) – 38CrMoAl8 were investigated by indentation method. For sliding wear estimation hardmetal (HM) – H15 (WC-15Co) and above mentioned CWTS-s Weartec and Vanadis 6 substrate were used. The prediction of coated system behavior in wear tests is presented in table 1. Wear and fatigue tests performed with coatings/substrate combinations are shown in table 2.

*Table 1.Coating and substrate parameters combinations with prognosis of **fatigue** and **wear resistance (r).** Shaded boxes are the best combinations..*

Substrate \ Coating E/H	TiCN 18.8	TiN 15.4	TiAlN 15.2	AlTiN 14.1	nACo 11.1
NS Carbon content 0.37 C, wt % $E = (250 – 300)$ GPa, $H = 850$ HV0.01 $E/H = 0.32$	High substrate *E/H*, High coating *E/H*, Different structure (presence of Al in the substrate) **Prognosis:** The lowest Cracking r/ Fatigue r	High substrate *E/H*, Medium coating *E/H*, Different structure (presence of Al in the substrate) Monolayer coating **Prognosis:** Low Cracking r/ Fatigue r	High substrate *E/H*, Similar chemical composition (presence of Al in the substrate), Medium coating *E/H* **Prognosis:** Average Cracking r/ Fatigue r	High substrate *E/H*, Similar chemical composition (presence of Al in the substrate), Medium coating *E/H* **Prognosis:** Best Cracking r/ Fatigue r	High substrate *E/H*, Similar chemical composition (presence of Al in the substrate), Low coating *E/H* **Prognosis:** Average Cracking r/ Fatigue r
SF The highest carbon content 2.8 C, wt % carbide grains (5 – 10) μm, uniform carbide distribution $E = 210$ GPa, $H = 843$ HV0.01 $E/H = 0.25$	Low substrate *E/H*, High coating *E/H*, Similar structure, Bigger carbides **Prognosis:** Average Cracking r/ Fatigue r/	Low substrate *E/H*, Medium coating *E/H*, Monolayer coating **Prognosis:** Low Cracking r/ Fatigue r	Low substrate *E/H*, Medium coating *E/H*, Different structure (presence of Al in the coating) **Prognosis:** Low Cracking r/ Fatigue r	Low substrate *E/H*, Medium coating *E/H*, Different structure (presence of Al in the coating) **Prognosis:** Low Cracking r/ Fatigue r	Low substrate *E/H*, Low coating *E/H*, Different structure (presence of Al in the coating) **Prognosis:** The lowest Cracking r/ Fatigue r
PM High carbon content 2.1 C, wt % carbide grains (1 – 3) μm, uniform carbide distribution $E = 199$ GPa, $H = 843$ HV0.01 $E/H = 0.24$	Low substrate *E/H*, High coating *E/H*, Similar structure **Prognosis:** Best Cracking r/ Fatigue r/ Wear r	Low substrate *E/H*, Medium coating *E/H*, Monolayer coating **Prognosis:** Low Cracking r/ Fatigue r/ Average Wear r	Low substrate *E/H*, Medium coating *E/H*, Different structure (presence of Al in the coating) **Prognosis:** Low Cracking r/ Fatigue r/ Average Wear r	Low substrate *E/H*, Medium coating *E/H*, Different structure (presence of Al in the coating) **Prognosis:** Low Cracking r/ Fatigue r/ Average Wear r	Low substrate *E/H*, Low coating *E/H*, Different structure (presence of Al in the coating) **Prognosis:** The lowest Cracking r/ Fatigue r/ Wear r

Substrate \ Coating	**TiCN** *E/H* 18.8 **A**	**TiN** 15.4 **B**	**TiAlN** 15.2 **C**	**AlTiN** 14.1 **D**	**nACo** 11.1 **E**
HM WC content 85%, wt % Co content 15%, wt % carbide grains $(1-2)$ μm, $E = 590$ GPa, $H = 1555$ HV0.3 $E/H = 0.37$	High substrate *E/H*, High coating *E/H*, Similar structure **Prognosis:** Best Wear r	High substrate *E/H*, Medium coating *E/H*, Monolayer coating **Prognosis:** Average Wear r	High substrate *E/H*, Medium coating *E/H*, Different structure **Prognosis:** Average Wear r	High substrate *E/H*, Medium coating *E/H*, Different structure **Prognosis:** Low Wear r	High substrate *E/H*, Low coating *E/H*, Different structure **Prognosis:** The lowest Wear r

Table 2. Coating and substrate combinations with performed wear and fatigue tests

Substrate \ Coating *E/H*	**TiCN** 18.8	**TiN** 15.4	**TiAlN** 15.2	**AlTiN** 14.1	**nACo** 11.1
SF	Indentation Fatigue	Indentation Fatigue	Indentation Fatigue	Indentation Fatigue	Indentation Fatigue
NS	Indentation Fatigue	Indentation Fatigue	Indentation Fatigue	Indentation Fatigue	Indentation Fatigue
PM	Indentation Fatigue/ Sliding Wear	Indentation Fatigue/ Sliding Wear	Indentation Fatigue/ Sliding Wear	Indentation Fatigue/ Sliding Wear	Indentation Fatigue/ Sliding Wear
HM	Sliding Wear	Sliding Wear	Sliding Wear	Sliding Wear	Sliding Wear

Chemical composition and mechanical properties of the substrate were explored (Table 3).

Table 3. Chemical compositions and mechanical properties of substrate materials

Substrate	Designation	Chemical composition, *wt%*							Hardness H_2	Modulus of elasticity E_2 (GPa)
		C	Si	Mn	Cr	Mo	V	Al		
SF CWTS	Weartec	2.8	0.8	0.7	7.0	2.3	8.9	-	843 HV0.01	199
PM CWTS	Vanadis 6	2.1	1.0	0.4	6.8	1.5	5.4	-	843 HV0.01	210
NS	38CrMoAl8	0.37	-	0.32	1.8	0.2	-	0.98	850 HV0.01	250–300
HM	H15 (WC-15Co)	-	-	-	-	-	-	-	1555 HV0.3	590

The substrate and coating chemical composition similarities are expected to result in better wear, fatigue and cracking resistance. As mentioned in [17] crystallographic similarity of substrate and coating layer yields strong bonding through epitaxial growth. TiCN coating should perform better on PM steel (Vanadis 6) with similar structure, smaller carbide size and uniform distribution of carbides. On the contrary the presence of aluminium in nitrided steel (38CrMoAl8) should make it more efficient as a substrate for TiAlN and AlTiN coatings.

Hardness and modulus of elasticity of substrates play an important role in formation of coated system properties. It is assumed that in indentation testing the lower is the substrate modulus of elasticity value the higher the cracking resistance of the coating should be. The substrates with high elasticity should work like a spring under the coating, allowing it to bend and deform (fracture) according to the contact region wear model described above. Hardness of substrate has little influence on crystalline structure and tribological properties of coatings. However toughness and adhesion are affected by substrate hardness. High hardness of substrate ensures better adhesion and toughness of coatings as mentioned in [23].

Five types of coatings monolayer TiN and multilayer gradient TiCN, TiAlN, AlTiN and nanocomposite coating nACo (nc-$(Al_{1−x}Ti_x)N$/a-Si_3N_4) were deposited on the substrates. For deposition of coatings plating PVD-unit PLATIT-π80 with the lateral rotating ARC-cathodes (LARC) technology was used. Before deposition procedure samples ((20x20x5) mm) were heat treated to a fixed hardness value (see Table 3), grinded, diamond polished (powder grain size 1 µm). After that samples were degreased ultrasonically in phosphate-alkali solution, rinsed in ethanol and dried in air. In a vacuum chamber samples were sputter-cleaned in argon plasma

and Ti adhesion layer was deposited. TiN layer was formed on top of the Ti interlayer. The other deposition process parameters are presented in Table 4.

Table 4. PVD parameters

Type of coating	Bias voltage (V)	Pressure (mbar)	Ti –Al / AlSi cathode arc current (A)	Temp. (°C)	Ar	N$_2$ flow (sccm)	C$_2$H$_2$
TiN	−75…−120	8×10^{-3}	100…125/ -	450	6	200	-
TiCN	−60…−120	$(5…7) \times 10^{-3}$	120..130/ -	450	6	165…180	7…39
nACo	−75…−150	$9 \times 10^{-3}…1.2 \times 10^{-2}$	82…125/ 65…100	435…475	6	200	-
TiAlN	−60…−150	$8 \times 10^{-3}…1.5 \times 10^{-2}$	85…125/ 65…115	475	6	200	-
AlTiN	−60…−150	$4 \times 10^{-3}…1.2 \times 10^{-2}$	60…125/52...130	430…450	6	150…200	-

The properties and surface roughness of studied coatings are presented in Table 3. The content of Al was about 50 and 75 at. % in the $(Ti_{1−x}Al_x)N$ and $(Al_xTi_{1-x})N$ coatings respectively.

Table 5. Mechanical and surface properties of coatings on PM

Coating designation	Type	Modulus of elasticity E (GPa)	Nano-hardness H (GPa)	E_1/H_1 ratio	Surface roughness R_a (nm)
TiN	Monolayer	438±8.0	28.5±0.6	15.4	70±8.4
TiCN	Gradient	500±9.0	26.6±1.4	18.8	85±9.0
TiAlN	Multilayer	301±9.0	19.9±1.2	15.2	90±10.8
AlTiN	Gradient	336±13	23.8±1.0	14.1	90±10.8
nACo	Gradient	323±13	29.0±1.5	11.1	80±9.0

The hardness and modulus of elasticity given in the Table 5 are comparable with those available in the literature. In [25] the TiN coating with a thickness of 2.1 μm on tool steel Böhler S790 ISOMATRIX (E_1 = 214 GPa) had the nanohardness of 27 GPa and modulus of elasticity E = 305 GPa. Fouvry [20] investigated a TiCN coating with a thickness of 2.5 μm on Vanadis 23 (E_1 = 230 GPa), which had modulus of elasticity E = 550 GPa.

The nanoindentation was performed on MTS Nano Indenter XP® in a depth mode, a target depth of 150 nm and average indentation force of 12 mN were applied. The thickness of the coatings measured by Kalotester kaloMax® was about 2.3 μm. Surface roughness values of coatings obtained by Mahr optical profilometer were measured with ±5% accuracy.

Cross-sectional micrographs of coatings reveal the columnar structure of coatings (Fig. 2). Ti additional adhesion layer for TiN was deposited to ensure the

good bonding conditions between substrate and coating. The deposition procedure other parameters are described in the next chapter.
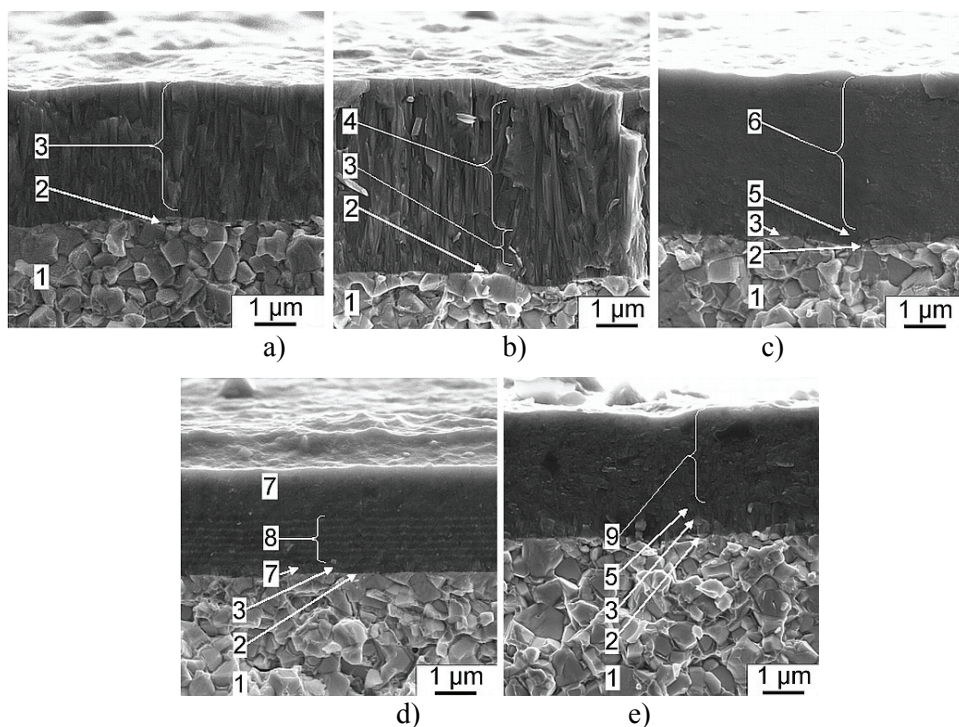

Fig. 2. SEM images of fractured surface of hard PVD coatings: a – TiN; b – TiCN; c – nACo; d – TiAlN; e – AlTiN. 1– substrate; 2 – Ti adhesion layer; 3 – TiN layer;4 – TiCN gradient coating; 5 – TiAlN gradient layer + AlTiN gradient layer; 6 – nc-AlTiN/a-Si$_3$N$_4$ gradient coating; 7 – TiAlN layer; 8 – TiAlN/AlN multilayer coating; 9 – AlTiN gradient coating.

2.2 Evaluation of adhesion of coatings

2.2.1 Adhesion testing

A Rockwell adhesion test followed the VDI 3198 standard [39] (Rockwell "C" indentation test) was performed on Zwick/ZHR 8150 with a load of 1471 N (150 kgf). The indented samples were analyzed with SEM. The type and the volume of failure zone were classified according to the character of cracking (see table 6).

Table 6. Classes, crack types and observation of results of Rockwell indentation test [39]

Class	Crack type	Observation
Class 0		no cracks nor adhesive delamination
Class 1		cracking without adhesive delamination of the coating
Class 2		partial adhesive delamination with or without cracking
Class 3		complete adhesive delamination

The formation of long conical cracks without considerable delamination of the coating complies with the Class 1 and nucleation of radial cracks with adhesive delamination corresponds to the Class 2. The adhesion and brittleness depend on microstructure and the mechanical properties of the coatings and substrate.

2.2.2 Scratch testing

The comparative scratch testing was performed along with Rockwell adhesion testing. During progressive load scratch test (prEN 1071-3) standard operating parameters of 100 N/min (loading rate) and 10 mm/min (lateral displacement speed) were used. The Rockwell C diamond indenter used for the test had a conical geometry with a 120° angle and a round tip with a radius of 200 μm (EN 10109-2). In adhesion testing CWTS samples with dimensions of (20x20x5) mm were coated with five above mentioned coatings.

2.3 Sliding wear performance of coatings

2.3.1 Rototribometer wear testing

Sliding wear tests were preformed on rototribometer (RT) (Fig. 3). This new testing method differs from pin-on-disk and ball-on-disk tests by the debris removal during wear test and possibility to use up to 12 samples in one test. Spherical coated sample assures the continuous contact between coated ball and counterbody what leads to more real thermal conditions and debris removal mechanisms during wear testing. The frequency of rotation (*n*) of tribometer varies from 0 to 1500 rpm. In the experiment the frequency of rotation *n* = 160 rpm (*v* =

2,5 m/s) which was selected according to the centrifugal load (normal load) $F_N = 1$ N. This value of normal load guarantees that mean Hertzian contact pressure $p = (500 - 600)$ MPa in the sliding contact does not exceed the yield strength of hard coating. The sliding wear test duration was 60 s and sliding distance was about $s = 145$ m. The tests were performed at (24 ± 1) ºC and relative humidity $65 - 70\%$.

The tribo couple consisted of fixed coated WC-15Co ball with diameter of 6 mm and C45 drum with inner diameter of 330 mm (thickness of drum wall was 5 mm). The kinematic scheme of rotoribometer and placement of specimens is shown in Figs. 4 and 5. The surface roughness of C45 steel drum obtained by Mahr optical profilometer was $R_a = 0.74$ μm with accuracy of ± 5 %.
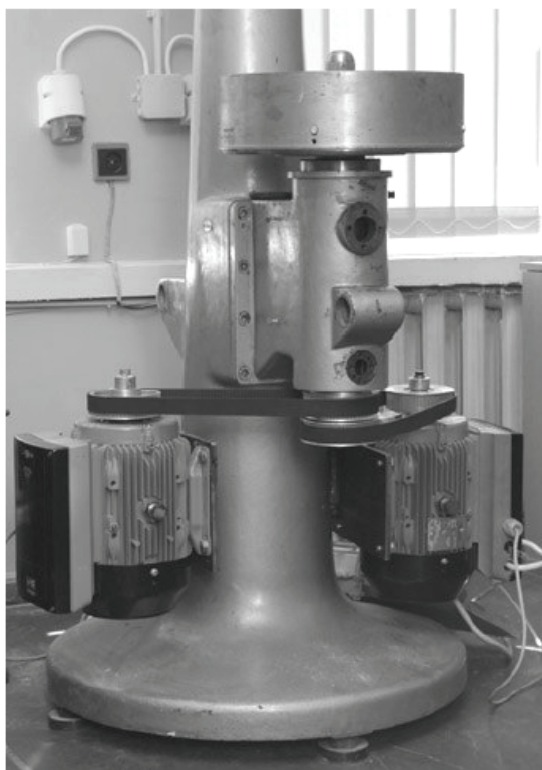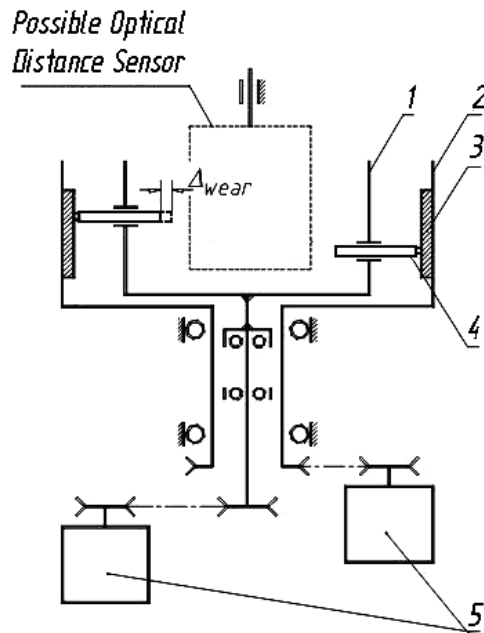

Fig. 3. Prototype of the rototribometer.

Fig. 4. Kinematic sheme of rototribometer.
1 – internal barrel; 2 – external barrel;
3 – drum (steel C45); 4 – cylindrical sample
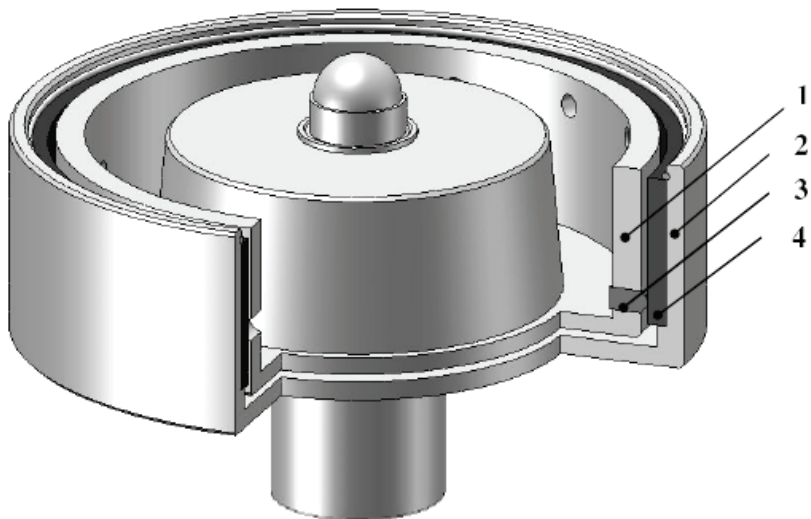*with glued coated WC-15Co ball; 5 – electric motors.*

Fig. 5. RT prototype drums.
1 – internal drum; 2 – external drum;
3 – cylindrical sample; 4 – friction surface [40].

2.3.2   Ball-on disk wear testing

Ball-on-disk (BoD) sliding wear testing was performed on +CSA instruments tribometer in dry conditions. The alumina (Al_2O_3; E =330 MPa; v = 0.21) ball d = 6 mm was used for test. The HM (WC-15Co) substrate coated plates with dimensions of (15x25x3) mm were used for the test. The value of normal load of 1 N was chosen leaning upon calculations of contact pressure that should not exceed the limit values. The mean Hertz contact pressure for all coating was in the range of (600 – 700) MPa depending on the modulus of elasticity (E) and Poisson ratio (v) of the coatings. The revolving drum linear velocity was set to v = 0.04 m/s (n = 100 rpm). The experimental lasted for 60 s and the sliding distance (s) was about 2.4 m. The temperature in the testing room was (28 ± 1) ℃ and the relative humidity during the test was (40 – 45) %.

2.3.3   Pin-on-disk wear testing

The pin-on-disk (PoD) wear testing was set up according to ASTM G99–95a standard. The stainless steel (STS) (AISI304) spherical end pin d = 6 mm was positioned perpendicular to the flat coated sample (20x20x5) mm attached to the rotating disk. The pin was pressed against the coated sample at a specified load (F_N = 5 N) and wear track diameter was 5 mm. The number of rotating cycles reached 1600 that corresponds to sliding distance s = 25 m. The mean Herzian pressure was in the range of p = (800 – 900) MPa. The revolve disk linear velocity was set up to v = 0.08 m/s (n = 300 rpm). The air temperature in testing laboratory was (21 ± 1) ℃ and relative humidity was held in the range of (35 – 40) %.

2.3.4 Sliding wear characterization

The main advantages of new sliding wear testing device are listed in table 7.

Table 7. The comparison of testing parameters of RT, BoD and PoD tribometers

Parameters / Wear test	Debris removal	Experimental duration (several samples at the same time)	Higher values of linear velocity	Friction pair linear velocity adjustment during wear test
RT	+	+	+	+
PoD	-	-	-	-
BoD	-	-	-	-

The sliding wear tests parameters are shown in Table 8.

Table 8. Sliding wear testing parameters

Testing parameters / Wear testing type	Normal load F_N (N)	Contact pressure p (MPa)	Frequency of rotation n (rpm)	Linear velocity υ (m/s)	Sliding distance s (m)	Ball or disk material and form	Counter-body material and form
RT test	1	540	160	2.5	140	HM WC-15Co; ball d=6mm	C45 steel; drum d_{inner} = 330 mm
BoD wear testing	1	630	100	0.04	2.4	HM WC-15Co; disk (20x2x5) mm	Alumina; Ball d=6mm
PoD wear testing	5	900	300	0.08	25	CWTS SF Weartec; disk (20x2x5) mm	Stainless steel AISI304; pin d=6mm

The wear rate in sliding contacts can be described by a general differential equation:

$$\frac{dh}{ds} = f(x),$$ (1)

where h is the wear depth (m) and s is the sliding distance (m), x is either load, velocity, temperature, material parameters, lubrication etc. Generally, the dominating parameters in sliding wear models are sliding velocity and the normal load. First parameter can be determined by the mechanism kinematics. The load influence determination is often more complicated. Applications of linear wear model have been successfully adapted to PVD hard coatings abrasive wear investigation [20]. For wear intensity prediction the coefficient of wear (CoW) of coatings were calculated. The linear wear model (Archard's wear law) first published by Holm [41] was used for dimensionless wear coefficient K calculation. The model is based on the experimental observations and was initially written in form:

$$\frac{V}{s} = K\frac{F_N}{H},$$ (2)

where V is the volume wear, s is the sliding distance, F_N is the normal load and H is the hardness. Classical wear model is usually applicable for uncoated systems [42], but it was successfully used for coated system wear description [20, 43].
The wear depth is more important than wear volume in engineering calculations. Dividing both sides of equation (2) by the apparent contact area, the wear depth is

$$h = k \cdot p \cdot s,$$ (3)

where h is the wear depth, p is the normal contact pressure over that particular discrete region, s is sliding distance, $k = K/H$ is the dimensional wear coefficient.
The replacement of dimensionless wear coefficient K with $k \cdot H$ in linear wear model allows calculating dimensional wear coefficient (mm^3/N·m):

$$k = \frac{\Delta V}{s \cdot F_N},$$ (4)

where ΔV is the coating volume removed during experimental corresponding to the sliding distance.
The coated ball volume wear (V_{ball}) was determined by measuring the wear scar radius according to geometric considerations (see Fig. 5) [20]:

$$S = 2 \cdot \pi \cdot r_{ball} \cdot h,$$ (5)

$$V_{ball} = \frac{1}{3}\pi \cdot h^2 (3 \cdot r_{ball} - h),$$ (6)

where r_{ball} the radius of spherical end of pin or ball and h the wear depth.

The equations (5) and (6) lead to

$$V_{ball} = \frac{1}{3}\pi \cdot \frac{S^2}{(2 \cdot \pi \cdot r_{ball})^2} r_{ball} \left(3 - \frac{h}{r_{ball}}\right),$$ (7)

If $h << r_{ball}$, the equation (7) can be deduced

$$V_{ball} = \frac{S^2}{4 \cdot \pi \cdot r_{ball}},$$ (8)

where S is the wear scar area on ball sample and $S = \pi \cdot a^2$, where a is the wear scar radius (see Fig. 6).
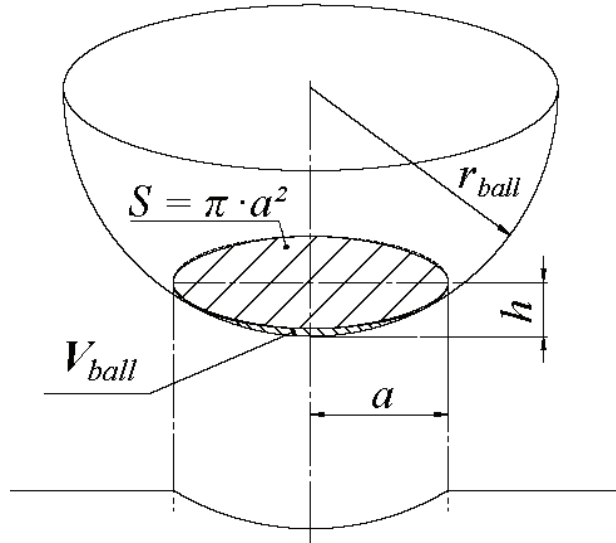

Fig. 6. Schematic diagram of the dry sliding RT wear test sphere cap (cross-section perpendicular to the sliding direction).

The coated disk volume wear (V_{disk}) at PoD and BoD tests was calculated by measuring wear track width assuming that pin and ball wear was minimal using formula [43] (see Fig. 7):

$$V_{disk} = \frac{\pi \cdot r_{track} \cdot b^3}{6 \cdot r_{ball}},$$ (9)

where r_{track} is the disk wear track radius, b the wear track width and r_{ball} the radius of spherical end of pin or ball.
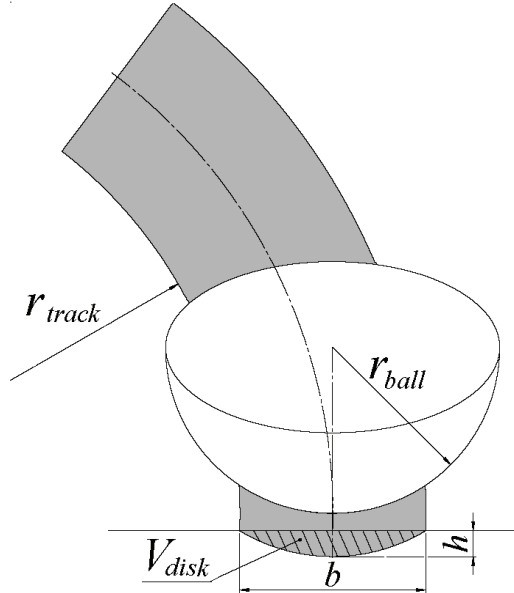
Fig. 7. Schematic diagram of the dry sliding of the BoD and PoD wear tests (cross-section perpendicular to the sliding direction).

2.4 Cyclic indentation testing of coated systems

The importance of cyclic indentation testing is usually underestimated. However it allows estimate the intensity and the character of crack propagation and fatigue wear.

For indentation experiment a servo hydraulic fatigue test system INSTRON 8800 and Vickers diamond pyramid indenter were used. The maximum number of indentation cycles reached up to 10 000. A total indenting load of 500 N for CWTS-s (PM Vanadis 6 and SF Weartec) substrates and 100 N for NS

(38CrMoAl8) was applied. The reason of selection of a high indenting force is based on the results of previous studies. According to Richter [17], hard coating cracking starts at 100 N indenting load. Indentation testing was carried out with a stress ratio $R = 0.1$ using a sinusoidal loading pattern. The loading frequency varied from 0.5 up to 15 Hz within 1 to 1000 and 10 000 cycles, respectively.

The Palmqvist method [44] was used for evaluation of radial cracks. This method is based on the length measurements of the radial cracks emanating from the indentation impression corners. The observations and estimation of the type and measurement of cracks length were made with an optical microscope. The optical microscope Axiovert 25 (ZEISS) has 500x magnification along with Buehler Omnimet Image Analysis System 5.40 and the package for image capture and basic measurement functions. It is suggested [31] not to use SEM for crack length measurement due to the difficulty in defining the corners of indentations.

The evaluation of cyclic indentation experiments results of different coated systems was based on the following: the qualitative evaluation criteria of the cracking (0 –VI) from crack formation, propagation to delamination of the coating was considered (Table 9).

Table 9. Crack types and crack evaluation criteria.

	0	I	II	III	IV	V	VI
Crack type							
Crack type description	Very weak secondary radial cracks, which emanate from the edge and around the corners of the imprint	Weak secondary radial cracks.	Medium secondary radial cracks and weak radial cracks – beginning of radial cracks formation	Medium secondary radial cracks and medium radial cracks – propagation of weak radial cracks	Medium secondary radial cracks and strong radial cracks.	Medium radial cracks, delamination of coating in the corners of the contact impression and cone (ring) cracks at the periphery of the imprint	Strong radial cracks and delamination of the coating around the corners of the indent impression

2.5 Evaluation of other parameters influence on sliding wear and fatigue

Residual stress

Residual stresses arising during physical vapor deposition process have influence the functional properties of coatings. The conventional deformation method (Stoney's method) and X-ray diffraction techniques (XRD) with use of a steel plate and strip as a substrate were used.

In the experiment nickel alloy (E_1 = 156.5 GPa) plate ((20x20x0.24) mm) and stainless steel C45 (E_1 = 200 GPa) strip ((30x4x0.35) mm) specimens were chosen The conventional deformation method Stoney's formula was used in [45] for residual stress calculations the thickness of substrate (h_1) exceeds tens of times the thickness of thin coating (h_2): $h_1/h_2 \geq 60$. Assumable the residual stress is distributed uniformly throughout coating thickness in plate specimen:

$$\sigma_{residual} = \frac{4E_2}{3(1-\mu_2)} \cdot \frac{h_2^2}{l^2 h_1} \frac{f_4}{f_2} w \tag{10}$$

and for a strip specimen:

$$\sigma_{residual} = \frac{4E_2}{3(1-\mu_2)} \cdot \frac{h_2^2}{l^2 h_1} \frac{f_4}{f_2} \delta \tag{11}$$

where $f_4 = h_1^4 + 4\gamma h_1^2 h_2 + 6\gamma h_1^2 h_2^2 + 4\gamma h_1 h_2^3 + \gamma^2 h_2^4; f_2 = h_1^2 + 2h_1 h_2 + \gamma h_2^2,$

$\gamma = \dfrac{E_1^*}{E_2^*}$ is the ratio of the elastic parameters of the coating to the elastic parameter

of the substrate, $E_1^* = \dfrac{E_1}{1-\mu_1}$, $E_2^* = \dfrac{E_2}{1-\mu_2}$

$\sigma_{residual}$ is the residual stress in the coating; E_1, E_2 is modulus of elasticity of coating and substrate; h_1 is coating thickness; h_2 is substrate thickness; μ_1, μ_2 is Poisson's ratio of coating and substrate; l is length of the substrate; w is measured deflection in the middle of the plate; δ is the deflection of the free end of the strip substrate.

For comparison, the residual stresses of coatings were determined by two-angle and the sin square psi XRD methods and with ANSYS finite element method simulation. In thin coating optimally high compressive stresses are beneficial as they prevent of cracks initiation and delamination of the coating.

Surface roughness

Functional characteristics of coatings depend on its surface properties. The influence of surface geometry of hard coatings on HSS substrates (S390) on tribological behavior was investigated. For estimation of surface roughness parameters (S_a, R_a) atomic force microscopy (AFM) and Mahr Perthometer (Göttingen, Germany) was used.

3   RESULTS AND DISCUSSION

3.1   Adhesion of coatings

Two comparative tests were used for coatings adhesion evaluation – scratch test and Rockwell "C" indentation test.

In scratch test dense chevron cracks at the borders of the scratch track (L_{c1}) were formed in the beginning of scratch testing $(0 – 20)$ N (see Fig. 4). First brittle failure of coatings except of nACo failed in form of cohesive chipping at the tracks edges (L_{c3}) and spallation at the track edges (L_{c4}) was observed at contact load of $(20 – 30)$ N. The micrographs showed parallel cracks (L_{c1}) at 5 N and semicircular coating cracks inside the scratch tracks (L_{c2}) and spallation (L_{c3}) at 10N loading in nACo scratch test. The load values presented in Table 10 are given with 10% accuracy. As follows from Table 10 there the critical load of adhesion is dependant on coating friction coefficient presented. Similarly to [46] lower friction coefficient of coating corresponds to higher values of critical load and better adhesion of coatings. The monolayer TiN coating adhesion appeared to be better than of the multilayer or gradient coatings. The same tendency was detected in [47].

Table 10.Critical load values versus coefficient of friction

Coating	TiN	TiCN	TiAlN	AlTiN	nACo
Coefficient of friction (BoD test)	0.2±0.02	0.25±0.03	0.32±0.08	0.35±0.09	0.43±0.09
Failiure mode at contact load Lc3 [N]	33	22	20	17	10

The comparative indentation adhesion test (Rockwell "C" indentation test) results are shown in Fig. 8. Coatings failure types and the volume of a failure zone were characterized by four classes corresponding to crack types (see Table 6). According to the test results coatings of higher *E/H* ratio withstand the load without nucleation of conical cracks (TiN and TiCN). The radial cracks of $(10 - 50)$ μm were generated, causing the exfoliation of coating layers that is a typical behavior of TiCN and TiN coatings under loading [48] (Class 1 and 2).
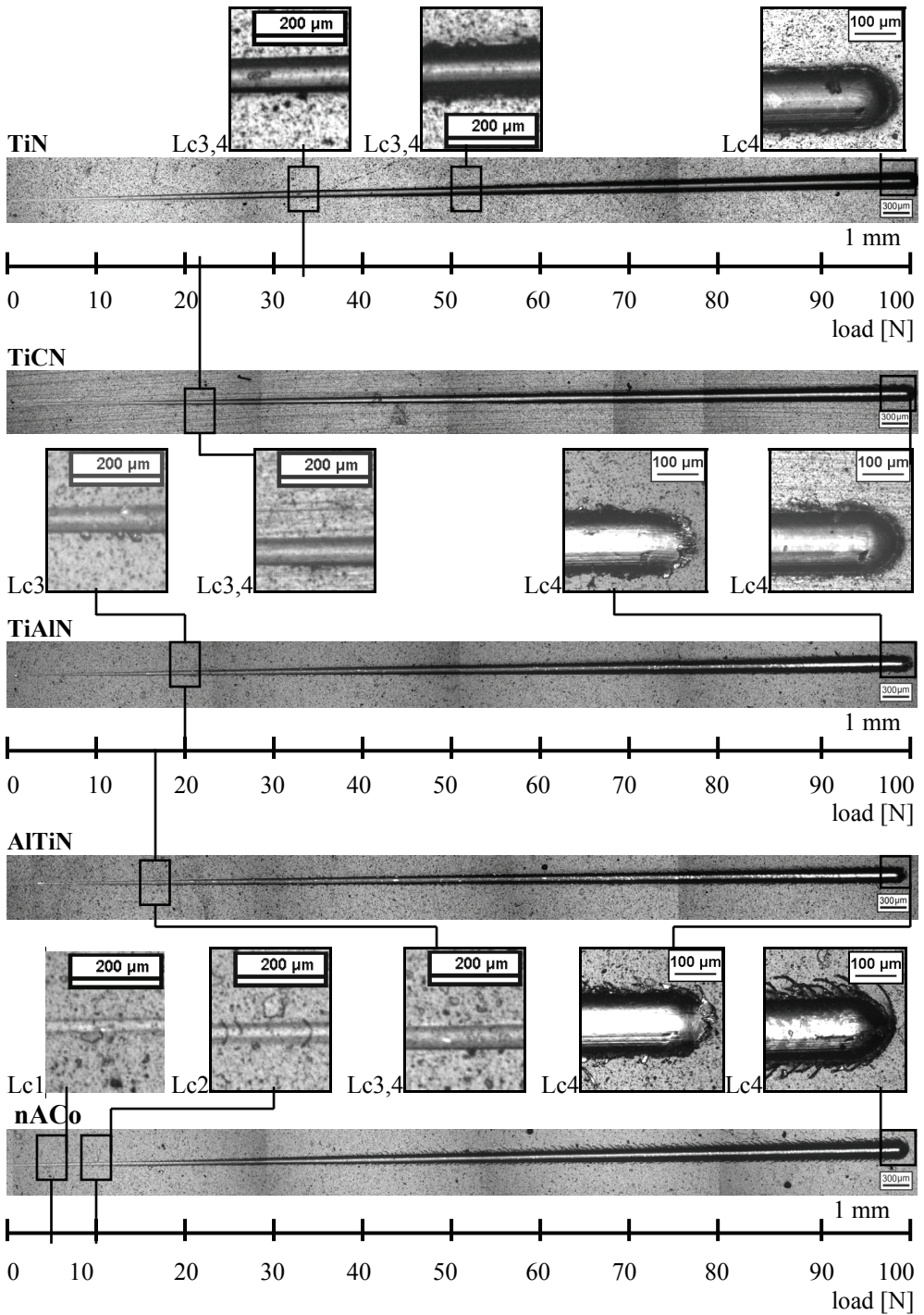
Fig. 8. The micrographs of the scratch test tracks and types of coatings failure versus load values.

The longest radial cracks were indicated in the TiN coating and larger in size exfoliations of the coating layer are observed (Class 2) (Fig. 9 a).
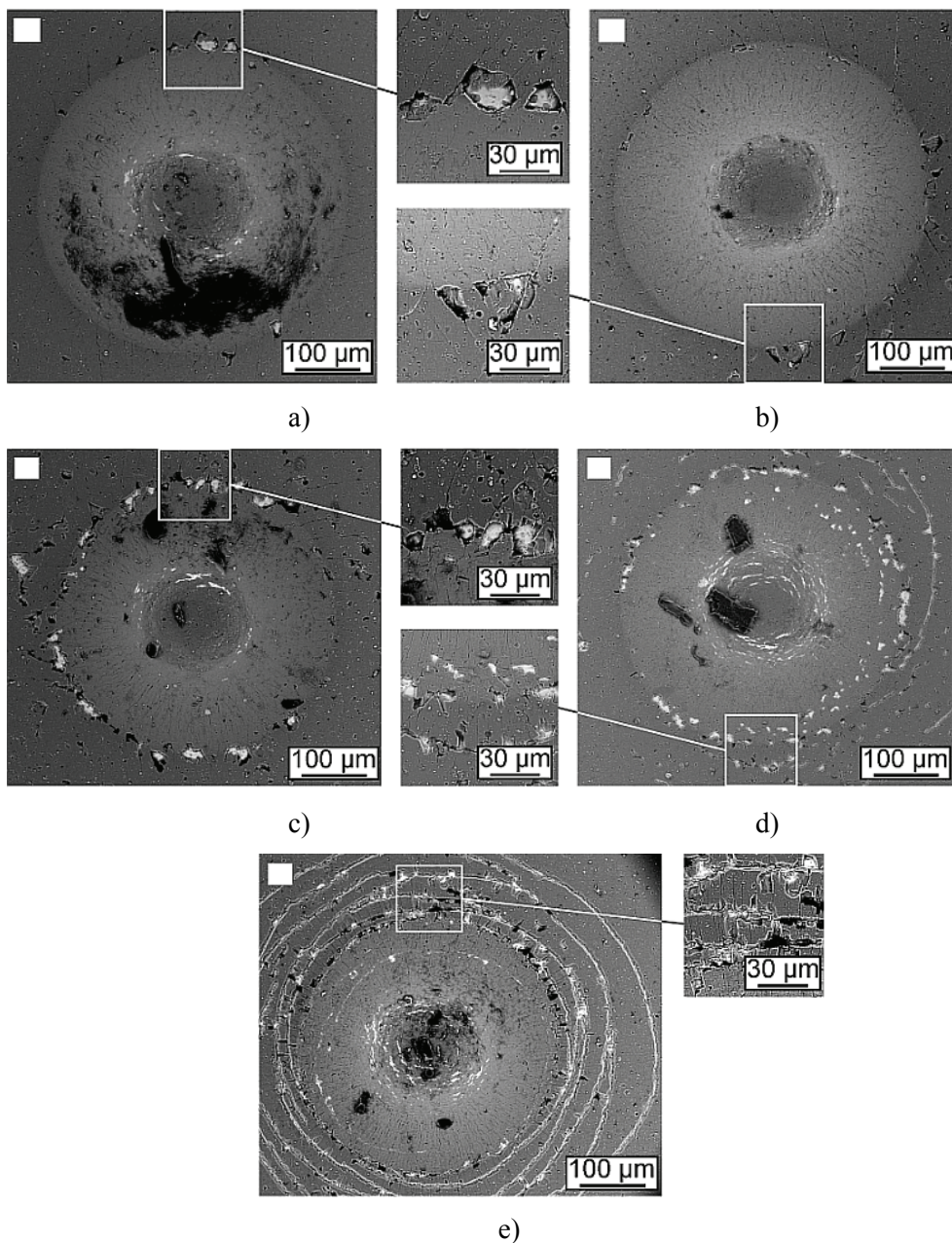

a)

b)

c)

d)

e)

Fig. 9. SEM micrographs of the adhesion test of coatings on CWTS:
a – TiN; b – TiCN; c –TiAlN; d – AlTiN and e –nACo.

The failure of TiAlN coating was similar to TiN coating. However, the conical cracks were also present (Fig. 9 c) (Class 3, see table 6). TiAlN coating failure resulted in the short radial cracks what accelerate chipping on the bordering area of coating-indenter contact. Emerged chips tend to make connections with the closest on the sides forming the ring or conical crack. The pores, non-metallic inclusions and others structural defects presented on the surface of coatings contribute to this process. The worst adhesion characteristics were observed in case of nACo coating (Fig. 9 e). The most drastically fractured nACo coating (Class 3, see table 6) had numerous short radial and closed conical cracks. First, brittle structure collapses around the indenter and then all the fracture energy goes on formation of radial cracks. Eventually those are blunted by the perpendicularly formed conical cracks and are not reaching the last "ring".

Among all the tested coatings, the TiCN seems to be most endurable (Class 1, see table 6). Most widely presented failure modes of coated systems are cohesive (chipping caused by the normal component of a stress tensor) (Class 2, see table 6) and the delamination with buckling and fracture mode (decohesion of a coating with the formation of microcracks, caused by a combination of shear and normal stresses) (Class 3, see table 6).

The results of both adhesion tests correlate well. Adhesion testing revealed that among multilayered and gradient coatings on CWTS-s the adhesion increases with *E/H* ratio value growth. TiCN coating with the highest *E/H* value of 18.8 showed the best bonding with substrate. It is assumed that low value of nACo coatings *E/H* ratio caused the most severed damage in indentation testing and had an effect on low value of critical adhesion load in the scratch testing.

3.2 Sliding wear of coatings

The results of the wear test performed with rototribometer presented in form of micrographs of wear scars on balls and wear track on counterbody made by optical microscope Axiovert 25 (ZEISS) and by stereomicroscope Zeiss Discovery V20 (see Figs.10 and 11). Buehler Omnimet Image Analysis System 5.40 package were used for wear track width and wear scar diameters measurement. The depth of wear track on C45 steel drum was measured by Mahr optical profilometer. The wear behavior of five sliding pairs was different.

Mostly brown colored debris (iron oxide) was produced in the test due to oxidative wear of C45 steel similarly to [49]. The debris formed in the wear test was pushed into the C45 steel drum surface resulting in different wear track colors. TiCN/C45 and TiN/C45 friction pairs showed the bright orange coloration of wear track on steel drum probably from the presence of iron oxide. The formation of iron oxide refers to tribo-oxidation process. The oxide particles cause the mild abrasive wear that seems to be predominant in dry friction between coatings and C45 steel.

It is typical of all coated ball specimens that the center of ball contact is less damaged or is not worn (Fig. 10). Hypothetically the high contact pressure at the center of ball-contact prevents the debris (oxide, softer conterbody (C45 steel) material and brittle fracture wear particles) ingress at this point contact reducing the wear here. The same effect was detected in [49].
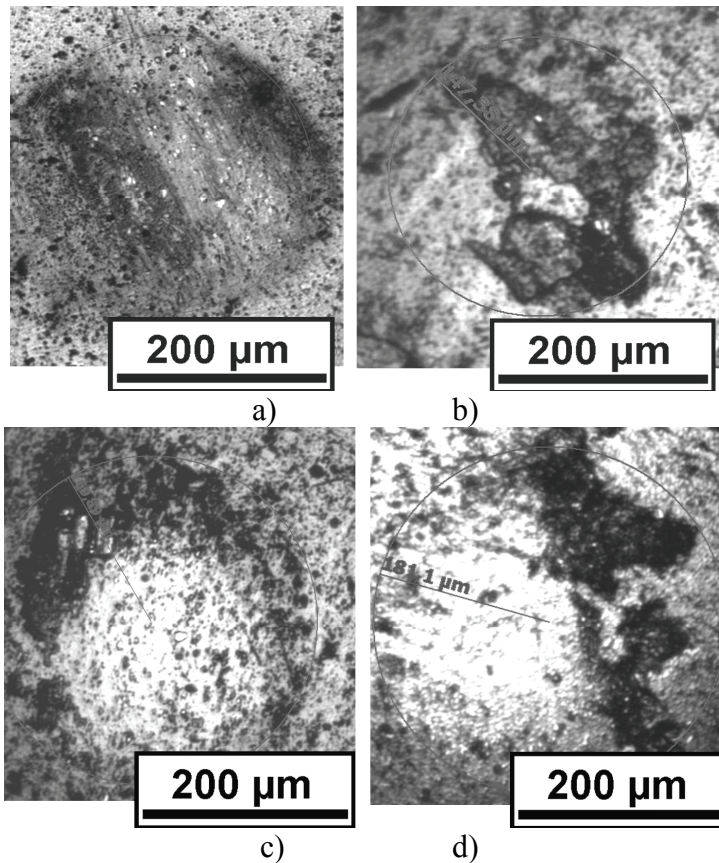
Fig.10 . Wear scars of the WC-15Co ball coated with:
a – TiCN; b – TiAlN; c – AlTiN; d – nACo
coatings in pair with C45 steel drum by RT test.
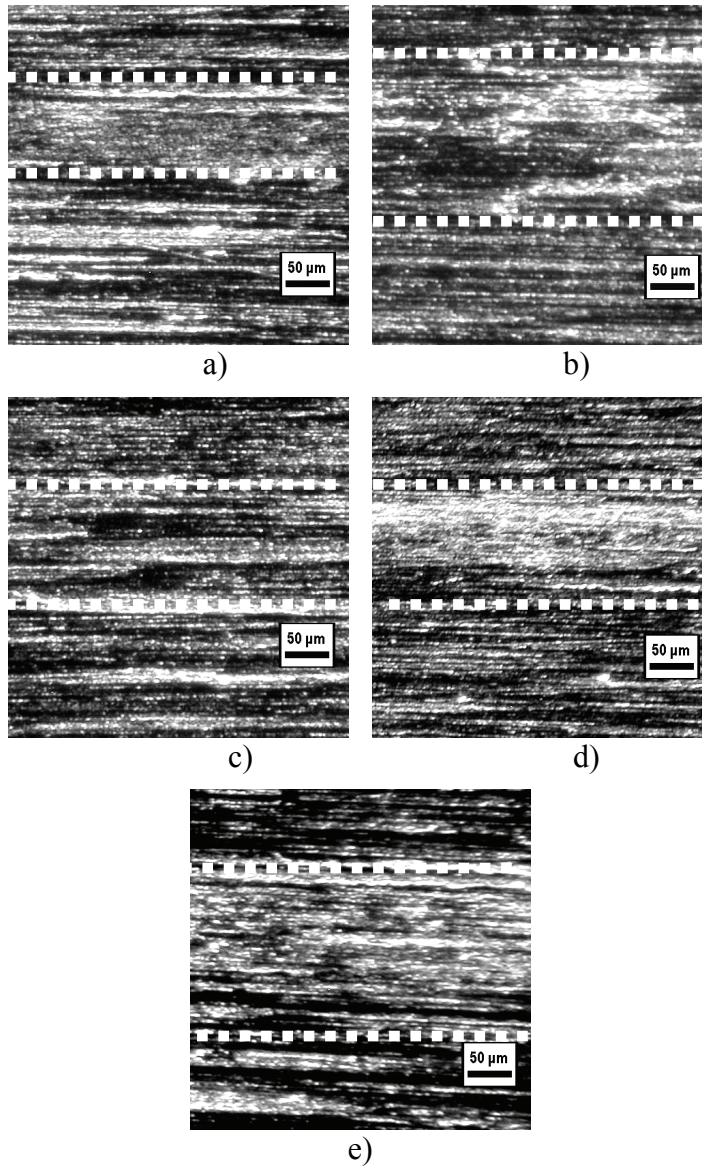
Fig.11. Wear tracks of the C45 steel drum versus WC-15Co ball coated with: a – TiCN; b – TiN; c – TiAlN; d – AlTiN; e – nACo coatings by RT test.

Ball-on-disk wear testing was performed for comparison with the rototribometer test results. The friction coefficients of coatings were measured in this test. The micrographs of coating wear tracks and alumina ball wear scar were made with optical microscope Axiovert 25 (ZEISS) (see Figs. 12 and 13). The wear track

width and wear scar diameter were measured with Buehler Omnimet Image Analysis System 5.40 package.

a)

b)

c)

d)

e)
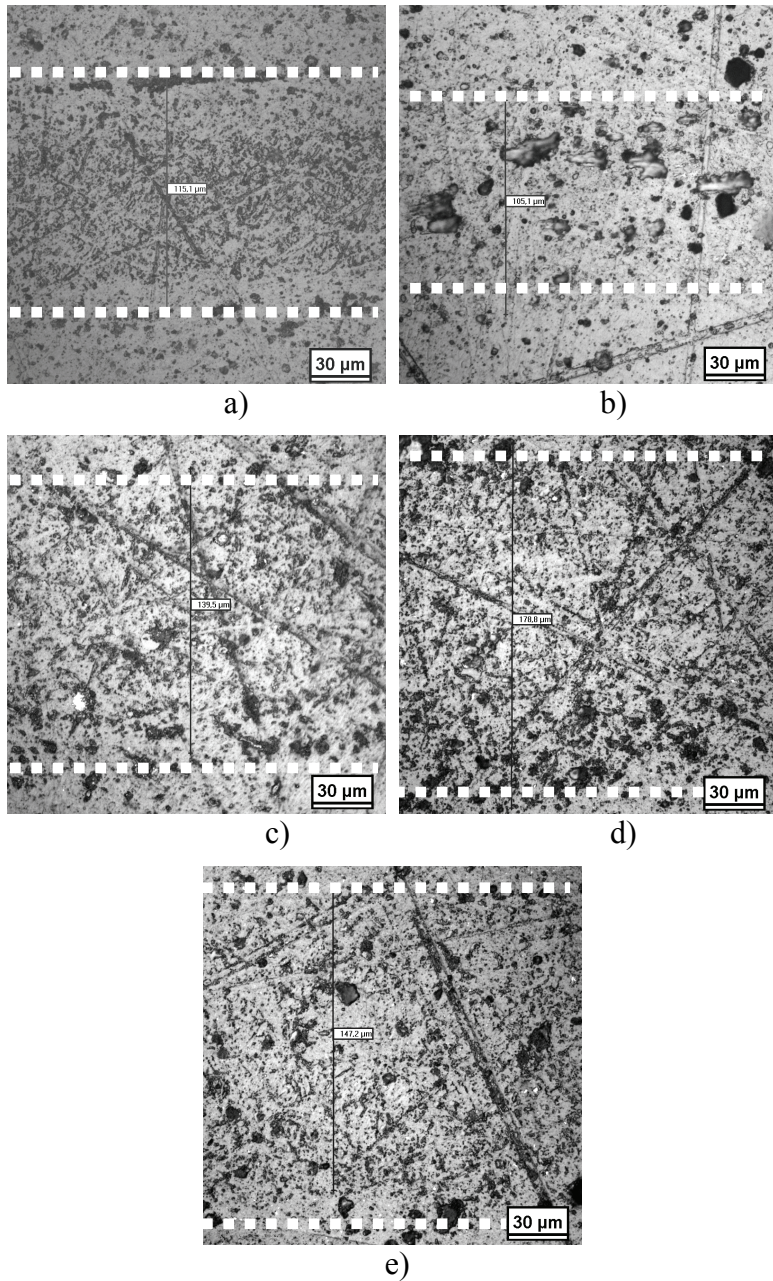
Fig. 12. Wear tracks of the WC-15Co disk wear tracks coated with: a – TiCN; b – TiN; c – TiAlN; d – AlTiN; e – nACo coatings in pair of alumina balls by BoD test.

The black colored debris was formed in the ball-on-disk test. The wear of coatings can be characterized by abrasion wear with minimal coating damage due to the low normal load (F_N = 1N) and frequency of ball rotation (n = 100 rpm).

Fig.13 . The micrograph of alumina ball wear scar after TiCN coating wear testing.

The results of C45 steel drum sliding wear on RT tribometers are presented in form of a diagram (Fig. 14).

Fig.14. Diagram of sliding wear testing results by RT. Drum (C45 steel) wear track width and versus coatings E/H ratio.

Additional pin-on-disk test was performed with higher contact pressure and CWTS was selected as a coatings substrate. The wear tracks on coated p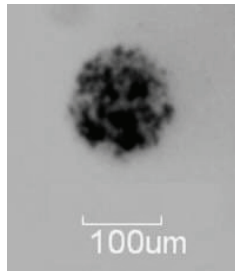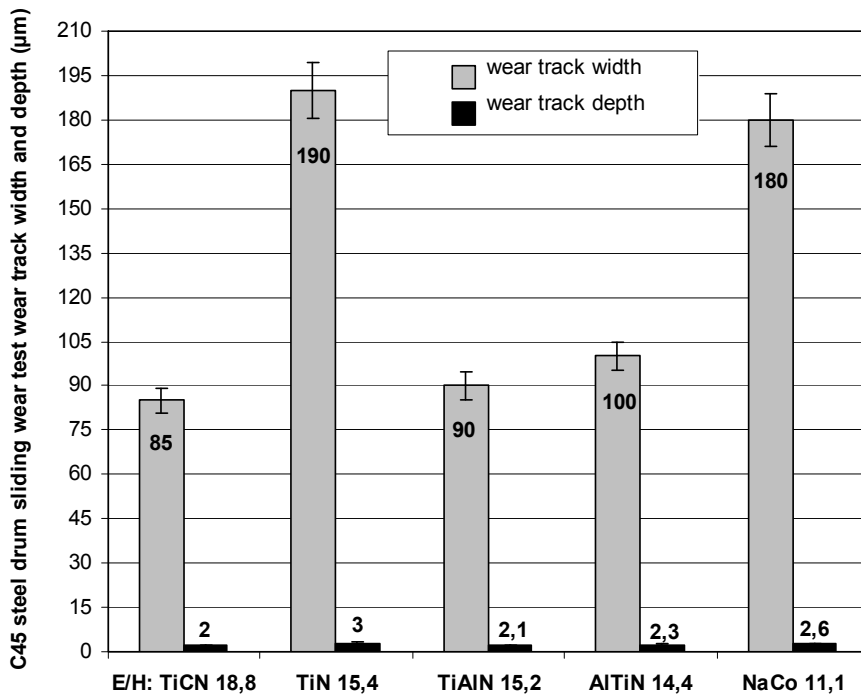lates are shown in Fig. 15. Similarly to rototribometer wear testing a ribbon of unworn or less worn coating was observed in the center of wear track caused by high contact pressure at this point and as a result presence of the less number of abrasive particles (Fig. 15). However the surface fatigue in form of microcracks perpendicular to sliding direction (Fig. 15 b 1) and microchips (Fig. 15) were detected in the central part of round wear track. The darker edges of wear tracks indicate the abrasion of coating and the exposure of substrate.

The three-body abrasive wear mechanism is typical for all sliding wear tests. The debris removed from the coated sample and stainless steel pin plays the role of a third body particle.
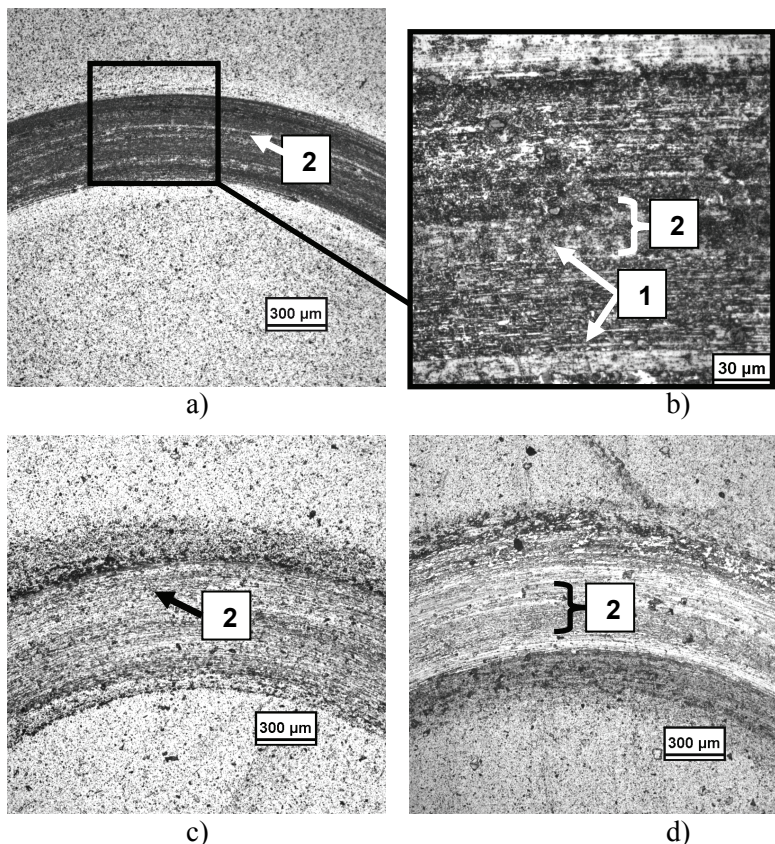

Fig.15. The optical micrographs of coatings surfaces on CWTS after wear testing with PoD tribometer. a – TiCN; b – TiCN; c – AlTiN; d – nACo.
1 – fatigue microcracks perpendicular to the sliding direction; 2 – ribbon of unworn or less worn coating.

All the data concerning the results of coatings wear is presented in form of a diagram (see Fig. 16) and was gathered in table 11. The results of testing by three methods are compatible except monolayer TiN. Among with multilayered and gradient coatings there is a tendency of increase in wear volume of coatings with decreasing *E/H* ratio. According to the diagram TiCN coating with the highest *E/H* ratio (18.8) had less damage. The most severed wear was observed in case of nACo coating with the lowest *E/H* ratio (11.1). The monolayer TiN with *E/H* ratio of 15.4 showed the highest wear.
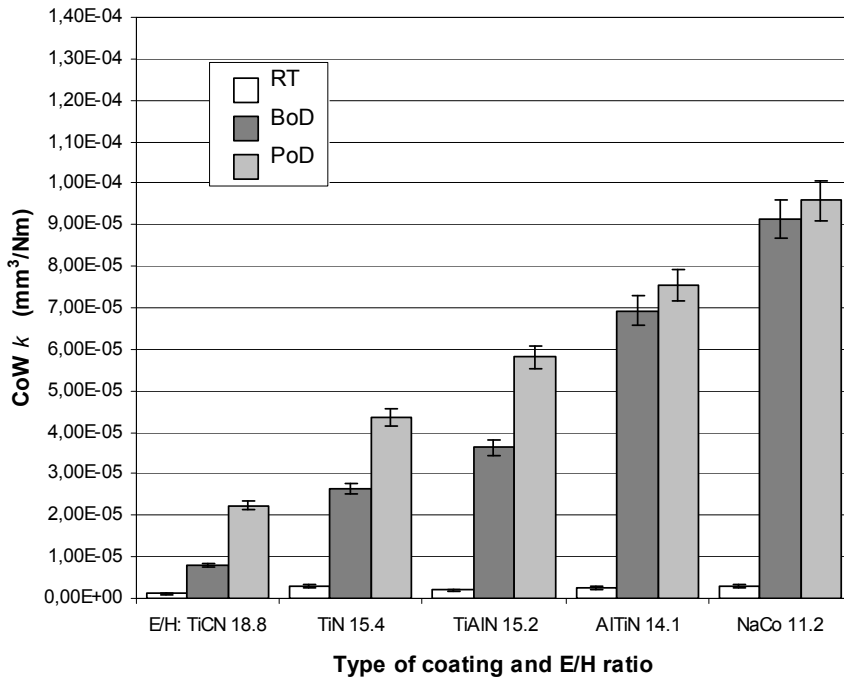
Fig.16. The effect of coatings E/H ratio on CoW of dry sliding wear tests.

The CoW of coatings of PoD and BoD tests calculated with (4), (8) and (9) along with coatings friction coefficients are listed in Table 11. The tendency of friction coefficient growth with *E/H* ratio decrease and friction coefficient increase was exposed. According to the sliding wear testing results there is a trend towards initial CoF rise with an increase of Al content in the coating.

Table 11. CoW k (mm^3/ N·m) *and* CoF *of coatings after RT, BoD and PoD tests*

Coating/ *E/H* ratio CoF and CoW k (mm^3/N·m)	TiCN/ 18.8	TiN/ 15.4	TiAlN/ 15.2	AlTiN/ 14.4	nACo/ 11.1
CoW; RT test	$1.23·10^{-6}$	$2.99·10^{-6}$	$1,96·10^{-6}$	$2,44·10^{-6}$	$2,99·10^{-6}$
CoW; BoD test	$7,85·10^{-6}$	$2,65·10^{-5}$	$3,64·10^{-5}$	$6,93·10^{-5}$	$9,15·10^{-5}$
CoW; PoD test	$2,23·10^{-5}$	$4,36·10^{-5}$	$5,81·10^{-5}$	$7,54·10^{-5}$	$9,59·10^{-5}$
CoF; BoD test	$0.20±0.02$	$0.25±0.03$	$0.32±0.08$	$0.35±0.09$	$0.43±0.09$

To conclude, the results of new method and device of sliding wear (rototribometer wear test), were compatible with commonly used pin-on-disk and ball-on-disk tests. The investigated coatings coefficients of friction showed a tendency to increase with growth of aluminium content in the coating. The influence of coatings *E/H* ratio and CoF on coatings wear volume and CoW was investigated. It was found that among multilayer and gradient coatings on CWTS substrates higher values of *E/H* and lower values of CoF are preferable in sliding wear contacts.

3.3 Fatigue wear under cyclic indentation of coated system

For coated system the cracking resistance at cyclic indentation was estimated by qualitative and quantitative analysis of the samples.

Mostly contact region model of coating on both substrates was observed after first indentation cycle as a result of high indenting load of 100 N and 500 N. However deformation of TiCN coating on NS after single indentation cycle was characterised by uplift model what could be a result of coating and structure chemical compound differences. For coatings with higher *E/H* ratio (TiN and TiCN) on CWTS the contact region model was observed at maximum number indentation cycles. Other coatings deformed according to uplift model with delamitation around the corners of imprint or at the periphery of the impression. For all coatings on NS substrate the damage evolution according to uplift model prevailed after 10 000 indentation cycles.

To describe and demonstrate the cracking criteria of coatings (see table 9) the micrographs of impressions were made (Figs. 17 – 19). TiCN on PM damage revealed crack evaluation criteria II (Fig. 17 c) with medium radial cracks (a length of 20 μm), TiAlN had medium and AlTiN strong radial cracks after 10 000 cycles. Both coatings showed delamination of the coating around the corners of the

impression. TiAlN was less damaged and it had higher *E/H* ratio than AlTiN (Fig. 19 a). The lowest cracking resistance was observed during nACo cyclic indentation testing. nACo with lowest *E/H* ratio on both substrates had the poorest cracking resistance with V evaluation criteria (Fig. 18 d and e). In addition to radial cracks and delamination of the coating at indent impression corners, the ring or cone cracks around the impression were formed, confirming the results of the adhesion test (Fig. 9 e).The monolayer TiN coating with one of the lowest cracking resistance and the formation of strong radial cracks with the length of about 47 μm despite high *E/H* ratio of TiN (Fig. 18 a) pointed out the preference of multilayered coatings over monolayer in fatigue resistance. The best cracking resistance of TiCN on cold work tool steels can be also explained by good adhesion due to the presence of the carbides in both substrates. Crystallographic similarity of the substrate and the coating seem to have an effect, ensuring strong bonding between them. The observations of both substrates coated with TiCN expose the advantages of PM steel Vanadis 6 over SF Weartec. PM Vanadis 6 smaller carbide size and uniform carbides distribution hampers the formation and propagation of cracks and delamination of the coating. However, PM Vanadis 6 as a substrate for TiN and nACo did not show benefits over SF Weartec.

The best cracking resistance of coating on NS showed AlTiN gradient coating (III criteria with minimal delamination around the corners of imprint. nACo on harder NS in cyclic indentation behaved differently to nACo on CWTS resulting in VI cracking evaluation criteria with delamination of the coating in the corners of imprint. The rest coatings damage complied with the VI cracking evaluation criteria with different (lower or higher) degrees of delamination from coating to coating (Fig. 20).

| a) | b) | c) |
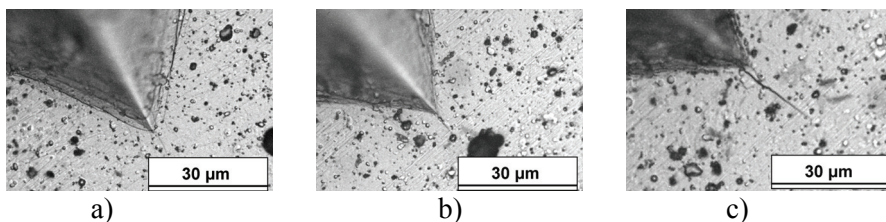
Fig. 17. Impression corner of TiCN on CWTS substrate with the appearance of 0 criteria after: a – 1 cycle; 0, I criteria after: b –1000 cycles; II criteria after: c – 10 000 cycles.

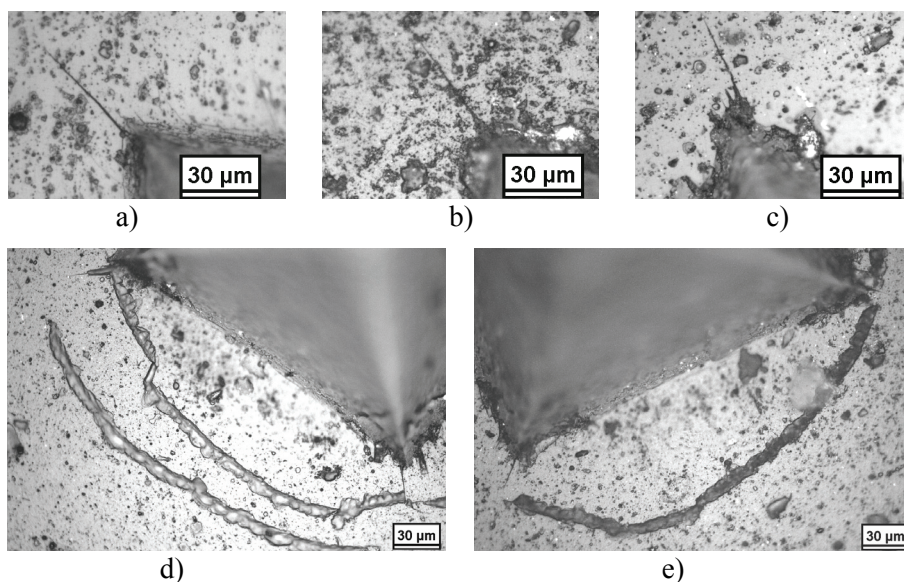*Fig. 18. Impression corner of coatings on CWTS after 10 000 cycles with the appearance of IV criteria: a –TiN; VI criteria: b – TiAlN and c –AlTiN; V criteria: d – nACo on SF and e – nACo on PM.*
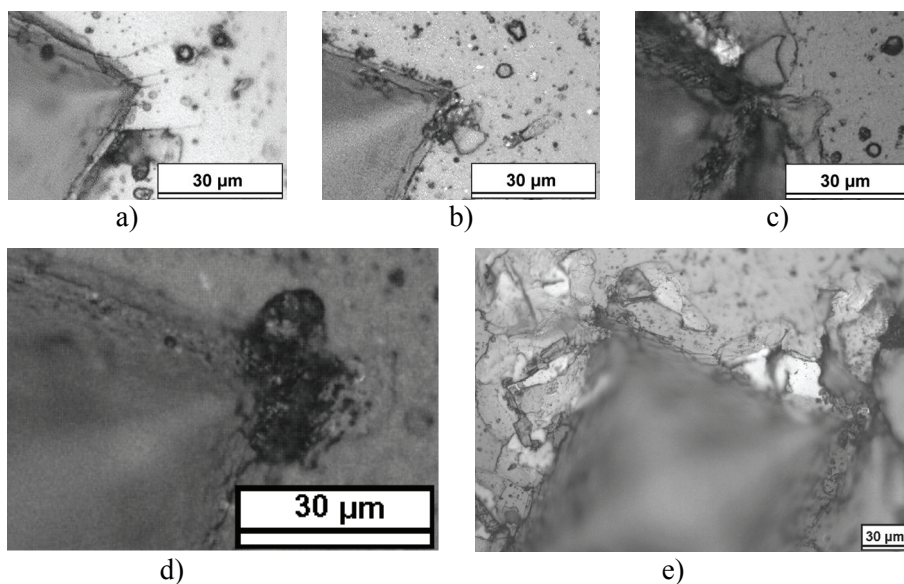

Fig. 19. Impression corner of coatings on NS after 10 000 cycles with the appearance of III criteria: a – AlTiN; VI criteria: b –TiN; c –TiAlN; d – nACo and e – TiCN.

The evaluation criteria of coatings cracking is presented in Table 12. For quantitative analysis the Palmqvist method [30] was used – the lengths of radial cracks from the impression corner were measured and presented on graphs (Figs. 20, 21) versus the number of indentation cycles. The error bars show the standard deviation of 2.3 μm.

Leaning on the facts mentioned above a hypothesis can be made that the crack type and cracking resistance of a cyclic loaded coated system is dependant on the coating *E/H* ratio and substrate. Coatings with the highest *E/H* ratio (TiCN and TiN) on softer substrates (CWTS) show radial cracking without delamination or minimal delamination. The lowest *E/H* values of coatings (nACo) lead to cone cracking and delamination. Harder substrates like NS eliminate the coating *E/H* ratio influence on fatigue resistance. All types of coatings on NS showed minimal or strong delamination. However the less damage of TiAlN and AlTiN coatings can be explained by structural and chemical composition similarities with substrates and coatings lower modulus of elasticity.

As the Vickers diamond pyramid was used the "quasi-plastic" damage mode prevailed in cyclic indentation testing. Vickers sharp indenter penetrates easily into the coating surface and cone cracking formation is suppressed by the radial cracks nucleation. In contrast to spherical indenter, radial cracks become the dominant mode of indentation fracture and lead to accelerated degradation of the coating if pyramid indenter is used. Fracture analysis revealed that apart from other coatings, in nACo the "brittle" damage mode occurred with the formation of cone cracks, driven by tensile stresses in addition to "quasi-plastic".

Table 12. Crack types and crack evaluation criteria of different coated systems

Number of indentation cycles / Coating/Substrate	1	10	50	100	1000	10 000
TiN mono/ SF	I	I	I	I, II	II	**IV**
TiN mono/ PM	I	I	I	I	II	**IV**
TiN mono/ NS	II	II	III	III	IV	**VI**
TiCN gradient/ SF	0, I	0, I	0, I	I	I	**III**
TiCN gradient/ PM	0	0	0	0, I	0, I	**II**
TiCN gradient/ NS	VI Perimeter delamination	VI Perimeter delamination	VI Perimeter delamination	VI Perimeter delamination	VI Perimeter delamination	VI Perimeter delamination
nACo gradient/ SF	I	I, II Starting delamination	II Delamination	II Delamination	V	**V**
nACo gradient/ PM	0	I Starting delamination	V	V	V	**V**
nACo gradient/ NS	I	I	I	II	II	**VI**
TiAlN multi/ SF	0, I	I	I	I, II	II, III	**VI**
TiAlN multi/ NS	I	I	II	II	III Some perimeter delamination	**VI** Perimeter delamination
AlTiN gradient/ SF	I	I	I	I	II	**VI**
AlTiN gradient/ NS	I	I	II	III	III	**III** Minimal delamination in the corners
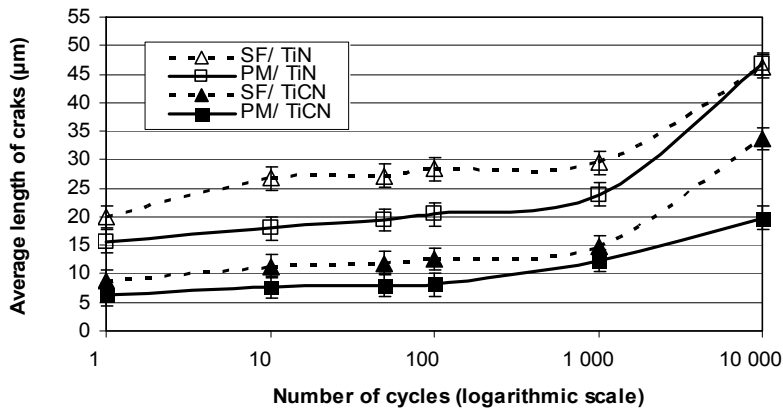
a)
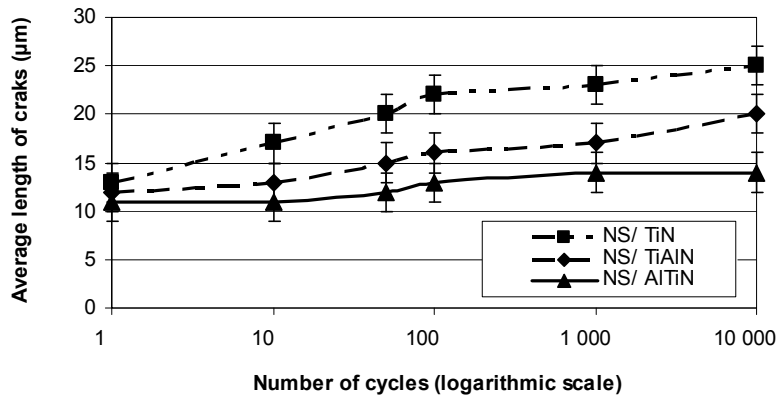
b)
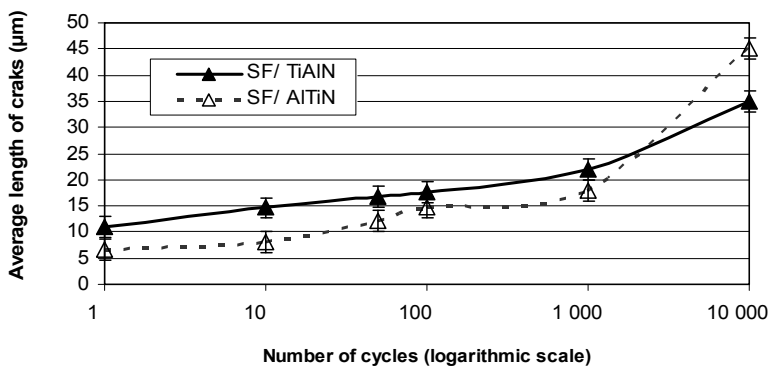
c)

Fig. 20. Effect of the fatigue test number of cycles on the average length of radial cracks: a – TiN and TiCN on CWTS; b – TiN, TiAlN and AlTiN on NS; c – TiAlN and AlTiN on CWTS substrate.
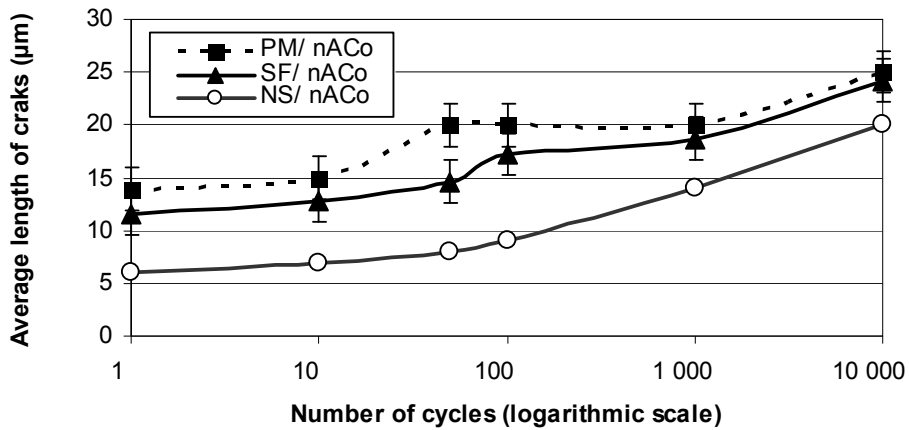
Fig. 21. Dependence of the average length of radial cracks on the number of indentation cycles for nACo coating on different substrates.

The dependence between radial cracking sequence and *E/H* ratio values was described in the form of a diagram (Fig. 22). To discard the monolayer TiN and nanocomposite coatings the tendency of radial crack length growth with decreasing *E/H* value was detected in cycle indentation tests in case of gradient and multilayer coatings on CWTS substrates. Nitrided steel substrate with higher hardness and modulus of elasticity comparing to cold work tool steels exposed the inverse tendency of the cracks length decrease with the coatings *E/H* ratio value decrement. Presumably the reason of TiAlN and AlTiN coatings better performance on NS substrate could be the presence of aluminium in NS. Chemical compounds and structure similarities had the same effect on TiCN on cold work tool steels.
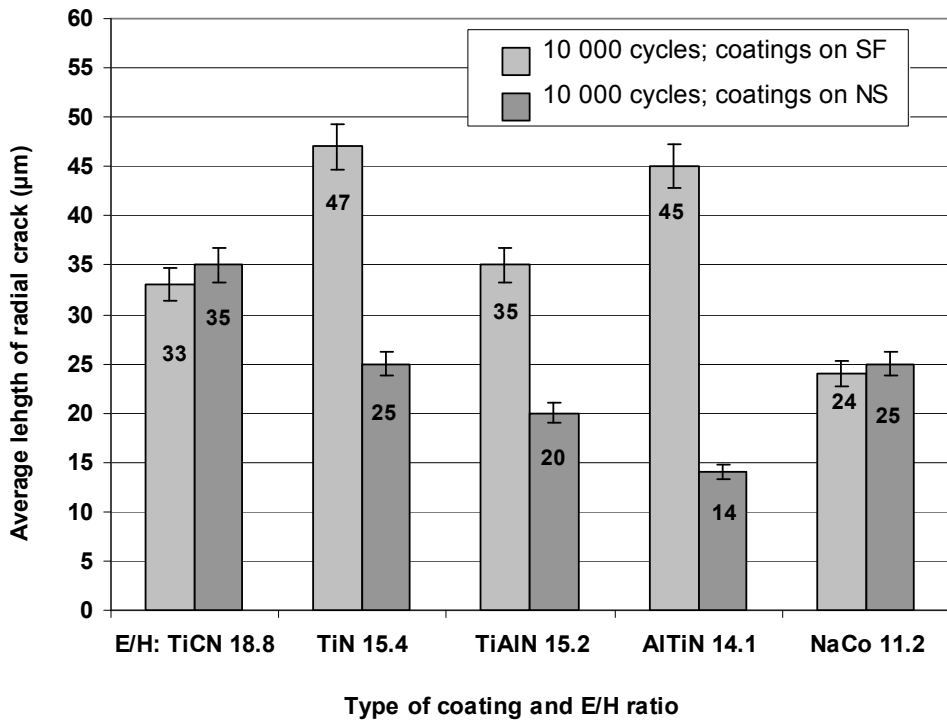
Fig. 22. The effect of the E/H ratio on the radial crack propagation (coatings on SF and NS).

3.4 Effect of other parameters on coatings wear characteristics

Residual stress

The residual stresses and surface roughness influence on sliding wear and fatigue characteristic should be considered. The conventional deformation method (Stoney's method) and X-ray diffraction techniques (XRD) with use of a steel plate and strip as a substrate were used for residual stress influence estimation.

Two-angle XRD method was used to determine internal stresses of PVD coatings. The residual stress in the coatings determined by both methods, were compressive stresses. The values of residual stresses are given in Table 13.

Table 13. Mean residual compressive stresses in the coatings

Residual stress and method (GPa) / Coating	TiCN	TiN	TiAlN	AlTiN	nACo
Calculated by Stoney's (10) and (11)	7.36	3.19	6.50	3.02	4.05
Measured by XRD	-	3.19	6.50	2.94	-
FEM simulation ANSYS	7,3±0,3	2,8±0,2	5,5±0,2	-	-
CoF; BoD test	0.20±0.02	0.25±0.03	0.32±0.08	0.35±0.09	0.43±0.09

In addition to mentioned residual stress evaluation methods FEM simulation was done. The results of simulation are presented in table 13 and Fig. 23.

Near surface residual compressive stresses are clearly beneficial resisting wear and fatigue. Among multilayer coatings higher residual stress values correspond to the lowest coefficient of friction (as well as wear coefficient) (see Table 13). The coatings fatigue properties are also influenced by residual stress. Due to the compressive residual stress coatings can resist fatigue inhibiting crack growth after crack initiation [50]. The coating with the best cracking resistance and lowest CoF – TiCN have the highest compressive residual stress ($\sigma_{residual}$ = 7.36 GPa).
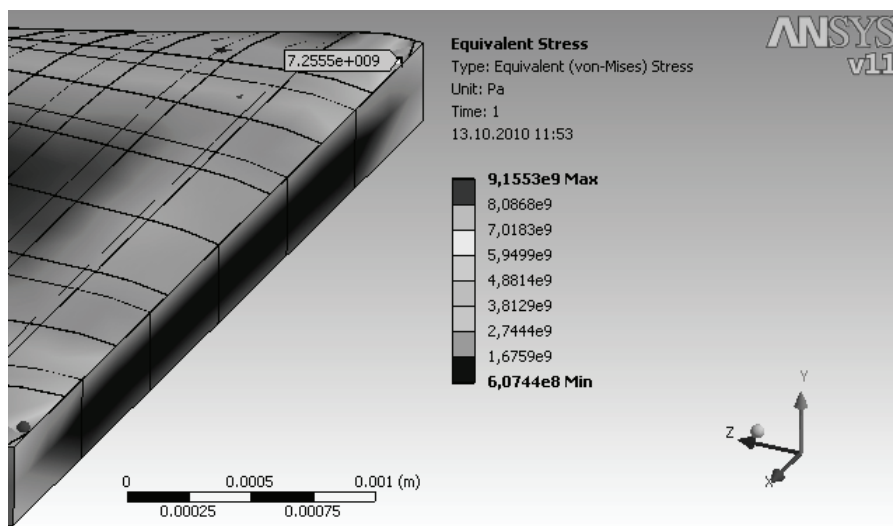
Fig. 23.FEM simulation of equivalent stress (residual stress) for coated sample (strip (30x4x0.35) mm).

Surface roughness

Surface topology (area of (50x50)μm, (10x10)μm and (5x5)μm) investigations by the AFM revealed that for investigated TiN, TiAlN, AlTiN and nACo coatings the non-Gaussian height distribution function (HDF) is mainly due to the macroparticles (see Fig. 24). The morphology of coating surfaces can be characterized by an alternation of the defect-free surface and macroparticles.

Surface topology (area of (50x50)μm, (10x10)μm and (5x5)μm) investigations by the AFM revealed that for investigated TiN, TiAlN, AlTiN and nACo coatings the non-Gaussian height distribution function (HDF) is mainly due to the macroparticles (see Fig. 24). The morphology of coating surfaces can be characterized by an alternation of the defect-free surface and macroparticles.
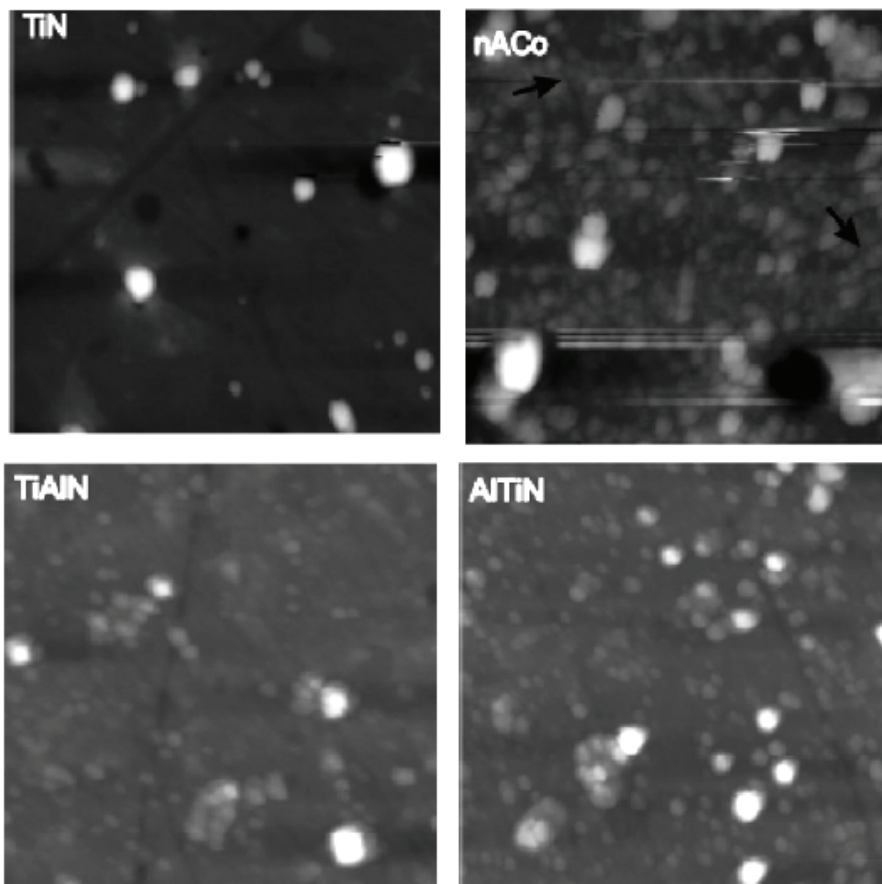
Fig. 24. AFM images (10μm×10μm) of the TiN, nACo,
TiAlN and AlTiN coatings surfaces.

Scratches of different lengths and depths were observed on the surface of a clean HSS substrate. However TiN, TiAlN and AlTiN coatings had relatively flat and defect-free surface that is in contrast with a cellular-like structure covering the entire surface of the nACo coating (see Fig. 25). This structure is partially aligned, probably with the deep HSS substrate scratches depicted by arrows (see Fig. 24). Therefore, the cellular-like structure should not be mixed up with the macroparticles and such structure could be an indication of the intrinsic kinetics of nACo growth on the substrate. It is assumed that surface defects on nACo coating could be the reason for poor friction and wear resistance (see Tables 11 and 14).

Table 14. Surface roughness and coating type

| Parameter	HSS	Wet polished TiCN	Dry polished TiCN	Wet polished AlCrN	Dry polished AlCrN	TiN	TiAlN	AlTiN	nACo
Roughness R_a (nm)	4	570	160	410	150	70±8	90±11	90±11	80±10
CoF	0,5	0,2	0,2	0,35	0,35	0,27	0,3	0,45	0,49

According to AFM surface topography investigations and sliding wear testing results, similarly to [30], the coefficient of friction (as well as wear coefficient) increases with multilayer coatings surface roughness parameter R_a decrement (see Table 14). Lower friction and stiction (adhesion) of coatings with rougher surfaces is caused by smaller real area of contact in the elastic region [51]. Fretting tests (2 N, 10 Hz, 100µm, 4000 cycles, RH=15%, Al_2O_3 ball d =10mm) were conducted on the HSS substrate. The initial value of coefficient of friction in the beginning of fretting test after 166 cycles varied depending on the coating type (see Table 14). There is a trend towards initial coefficient of friction rise with an increase of Al content in the coating.

The dependence of two additional coatings (TiCN and AlCrN) surface fatigue and cracking resistance dependence on coatings surface roughness was also considered in this work. The Vickers diamond pyramid indenter was cyclically pressed with 500 N load at single point during indentation surface fatigue testing. The results of cyclic indentation test are presented in Fig. 25. The result are comparable with industrial trials of four punches for blanking of 4 mm soft annealed sheet steel C60E (for more descriptions see VII). The better surface fatigue wear resistance of rougher surfaces (see Figs. 25 and 26) can be explained by compressive residual stresses in the coatings (see Table 13) [38]. The surface roughness determines the character of control over fatigue process. The smooth surface fatigue is controlled by crack nucleation and rough surface by crack propagation.
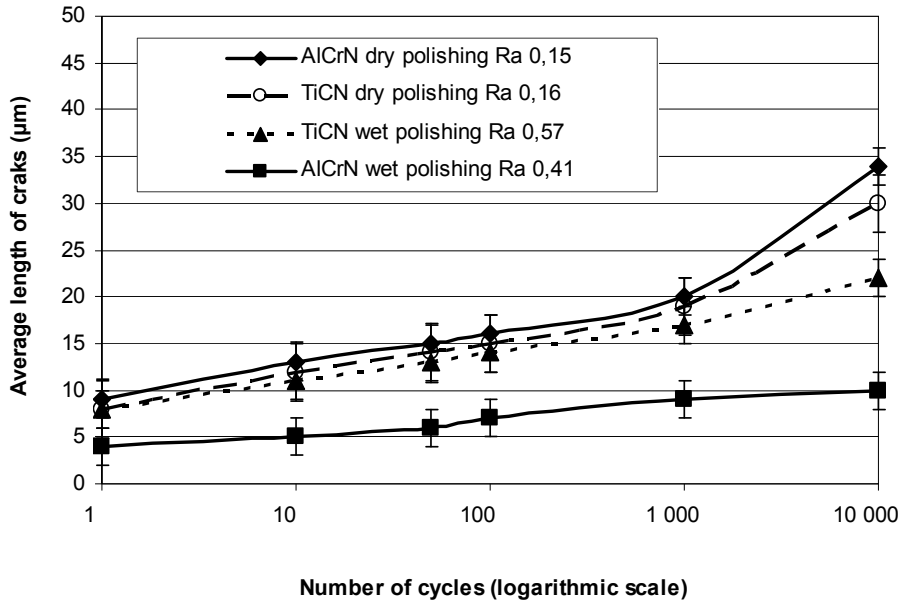
Fig. 25. Indentation surface fatigue testing results.

a) R_a 0.41

b) R_a 0.57

c) R_a 0. 15
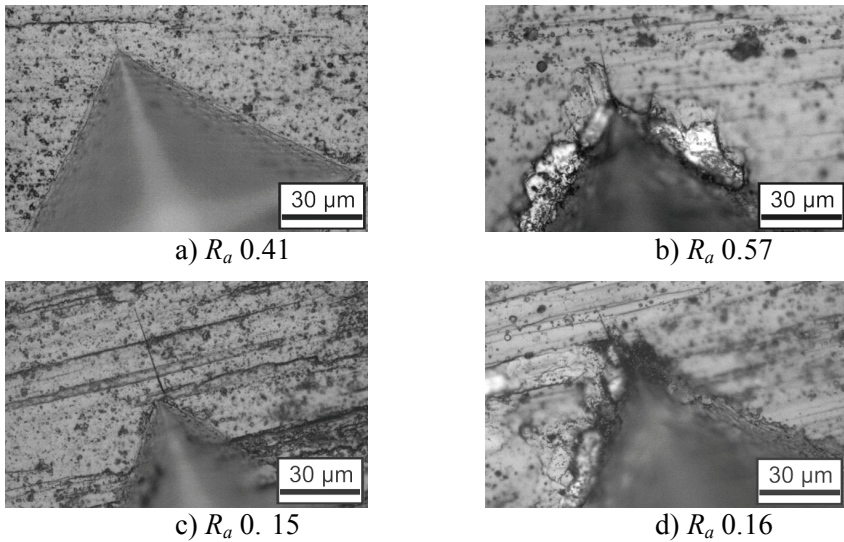

d) R_a 0.16

Fig. 26. Impression corner of a – AlCrN and b –TiCN coatings on wet polished S390 steel; c –AlCrN and d –TiCN coatings on dry polished S390 steel after 10 000 indentation cycles.

4   CONCLUSIONS

The influence of physico-mechanical of coatings, surface roughness and residual stress parameters on surface fatigue, cracking resistance, adhesion and sliding wear of the coated system has been investigated. The current conclusions can be made:

1) A new express method and device (rototribometer) for dry sliding wear testing can be successfully exploited. The results of rototribometer test were comparable with pin-on-disc and ball-on-disc standard wear test results.

2) Multilayer and gradient coatings on cold work tool steels and WC-15Co substrates in conditions of dry sliding wear test revealed the tendency of the increase of coefficient of friction and coefficient of wear with E/H ratio decrease. The values of the coefficient of friction and the coefficient of wear of multilayer and gradient coatings tend to grow with decreasing surface roughness parameter R_a (in the range of tens of nanometers) and residual stress. The optimal residual compressive stress ($\sigma_{residual} = (6.5 - 8)$ GPa) is preferable for minimal sliding wear.

3) Higher cracking resistance and better fatigue properties of coatings on cold work tool steels ($E/H = 0.24 - 0.25$) are guaranteed by high E/H ratio, coating multilayer and substrate fine-grained structures, chemical composition similarity of coating and substrate, also by optimal surface roughness ($R_a = (0.4 - 0.6)$ μm) and compressive residual stress ($\sigma_{residual} = (6.5 - 8)$ GPa). However the E/H ratio influence on coatings on nitrided steel ($E/H = 0.32$) was opposite to cold work tool steel substrate ($E/H = 0.24 - 0.25$).

4) Better adhesion of coatings on cold work tool steels at monolayer structure and higher E/H ratio was observed. Rockwell C adhesion test results were comparable with Vickers single loading test results.

The following activities are planned for future work:

- The modification of rototribometer prototype should be done to make it possible to perform the in-situ measurements of coatings linear wear.
- FEM models for prediction of sliding and indentation fatigue wear of coatings should be created. FEM models of coated systems will give more precise information concerning the E/H ratio value influence on fatigue wear of coatings. The surface roughness and residual stress parameters should be taken into account in FEM models. The optimal values of surface roughness and residual stress for different coatings applications should be determined.

5 REFERENCES

1. **Leyland, A., Matthews, A.** On the significance of the H/E ratio in wear control: a nanocomposite coating approach to optimised tribological behaviour. *Wear*, 2000, 246, 1 – 2, p.1 – 11.
2. **Ohnuma, H., Nihira, N., Mitsuo, A., Toyoda, K., Kubota, K., Aizawa, T.** Effect of aluminium concentration on friction and wear properties of titanium aluminium nitride films. *Surf. Coating Tech.*, 2004, 177 – 178, p. 623 – 626.
3. **Mo, J.L., Zhu, M.H., Lei, B., Leng, Y.X., Huang, N.** Comparison of tribological behaviours of AlCrN and TiAlN coatings deposited by physical vapour deposition. *Wear*, 2007, 263, p.1423 – 1429.
4. **Bressan, J.D., Hesse, R., Silva J, E.M.** Abrasive wear behaviour of high-speed steel and hard metal coated with TiAlN and TiCN. *Wear*, 2001, 250, p. 561 – 568.
5. **Halling, J.** Surface films in tribology, Tribologia 1 (2), 1982, p. 15.
6. **Cook, R.F., Pharr, G.M.** Direct observation and analysis of indentation cracking in glasses and ceramics. *J. Am. Ceram. Soc.*, 1990, 73, p. 787 – 817.
7. **Chiang, S.S., Marshall, D.B. Evans, A.G.** The response of solids to elastic/plastic indentation. I. Stresses and residual stresses. *J. Appl. Phys.*, 1982, 53, p. 298 – 311.
8. **Chiang, S.S., Marshall, D.B., Evans, A.G.** The response of solids to elastic/plastic indentation: II. Fracture Initiation, *J.Appl. Phys.*, 1982, 53, p. 312 – 317.
9. **Johnson, K. L.** Contact mechanics. Cambridge University Press, Cambridge, 1985.
10. **Mencík, J., Swain, M.V**. Materials Forum, 1994, 18, p. 277.
11. **Oliver, W.C., Pharr, G. M.** An improved technique for determining hardness and elastic modulus using load and displacement sensing indentation experiments. *Journal of Materials Research*, 1992, 7, p. 1564 – 1583.
12. **Bouzakis, K.-D., Hadjiyiannis, S., Skordaris, G., Mirisidis, I., Michailidis, N., Efstathiou, K., Pavlidou, E., Erkens, G., Cremer, R., Rambadt, S., Wirth, I.** The effect of coating thickness, mechanical strength and hardness properties on the milling performance of PVD coated cemented carbides inserts. *Surf. Coating Tech.*, 2004, 177 – 178, p. 657 – 664.
13. **Grzesik, W., Zalisz, Z., Krol, S., Nieslony, P.** Investigations on friction and wear mechanisms of the PVD-TiAlN coated carbide in dry sliding against steels and cast iron. *Wear*, 2006, 261, p. 1191 – 1200.
14. **Bunshah, R. F.** Handbook of Hard Coatings. Noyes Publications, USA, 2001.

15. **Tarrés, E., Ramirez, G., Gaillard, Y., Jiménez-Piqué, E., Llanes, L.** Contact fatigue behavior of PVD-coated hardmetals. *Int. J. Refract. Met. H. Mater.*, 2009, 27, p. 323 – 331.

16. **Stachowiak, G. W., Batchelor, A.W.** *Engineering Tribology.* Butterworth Hienemann, 2001.

17. **Richter, J.** Application of Vickers indentation for assessment of PVD TiN coated new nonledeburitic high-speed steels. *Surf. Coat. Tech.*, 2003, 162, p. 119 – 130.

18. **Tarrés, E., Ramirez, G., Gaillard, Y., Jiménez-Piqué, E., Llanes, L.** Contact fatigue behavior of PVD-coated hardmetals. *Int. J. Refract. Met. H. Mater.*, 2009, 27, p. 323 – 331.

19. **Kim, D.K., Jung, Y.-G., Peterson, I.M., Lawn, B.R.** Cyclic contact fatigue of intrinsically brittle ceramics in contact with spheres. *Acta Mater.*, 1999, 47, p. 4711 – 4725.

20. **Fouvry, S., Liskiewicz, T., Paulin, C.** A global–local wear approach to quantify the contact endurance under reciprocating-fretting sliding conditions. *Wear*, 2007, 263, p. 518 – 531.

21. **Cook, R.F., Pharr, G.M.** Direct observation and analysis of indentation cracking in glasses and ceramics. *J. Am. Ceram. Soc.*, 1990, 73, p. 787 – 817.

22. **Sglavo, V.M., Green, D.J.** Indentation determination of fatigue limits in silicate glasses. *J.Am. Ceram. Soc.*, 1999, 82, p. 1269 – 74.

23. **Guiberteau, F., Padture, N.P., Cai, H., Lawn, B.R.** Simple cyclic Hertzian test for measuring damage accumulation in polycrystalline ceramics. *Philos. Mag. A*, 1993, 68, p. 1003– 1016.

24. **Lankford, J., Davidson, D.L.** The crack initiation threshold in ceramic materials subject to elastic/plastic indentation. *J. Mater. Sci.* 1979, 14, p. 1662 – 1668.

25. **Shetty, D.K., Wright, I.G., Mincer, P.N., Clauer, A.H.** Indentation fracture of WC-Co cermets. *J. Mater. Sci.*, 1985, 20, p. 1873 – 1882.

26. **PalDey, S., Deevi, S.C.** Single layer and multilayer wear resistant coatings of (Ti,Al)N: a review. *Mater. Sci. Eng.*, 2003, 342, p. 58 – 79.

27. **Bhushan, B.** Modern Tribology Handbook. CRC Press, 2001, p. 49 – 80.

28. **Smith, I.J., Gillibrand, D., Brooks, J.D., Münz, W.-D., Harvey, S., Goodwin, R.** Dry cutting performance of HSS twist drills coated with improved TiAlN. *Surf. Coat. Technol.* 1997, 90, p. 164 – 167.

29. **Dr. M. Morstein, Dr. J. Prokazka (**PLATIT- http://www.platit.com), personal communication.

30. **Lou, F., Pang, X.L., Gao, K.W., Tao, C.H.** Substrate Roughness Effects on Chromium Oxide Coating Adhesion and Wear Resistance. *Advanced Materials Research*, 2010, 97 – 101, p. 1261 – 1264.

31. **Takago, S., Gotoh, M., Sasaki, T., Hirose, Y.** The residual stress measurement of TiCN PVD films. *JCPDS-International Centre for Diffraction Data*, 2002, Advances in X-ray Analysis, 45, p.365 – 370.

32. **Murotani, T., Hirose, H., Sasaki, T., Okazaki, K.** Study on stress measurement of PVD-coating layer. *Thin Solid Films*, 2000, 377 – 378, p. 617 – 620.

33. **Matsue, T., Hanabusa, T., Ikeuchi, Y., Miki, Y., Maitani, E.** Residual stress and its thermal relaxation of TiN materials. *J. Soc. Mat. Sci. Japan*, 2000, 49 – 7, p. 735 – 741.

34. **Gunnars, J., Wiklund, U.,** Determination of growth-induced strain and thermo-elastic properties of coatings by curvature measurement. Mater. Sci. Eng., 2002, 336, p.7 – 21.

35. **Holmberg, K., Ronkainen, H., Laukkanen, A., Wallin, K,. Hogmark, S., Jacobson, S., Wiklund, U., Souza R. M, Ståhle, P.** Residual stresses in TiN, DLC and MoS2 coated surfaces with regard to their tribological fracture behaviour. *Wear*, 2009, 267, 12, p. 2142 – 2156.

36. **Wiklund, U., Gunnars, J., Hogmark, S.** Influence of residual stresses on fracture and delamination of thin hard coatings. *Wear*, 1999, 232 p. 262 – 269.

37. **Gotoh, M., Takago, S., Sasaki, T., Hirose, Y.** Effect of the residual stress on the mechanical strength of the thin films. *JCPDS-International Centre for Diffraction Data*, 2003, Advances in X-ray Analysis, 46, p.173 – 178.

38. **Totten., G.E., Howes, M., Inoue, T.** Handbook of residual stress and deformation of steel. ASM International, USA, 2002.

39. VDI 3198:1992–08, Coating (CVD, PVD) of cold forging tools, VDI-Verlag, Dusseldorf, 1991.

40. **Salumäe, T.** Wear measurement methods for rototribometers. BSc thesis. Institute of Mechatronics, Tallinn University of technology, 2008.

41. **Holm, R.** Electric contacts. Almqvist & Wiksells Boktyckeri AB, Uppsala, 1946.

42. **Põdra, P.** FE Simulation of Sliding Contacts. Doctoral Thesis. Royal Institute of Technology, KTH, Sweden, Stockholm, 1997.

43. **Yang, Q., Zhao, L.R.** Dry sliding wear of magnetron sputtered TiN/CrN superlattice coatings. *Surf. Coat. Tech.*, 2003, 173, p. 58 – 66.

44. **Palmqvist, S.** The work for the formation of a crack during Vickers indentation as a measure of the toughness of hard metals (in Ger.). *Arch. Eisenhuttenwes.*, 1962, 33, p. 629 – 634.

45. **Lille, H., Kõo, J., Ryabchikov, A., Toropov, S., Veinthal, R., Surzhenkov, A.** Comparative analysis of residual stresses in flame-sprayed and electrodeposited coatings using substrate deformation and hole-drilling methods. Küttner, R. (Eds.). *Proceedings of the 7th international conference of DAAAM Baltic Industrial Engineering,* 24 – 26th April 2010, TUT Press, Tallinn, Estonia, 2010, p. 474 - 479.

46. **Chen, Xi., Yan, Mi.,Yang, D., Hirose, Y.** A method for predicting critical load evaluating adhesion of coatings in scratch testing. *Journal of Zhejiang University Science*, 2003, 4, 6, p. 709 – 713.

47. **Braic, M., Braic, V., Balaceanu, M., Pavelescu, G., Vladescu, A.** Plasma deposition of alternate TiN/ZrN multilayer hard coatings. *Journal of Optoelectronics and Advanced Materials*, 2003, 5, 5, p. 1399 – 1404.
48. **Bouzakis, K.-D., Siganos, A., Leyendecker, T., Erkens, G.** Thin hard coatings fracture propagation during the impact test. *Thin Solid Films*, 2004, 460, p. 181 – 189.
49. **Gee, M.G., Wicks, M. J.** Ball crater testing for the measurement of the unlubricated sliding wear of wear-resistant coatings. *Surf. Coat. Tech.*, 2000, 133 – 134, p. 376 – 382.
50. **Donachie, M.J.** Titanium: a technical guide. ASM International, USA, 2000.
51. **Peng, W., Bhushan, B.** Three-dimensional contact analysis of layered elastic/plastic solids with rough surfaces. *Wear*, 2001, 249, p. 741 – 760.

ABSTRACT

In this work fatigue, cracking and sliding wear resistance of five types of mono, multilayered and gradient PVD coatings – TiN, TiCN, TiAlN, AlTiN and nanocomposite gradient nACo® (nc-Al$_{1-x}$Ti$_x$N/a-Si$_3$N$_4$) on cold work tool steels, nitrided steels and hardmetals are estimated. Methods of prediction and characterisation of coatings functional properties dependance on their physical-mechanical properties are offered.

The new method of rototribometer is used for sliding wear resistance assessment. Tribological test system consists of coated hardmetal (WC-15Co) sphere and drum made from constructional steel (C45). The examination of worn samples is presented if form of wear scars optical micrographs and profilograms of worn surfaces. The pin-on-disk and ball-on-disk test are carried out showing that both test results are comparable with new rototribometer test. Coefficient of friction, volume wear and coefficient of wear is dependant on coatings elastic modulus/hardness ratio (E/H ratio). Among multilayer and gradient coating the highest E/H ratio values guarantee better wear characteristics.

The fatigue cracks initiation and growth are evaluated by means of cyclic Vickers indentation method and analyzed by Palmqvist method. The cyclic indentation experiment results are presented graphically displaying radial cracks length versus the number of indentation cycles. In addition qualitative evaluation criteria of the cracking (0 –VI) from crack formation, propagation to delamination of the coating is considered for fatigue resistance detailed description. Resistance to fatigue crack initiation and propagation depends on coatings E/H ratio of the coating. On cold work tool steels the highest E/H ratio, coating multilayer structure, coating and substrate structure and chemical composition similarity inhibit cracking and show better resistance to fatigue wear. However opposite influence of E/H ratio was discovered in case of nitrided steel substrate.

Among other factors that have an effect on the coatings durability are residual stress and surface roughness of substrate. These parameters are taken into account in a more brief way. There is strong wear parameters dependence on residual stress. The optimal higher values of compressive stress are preferable. The optimal coatings surface roughness value for punches is offered. However the influence of surface roughness on wear parameters should be more specified. The optimal values for concrete applications have to be founded.

Investigation of different coating/substrate combinations gives an opportunity to ascertain the available data and enlarge the knowledge concerning substrate properties influence on coated system characteristics. Studied mechanisms of fatigue cracking and wear mechanisms should assist on the selection of optimal coating for metal tooling applications.

Keywords: PVD coatings, sliding wear resistance, fatigue wear resistance, coatings E/H ratio, residual stresses, surface roughness

KOKKUVÕTE

Selles töös hinnatakse tööriistaterastele, nitriiditud terastele ja kõvasulamitele sadestatud PVD mono-, mitmekihilise- ja gradientpinnete – TiN, TiCN, TiAlN, AlTiN ning nanokomposiitpinde nACo (nc-Al$_{1-x}$Ti$_x$N/a-Si$_3$N$_4$) liugekulumist, väsimuskulumist ja vastupanu pragunemisele sõltuvalt pinnete füüsikalis-mehaanikalistest omadustest.

Pakutud on uus meetod ja aparatuur – rototribomeetri testimismeetod pinnete liugekulumise katsetamiseks. Uus tribosüsteem koosneb kõvasulamist (WC-15Co) pinnatud kuulist ja konststruktsiooniterasest (C45) trumlist. Kulutatud katsekehade analüüs koosneb kulumisarmide läbimõõdu mõõtmisest mikroskoobi vahendusel ja nende sügavuse mõõtmisest profilomeetriga. Standardsete liugekulumiskatsete tulemused ja uue meetodi tulemused on kooskõlas. Vastavalt nende tulemustele pinnete hõõrdetegur, kulumi- ja kulumistegur on sõltuvuses elastsusmooduli/ kõvaduse suhtest (*E/H* suhe). Mitmekihiliste ja gradientpinnete seas kõrgem *E/H* suhe tagab pindele parema libisemiskulumiskindluse.

Väsimuskulumise ja vastupanu pragunemisele hindamiseks kasutati tsüklilise indentatsiooni meetodit ja tulemuste analüüsimiseks Palmqvisti meetodit. Tulemuste hindamiseks kasuatati radiaalpragude pikkuse ja tsükklite arvu vahelist seost. Kvalitatiivne analüüs on esitatatud pragunemise kriteeriumite (0 –VI) näol prao tekkimisest, arenemisest kuni pinde lahtitulekuni. Katsetulemused näitasid, et pinde kõrge *E/H* suhe, pinde mitmekihiline struktuur, pinde ja alusmaterjali struktuuri ja keemilise koostise sarnasus alandab väsimuskulumist ja tõstab vastupanu pragunemisele tööriistaterasest alusmaterjali korral, kuigi täiesti vastupidine *E/H* suhe mõju oli avastatud nitriiditud aluste puhul.

Teised faktorid, mis avaldavad mõju pinnete vastupidavusele, on jääkpinged ja pinnakaredus. Nende mõju uurimine polnud põhieesmärk. On selgelt näha, et survejääkpinged on eelistatud pinnete funktsionaalsuse parendamiseks. On pakutud optimaalse pinnakareduse väärtused stantsimisrakistes, kuigi pinnakareduse mõju pinnete omadustele teistes rakendustes vajab täpsustamist.

Erinevate pinnete/alusmaterjalide kombinatsioonide uurimine annab võimaluse pindekarakteristikutele mõjuvate faktorite andmebaasi laiendamiseks. Uuritud liuge- ja väsimuskulumise mehhanismid aitavad valida optimaalset pinnet konkreetsete tööriistade tööea pikendamiseks.

Võtmesõnad: PVD pinded, liugekulumine ja väsimuskulumine, pinnete kulumis-kindlus, *E/H* suhe, jääkpinged, pinnakaredus.

CURRICULUM VITAE

1. Personal data

Name and surname	Alina Sivitski
Date and place of birth	25.01.1982, Tallinn, Estonia

2. Contact information

Address	19086 Tallinn, Ehitajate tee 5, Estonia
Phone	+372 56154427
E-mail	alina.sivitski@ttu.ee

3. Education

Educational institution	Graduation year	Education (field of study/degree)
Tallinn University of Technology	2010	Faculty of Mechanical Engineering, Mechanical and Instrumental Engineering/ PhD.
Tallinn University of Technology	2010	Faculty of Social Sciences, Engineering Educator/ MSc.
Tallinn University of Technology	2006	Faculty of Mechanical Engineering, Product Development/ MSc.
Tallinn University of Technology	2004	Faculty of Mechanical Engineering, Product Development/ BSc.

4. Language competence/skills (fluent; average; basic skills)

Language	Level
Estonian	Fluent
Russian	Mother tongue
English	Fluent

5. Special Courses

Name of the course	Time of the study and place	Educational organization
E-course (online) construction	06.03 – 11.05.2007, Tallinn University of Technology	Open University

6. Professional Employment

Period	Organization	Position
Veebruar 2007 – present	Tallinn University of Technology/ Institute of Mechatronics/ Chair of Machine Elements and Fine Mechanics	Teaching assistant
Oktoober 2006 – Jaanuar 2007	Tallinn University of Technology/ Institute of Mechatronics/ Chair of Machine Elements and Fine Mechanics	Researcher
Märts 2006 – August 2006	Desfactory OÜ	Mechanics designer
Oktoober 2004 – August 2005	Karl Storz Video Endoscopy Estonia OÜ	CAD-engineer
August 2003 – Juuni 2004	Norma AS	Engineer-designer

7. Scientific work

Period of the project	Project name	Project no.
2008 – 2013	Hard coatings and surface engineering	SF0140091s08
2008 – 2010	Optimisation of tribological properties of PVD hard coatings	ETF7442
2006 – 2007	Synthesis of Mechatronics and Measurement Systems: Modeling, Optimisation and Quality Control	SF0142506s03

8. Main areas of scientific work/Current research topics

    a)   Hard coatings and surface engineering SF0140091s08
    b)   Optimisation of tribological properties of PVD hard coatings ETF7442

9. Other research projects

    a)   Graduate school „Functional materials and processes", European Social Fund under project 1.2.0401.09 – 0079
    b)   Graduate school „New manufacturing technologies and processes", Socrates, 2007-2008.
    c)   Managing a multicultural workforce – key issues in the Baltic Sea region, Sokrates/Curriculum Development programme 29323-IC-1-2005-1-FI-ERASMUS-MODUC-1, 2006-2008.

ELULOOKIRJELDUS

1. Isikuandmed

     Ees- ja perekonnanimi   Alina Sivitski
     Sünniaeg ja -koht   25.01.1982, Tallinn
     Kodakondsus   Eesti

2. Kontaktandmed

     Aadress   19086 Tallinn, Ehitajate tee 5,
                                      Eesti
     Telefon   +372 56154427
     E-posti aadress   alina.sivitski@ttu.ee

3. Hariduskäik

Õppeasutus (nimetus lõpetamise ajal)	Lõpetamise aeg	Haridus (eriala/kraad)
Tallinna Tehnikaülikool	2010	Mehaanikateaduskond, Tootearenduse õppesuund/ tehnikateaduste doktor
Tallinna Tehnikaülikool	2010	Sotsiaalteaduskond, Tehnikaõpetaja/ haridusteaduse magister
Tallinna Tehnikaülikool	2006	Mehaanikateaduskond, Tootearenduse õppesuund/ tehnikateaduste magister
Tallinna Tehnikaülikool	2004	Mehaanikateaduskond, Tootearenduse õppesuund/ tehnikateaduste bakalaureus

4. Keelteoskus (alg-, kesk- või kõrgtase)

Keel	Tase
Eesti	kõrgtase
Vene	emakeel
Inglise	kesktase

5. Täiendusõpe

Täiendusõppe nimetus	Õppimise aeg ja koht	Täiendusõppe läbiviija nimetus
E-kursuse loomine	06.03 – 11.05.2007 Tallinna Tehnikaülikool	Avatud Ülikool

6. Teenistuskäik

Töötamise aeg	Tööandja	Ametikoht
Veebruar 2007 –	Tallinna Tehnikaülikool/ Mehhatroonikainstituut/ Masinaelementide- ja peenmehaanika õppetool	Assistent
Oktoober 2006 – jaanuar 2007	Tallinna Tehnikaülikool/ Mehhatroonikainstituut/ Masinaelementide- ja peenmehaanika õppetool	Erakorraline teadur
Märts 2006 – august 2006	Desfactory OÜ	Mehaanika projekteerija
Oktoober 2004 – august 2005	Karl Storz Video Endoscopy Estonia OÜ	CAD insener
August 2003 – juuni 2004	Norma AS	Konstruktor

7. Teadustegevus

2008 – 2013	Projekt "Kõvapinded ja pinnatehnika"	SF0140091s08
2008 – 2010	Projekt "Aurustussadestatud kõvapinnete triboloogia omaduste optimiseerimine"	ETF7442
2006 – 2007	Projekt "Mehhatroonika ja mõõtesüsteemide süntees: modelleerimine, optimeerimine ja kvaliteediohje"	SF0142506s03

8. Teadustöö põhisuunad
   a) Kõvapinded ja pinnatehnika SF0140091s08
   b) Aurustussadestatud kõvapinnete triboloogia omaduste optimiseerimine ETF7442

9. Teised uurimisprojektid
   a) Doktorikool „Funktsionaalsed materjalid ja tehnoloogiad", Euroopa Liit, Euroopa Sotsiaalfond, 2009 – 2010.
   b) Doktorikool „Uued tootmistehnoloogiad ja -protsessid", Socrates, 2007-2008.
   c) Managing a multicultural workforce – key issues in the Baltic Sea region, Sokrates/Curriculum Development programme 29323-IC-1-2005-1-FI-ERASMUS-MODUC-1, 2006-2008.

PAPER I

Sivitski, A.; Ajaots, M.; Põdra, P. Wear of PVD hard coatings in sliding contacts (review). Küttner, R. (Eds.). *Proceedings of the 6th international conference of DAAAM Baltic Industrial Engineering*, 24 – 26th April 2008, TUT Press, Tallinn, Estonia, 2008, p. 549 – 554.

WEAR OF PVD HARD COATINGS IN SLIDING CONTACTS

Sivitski, A.; Ajaots, M.; Põdra, P.

Abstract: *Tribological behaviour of PVD thin hard coatings has been analysed in this paper. Only few studies on PVD coatings' tribology in sliding contacts have been published up to now. The mechanisms that influence sliding friction and wear phenomena of PVD hard coatings are, therefore, yet poorly understood. The works available generally rely on experimental approach with no deeper explanation of physical phenomena or respective mathematical models. The aim of this work is to compare the capability of the wear models, to present the complex of parameters that influence sliding wear rate and to introduce an analysis of practical procedure for determining the wear of (Ti,Al)N based hard coatings' in sliding contacts.*

Key words: Sliding wear models; PVD hard coatings; Wear analysis

1. INTRODUCTION

PVD thin hard coatings are primarily used to minimize friction and increase wear resistance of metal-cutting and -forming tools, as well as in some bearings, gearings and other applications [1]. In most of the available works [2], [3], [4], [5] mainly dry sliding conditions and abrasive wear mechanisms have been considered along with pin-on-disc tests. The use of PVD hard coatings in engineering applications to greater extent, would assume that their wear and friction behaviours in respective conditions, where abrasion is often not acceptable, are better known. The empirical methods used in works above support the development of materials'

tribological properties but do not suggest which coating type is the most suitable for particular application and do not allow the practicing engineer to predict the wear in particular contact. Mathematical wear models have to be identified and verified with appropriate experiments for prognosis of wear performance. Many of known wear models are hardly applicable in engineering design, due to complexity and use of specific and rare parameters. The linear wear model, also referred to as Archard's wear model, and some of its modifications, have therefore been used most extensively in practical engineering applications.

2. WEAR ANALYSIS METHODS AND WEAR MODELS IN SLIDING CONTACTS

One of the most important engineering tasks is the prediction of wear rate and its minimization in particular contact. The wear rate in sliding contacts can be described by a general differential equation:

$$\frac{dh}{ds} = f(x), \quad (1)$$

where h is the wear depth (m) and s is the sliding distance (m), x is either load, velocity, temperature, material parameters, lubrication etc). Generally, the dominating parameters in sliding wear models are sliding velocity and the normal load. First parameter can be determined by the mechanism kinematics. The load influence determination is often more complicated. Hertz formulae can be used for contact

stress distribution in the cases of non-conforming contacts of elastic bodies. The main disadvantage of the Hertz theory is that it is based on some assumptions that idealize the properties of contacting bodies and the contact conditions. In fact, properties of the coating and surface layer at contact zones change during wearing process under the influence of high contact pressure and sliding velocities. The chemical reactions, resulting in the formation of secondary compounds and structures, also occur in the contact area. Hertz theory neglects the fact that, in contact interaction, stresses increase in a thin surface layer, the thickness of which is comparable with the size of contact region. Thus, the properties of a thin surface layer play an important role in the subsurface stress and wear analysis [6]. In those cases numerical method such as finite element analysis (FEA), must be used for contact stress distribution determination and wear simulation [7].

Application of FEA is limited in some cases, as it is not fast enough to cover the whole lifetime of the contacting body using complex material model and sufficient elements in contact [8]. According to last statement in FEA the number of elements and extra features to consider (friction, plasticity, etc) must be minimized. If major simplifications are allowed, the Winkler's surface model can be used for saving computing time. In Winkler's model the interacting contact surfaces are modelled as a set of "springs", resisting on the rigid base.

Applications of wear simulation methods with FEA and linear wear model have been successfully adapted to PVD hard coatings abrasive wear investigation [9]. According to linear wear model, the volume rate is proportional to the normal load. The model is based on experimental observations and was initially written in form

$$\frac{V}{s} = K \frac{F_N}{H}, \quad (2) \qquad [10],$$

where V is the volume wear (m^3), s is the sliding distance (m), F_N is the normal load, H is the hardness (Pa) and K is the wear coefficient.

The wear depth is more important than wear volume in engineering calculations. Dividing both sides of equation (2) by the apparent contact area, the wear depth is

$$h = kps, \qquad (3)$$

where h is the wear depth, p is the normal contact pressure (Pa) over that particular discrete region, s is sliding distance, $k=K/H$ is the dimensional wear coefficient (Pa^{-1}).

It can be concluded that in case of coated materials the specimen structure is not homogenous. In addition, the contact pressure varies during the wear process. Thus, it is perspective to use linear wear model combined with numerical structural analysis methods such as FEA for hard coatings' wear study.

3. THE PARAMETERS THAT INFLUENCE WEAR OF PVD HARD COATINGS

The wear rates of PVD hard coatings are influenced by many parameters [2], [3], [4], [5]. The list of the main parameters is presented in table 1. More detailed overview of effect of the parameters on hard coatings wear has been offered below.

Wear mechanism is one of the parameters that have an effect on the evolution of the PVD hard coatings' wear process. Adhesion, two-body and three-body abrasive, tribo-oxidation and surface fatigue wear mechanisms can occur. Studies of wear resistant coatings reveal that coatings are most effective when resisting abrasive wear [1]. However, it has been mentioned that thin hard coatings are effective only if fine particles are present in the contact. If the size of the abrasive is larger and comes near to coating thickness then coatings' abrasive wear resistance decrease. Different types of hard coatings can be applied as solid lubricants to

suppress the adhesive wear in poorly lubricated and high stress contacts. For example, TiN coatings prevent the adhesion and seizure between the cutting tool and metal chip [1]. The same coating has been successfully used for increasing the wear resistance in gearing.

Coating hardness is the main parameter, which affects the wear rate of hard coatings. If investigated wear mechanism is adhesive or two-body abrasive mechanism the wear coefficient proved to have a linear dependence on the coating hardness. In three-body abrasive wear mechanism, the wear coefficient dependence on the coating hardness is absent [9] (Fig. 1).
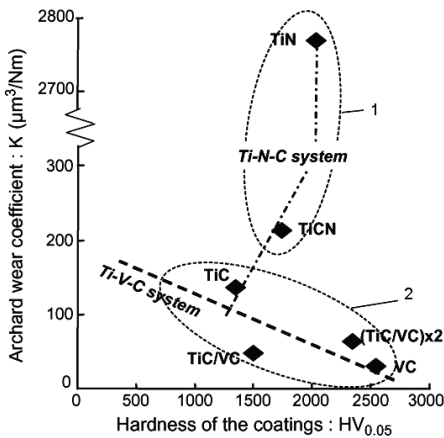

Fig. 1. The wear coefficient K versus coating hardness $HV_{0.05}$ for alumina ball as counterbody. 1– three-body abrasion; 2– two-body abrasion process [9].

Substrate material hardness influences on wear rate must be determined. It has been verified that wear rates increase with the substrate material hardness growth [5].

Surface roughness is an important factor in wear process. Generally, the smoother surface proves the lower wear rates. However, extra smooth surfaces in small scales require the optimal roughness verification due to the increase of contact bodies' atoms attraction. The appropriate surface roughness of coating and substrate is offered in table 1.

Table 1. The parameters that influence the wear of PVD hard coatings.

Friction and wear test parameters	

Wear mechanism
 -adhesive
 -abrasive
  two-body
  three-body
 -erosive wear
 -tribo-oxidation
 -surface fatigue
	Sliding velocity and distance
	 -constant velocity
	 -variable velocity
	 (0,5-10) m/s
	 -rotation motion
	 -reciprocating motion
	 -displacement amplitude
	  ±5 mm

Normal and tangential load -constant -variable ((5-500) N)	**Temperature** -room (~20 ºC) -high (up to 300°C)
Wear tests duration -50-5000 cycles	**Relative humidity** -50-60%
Specimen shape, geometrical deviations and size -plate is preferable	**Counterbody material, physical and chemical properties, surface roughness, shape geometrical deviations and size**
Coating characteristics	
Coating surface properties -surface roughness Ra =(0,01-0,2) µm	**Coating crystal structure and structural defects** - crystal structure type (cubic;hexagonal; mixed)
Coating chemical compound and properties -Al concentration -(Ti:Al) atomic ratio -oxidation resistance in air (400-1200) ºC	**Coating and substrate physical properties** -microhardness (1000-3000) HV - nanohardness (18-52)GPa -Young's module (200-600) GPa -Poisson's ratio (0,2 -0,3) -thermal conductivity (1,7-0,055) Kcm^2/s
Coating thickness -varies 1-5 µm for monolayered	**Number of coating layers** -monolayered -multilayered
Substrate characteristics	
Substrate material crystal structure and structural defects -crystal structure type (depends on material)	**Substrate physical properties** -microhardness - nanohardness -Young's modulus -Poisson's ratio -(depends on material)
Substrate interface strength -depends on material	**Substrate surface properties** -surface roughness Ra =(0,01-0,05) µm

Chemical compound of the coating also influences the wear process. Previous research [2] has shown that wear rate of TiAlN films decreases with increasing Al content because of protective layers of amorphous aluminium oxides, which are formed on the top of TiAlN film at high temperatures [2]. Last fact explains a much improved oxidation resistance at elevated temperatures of TiAlN coatings compared to TiN. It is known that CrN coatings as well as AlCrN have much slower oxidation in air in contact with copper [1]. The reason of TiN oxidation is the catalytic effect of copper. TiN oxidation leads to the formation of titanium oxide that is rapidly worn away. The better corrosion resistance of AlCrN explains the lower friction coefficient and wear rates revealed in AlCrN and TiAlN studies [4].

Crystal structures of hard coatings vary from cubic to hexagonal structure. The PVD hard coating compositions deposited from cathode materials have different atomic ratios (Ti:Al) what influence the coating crystal structure. The cubic crystal structure is the most preferable for TiAlN coatings as wear rate is the lowest [2] .

Crystal structure defects affect the wear characteristics. The presence of pores in the coatings' structure decreases the wear resistance. It has been shown [5] that even if the two coatings' has the same hardness, the wear coefficient can vary due to structural defects.

Coatings thickness is a critical factor that affects the hard coatings wear rates. It has been shown [11] that mechanical properties and the hardness of thin TiAlN coatings with thickness in range of (3–8) μm for cemented carbides significantly affect the wear rates. On the contrary, thick (8–10) μm coatings' wear depends mainly on the thickness of coating itself. Coating thickness is effected by deposition time. According to coating growth mechanism the thicker is coating the greater is superficial **grain size** that leads to hardness and wear resistance reduction [11]. This explains why thin coatings have superior mechanical strength.

Substrate material properties must be taken into account in coatings wear studies. Hard coatings are generally applicable to protect wear of softer material. The substrate material choice depends on the fact that deposition temperature must be lower than material critical temperature. (Ti,Al)N based coatings are deposited at T=500 ºC and therefore is not suitable for alloys which are not thermostable.

The substrate interface strength proved to have an effect on coating wear rate and thus, on lifetime [3]. The stronger are interface the longer is coating lifetime. Lately multilayered coatings are developed to guarantee a strong adhesion between coating and the substrate and to obtain wear-protective coatings with low chemical reactivity and low friction, as well as to increase the hardness and toughness of the coating [11], [12].

Sliding velocities and **displacement amplitudes** have to be defined. It is suggested [3] that the sliding distance reduction leads to the wear rate decrease due to the decrease of nominal contact pressure at the specimen surface.

Temperature effect on wear is questionable. No correlation between friction coefficient and test temperature has been found in some studies [5]. However, the wear rate of TiAlN decreased above temperature of 673 K, because of the formation of Al_2O_3 [2].

To conclude, the linear correlation between coating hardness and wear coefficient of adhesive wear mechanism in dry sliding condition is present. However, sliding velocity and temperature effect as well as other parameters influence on wear resistance needs further investigation.

4. PVD HARD COATINGS IN SLIDING CONTACTS

Since there are many parameters that affect the wear of PVD hard coatings a method integrating experimental research and

simulations must be applied. None of available works considers the influence of several (3-5) parameters at once. The experimental research provides data concerning wear rate and sliding friction coefficient versus wear process parameters. The statistical analysis of experimental data allows finding the correlation between the wear model and the experimental results. The obtained equations can be used for wear prediction in engineering design.

4.1. TRIBOMETERS

The pin-on-disc, Calo-wear (KaloMax), and tribometers with reciprocating motion are mostly used for sliding wear investigation. Coated plate specimens versus pin or ball specimen are preferable to use in wear tests (Fig. 2, 3). The wear process of point contact is in the centre of attention as it can be a starting point for more complicated types of contact wear studies.
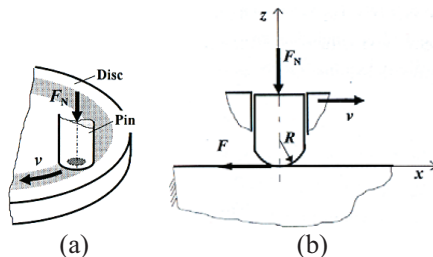

(a)   (b)

Fig. 2. The schematic of pin-on-disk (a) and reciprocating (b) tribometer.

Each wear testing method has its advantages and shortcomings. The disadvantage of pin-on-disc tribometer (Fig. 2 (a)) is possible accumulation of counterbody material in the inner areas of wear tracks. For example, Si_3N_4 counterboby leads to silicon presence in the wear track in pin-in disk tests [4]. The exhaust of the debris out of the contact zone in reciprocating test (Fig. 2 (b)) has been observed at once [4].

Another method calo-wear test with KaloMax (Fig. 3) has a high wear volume uncertainty [13], mainly due to variation in normal force on the sample and the wear of

the sphere (ball). The normal force control between the sphere and the specimen is enabled as it is derived only from the weight of the sphere.
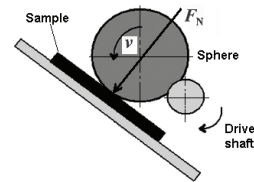

Fig. 3. The schematic of calo-wear (KaloMax) tribometer.

As fine distinctions between different sliding tests modes have been found the comparative tests should be done. The main friction and wear test parameters are offered in table 1.

4.2. THE WEAR PHENOMENA ANALYSIS

The wear process characteristics vary. Dimensional linear wear (μm) [3] and wear rate ($\mu m^3/Nm$) [9] versus sliding distance (m) or coating hardness (HV) are usually measured (Fig. 1). The width of wear track is also considered. Coefficient of sliding friction is measured against either sliding distance (m) or number of cycles. All characteristics must be calculated along with respective uncertainties for these materials according to test results with sliding wear testing machines.

SEM analysis should be done to control the coating quality after sliding tests. Optical microscopy is also needed for the wear scar's morphology definition. X-ray difractometer is used to define chemical components and the phase structures of the micro-zones inside the wear scars.

5. CONCLUSION

Summarizing, many of previous studies give the superficial knowledge of hard coatings wear based on empirical studies. The wear phenomena should be investigated.

The wear rate of PVD hard coatings in

5

sliding contacts depends primarily on sliding distance, coating hardness and normal load. Adhesive mechanism is acceptable. In this case, the linear correlation between wear coefficient and coating hardness is present.

The linear wear model (2) combined with FEA simulations is the most preferable in coating studies of sliding contacts for considering the nonhomogeneity of material and variations of contact pressure.

The maximum possible number of parameters that influence the wear characteristics must be taken into account. The applications of specific hard coatings with particular wear characteristics should be offered.

Comparative wear tests should be done to obtain reliable results.

6. REFERENCES

1. Stachowiak, G. W. Batchelor, A.W. Engineering Tribology. Butterworth Hienemann, 2001.

2. Ohnuma, H. Nihira, N. Mitsuo, A. Toyoda, K. Kubota, K. Aizawa, T. Effect of aluminium concentration on friction and wear properties of titanium aluminium nitride films. *Surf. Coating Tech.* 2004, **177 –178**, 623–626.

3. Grzesik, W. Zalisz, Z. Krol, S. Nieslony. Investigations on friction and wear mechanisms of the PVD-TiAlN coated carbide in dry sliding against steels and cast iron. *Wear.* 2006, **261**, 1191–1200.

4. Mo, J.L. Zhu, M.H. Lei, B. Leng, Y.X. Huang, N. Comparison of tribological behaviours of AlCrN and TiAlN coatings deposited by physical vapour deposition. *Wear.* 2007, **263**, 1423-1429.

5. Bressan, J.D. Hesse, R Silva Jr, E.M. Abrasive wear behaviour of high-speed steel and hard metal coated with TiAlN and TiCN. *Wear.* 2001, **250**, 561–568.

6. Goryacheva, I.G. *Contact Mechanics in Tribology*. In *Solid Mechanics and Its Applications,* Vol 61 (editor Gladwell, G. M. L). Kluwer Academic Publishers Group, The Netherlands, 1998.

7. Põdra, P. Doctoral Thesis, Royal Institute of Technology, KTH, Stockholm, Sweden. FE Wear Simulation of Sliding Contacts. Doctoral Thesis. Norstedts Trycferier AB, Stockholm, 1997.

8. Telliskivi, T. Simulation of wear in a rolling–sliding contact by a semi-Winkler model and the Archard's wear law. *Wear*, 2004, **256**, 817-831.

9. Fouvry, S. Liskiewicz, T. Paulin, C. A global–local wear approach to quantify the contact endurance under reciprocating-retting sliding conditions. *Wear*, 2007, **263**, 518-531.

10. Holm, R. *Electric contacts.* Almqvist & Wiksells BoktyckeriAB, Uppsala, 1946.

11. Bouzakis, K.-D. Hadjiyiannis, S. Skordaris, G. Mirisidis, I. Michailidis, N. Efstathiou, K. Pavlidou, E. Erkens, G. Cremer, R. Rambadt, S. Wirth, I. The effect of coating thickness, mechanical strength and hardness properties on the milling performance of PVD coated cemented carbides inserts. *Surf. Coating Tech.* 2004, **177-178**, 657-664.

12. Bunshah, R. F. Handbook of Hard Coatings. Noyes Publications, USA, 2001.

13. Podgursky, V. Gregor, A. Adoberg, E. Kulu, P. Wear of hard coatings, evaluated by means of kaloMax. Proc. Estonian Acad. Sci. Eng., 2006, **12**, 419–426.

7. ADDITIONAL DATA ABOUT AUTHORS

Alina Sivitski

M.Sc.Eng in product development, 2006, Tallinn University of Technology, Estonia. Major field of study: Fine mechanics and Tribology. E-mail: alina.sivitski@ttu.ee

Maido Ajaots

Ph. D in engineering sciences, tribology, 1977. Tallinn University of Technology, Estonia. E-mail: majaots@staff.ttu.ee

Priit Põdra

Ph. D in engineering sciences, machine elements, 1997. Kungliga Tekniska Högskolan, Stockholm, Sweden.
E-mail: priitp@staff.ttu.ee

PAPER II

Sivitski, A.; Gregor, A.; Saarna, M.; Kulu, P.; Sergejev, F. Application of the indentation method for cracking resistance evaluation of hard coatings on tool steels. *Estonian Journal of Engineering*, 2009, 15, 4, p. 309 – 317.

Application of the indentation method for cracking resistance evaluation of hard coatings on tool steels

Alina Sivitski[a], Andre Gregor[b], Mart Saarna[b], Priit Kulu[b] and Fjodor Sergejev[b]

[a] Department of Mechatronics, Tallinn University of Technology, Ehitajate tee 5, 19086 Tallinn, Estonia; alina.sivitski@ttu.ee
[b] Department of Materials Engineering, Tallinn University of Technology, Ehitajate tee 5, 19086 Tallinn, Estonia; andre.gregor@ttu.ee

Abstract. In this paper cracking resistance and fatigue properties of five hard coatings – TiN, TiCN, TiAlN, AlTiN and nanocomposite nc-AlTiN/a-Si$_3$N$_4$ (nACo®) on tool steels Weartec^{TM} and Vanadis 6 are evaluated by means of the cyclic Vickers indentation method. The analytical part covers an evaluation of damage evolution of the coated system versus the number of cycles. The comparative adhesion testing was conducted with the use of the Rockwell C technique. It was found that the type of cracks formed in the coated systems under cyclic loading depends on the Young modulus/hardness ratio. The data obtained permits to compare the cracking and fatigue resistance of the coated systems and to select the optimal coating for bulk and sheet metal forming tools.

Key words: PVD, hard coating, multilayers, indentation method, cracking, delamination.

1. INTRODUCTION

The functional properties of hard coatings have gained increasing importance as their application for sheet metal cold forming tools has grown recently. Fatigue and cracking resistance are the most important properties in such long-term applications where alternating loads are applied. Investigations of the coating crack development intensity and fatigue are commonly carried out using the indentation method for its ability to measure mechanical properties in the microscopic range [1–5].

The main elements of damage evolution and fatigue response in coated brittle systems are mechanical properties like the Young modulus/hardness ratio (E/H ratio) [4,6], microstructure and deposition technique. Two major crack types were observed in brittle materials during indentation tests: cone and radial (Palmqvist)

cracks [1,4,5]. The elastic brittle hard coatings do not show plastic deformation up to tensile fracture (normal stress) and may not suffer fatigue damage. Thus the crack propagation of the coated system may be attributed to the ratcheting deformation of the substrate under cyclic indentation. Two damage modes of coated systems: the tensile-driven cone cracking ("brittle" mode) and shear-driven microdamage accumulation ("quasi-plastic" mode) were determined [5].

This paper investigates cracking resistance of hard ceramic coatings subjected to cyclic Vickers indentation. The dependence of the crack types and the intensity of crack development on the coating type, deposition technique and substrate material are determined.

2. EXPERIMENTAL PROCEDURE

2.1. Materials

A spray formed (SF) cold work tool steel – Weartec™ and powder metallurgical (PM) high-speed steel (HSS) Vanadis 6, produced by Uddeholm, were used as substrates for coating deposition (Table 1). According to the manufacturer, PM steels have smaller carbide size and more homogeneous structure than SF steels resulting in better chipping/cracking resistance.

Five different PVD coatings, among them monolayer TiN and multilayer gradient TiCN, nanocomposite nc-(AlTi)N/a-Si_3N_4 (nACo®), TiAlN and AlTiN, were studied. TiAlN and AlTiN coatings were deposited only on Weartec™ substrate to reduce the number of experiments. Cross-sections of coated specimens, observed on the scanning electron microscope (SEM) are presented in Fig. 1. Mechanical properties of the coatings (Table 2) were obtained by MTS Nano Indenter XP® in a depth mode with a target depth of 150 nm and average indentation force of 12 mN. The thicknesses of the coatings, measured by Kalotester kaloMax®, was about 2.3 µm. The results presented in Table 2 are in good correlation with those available in the literature. In [7] the TiN coating with a thickness of 2.1 µm on HSS had the nanohardness of 27 GPa and Young's modulus about 305 GPa. Fouvry et al. [8] investigated a TiCN coating with a thickness of 2.5 µm on HSS which had Young's modulus of 550 GPa. The substrate material and coating surface roughness were measured by a surface roughness measuring instrument of Taylor Hobson Ltd. Surtronic 3+ (using CR filter) with an accuracy of 2% (Tables 1 and 2).

Table 1. Chemical compositions, mechanical and surface properties of substrate materials

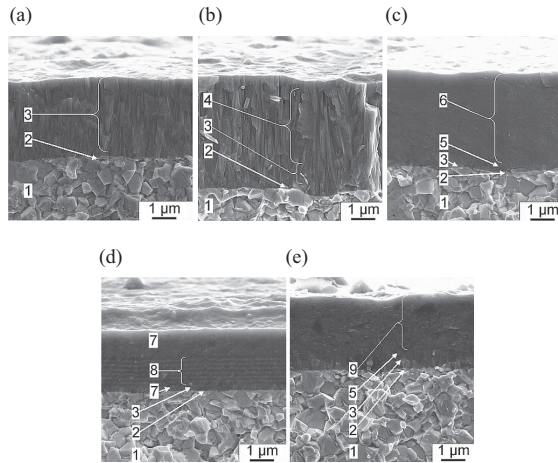| Substrate	Chemical composition, wt%						Hardness HRC/HV30	Young's modulus E, GPa	Surface roughness R_a, µm
	C	Si	Mn	Cr	Mo	V			
Weartec™	2.8	0.8	0.7	7.0	2.3	8.9	64/843	199	0.51 ± 0.10
Vanadis 6	2.1	1.0	0.4	6.8	1.5	5.4	64/843	210	0.51 ± 0.10

Fig. 1. SEM images of fractured surface of PVD coatings: (a) TiN; (b) TiCN; (c) nACo; (d) TiAlN; (e) AlTiN. 1 – substrate; 2 – Ti adhesion layer; 3 – TiN layer; 4 – TiCN gradient coating; 5 – TiAlN gradient layer + AlTiN gradient layer; 6 – nc-AlTiN/a-Si_3N_4 gradient coating; 7 – TiAlN layer; 8 – TiAlN/AlN multilayer coating; 9 – AlTiN gradient coating.

Table 2. Mechanical and surface properties of coatings

Coating/ Substrate	Type	Young's modulus E, GPa	Nano-hardness, GPa	E/H ratio	Surface roughness R_a, μm
TiN	Monolayer	438±80	28.5±0.6	15.4	0.08±0.01
TiCN	Multilayer	500±90	26.6±1.4	18.8	0.10±0.04
nACo®	Nanocomposite	323±13	29.0±1.5	11.1	0.10±0.04
TiAlN	Multilayer	301±90	19.9±1.2	15.2	0.10±0.04
AlTiN	Multilayer	336±13	23.8±1.0	14.1	0.05±0.01

2.2. Coating deposition procedure

Heat-treated samples (plates) of the size $20 \times 20 \times 5$ mm of two different substrate materials were grinded, diamond polished (powder grain size 1 μm) and degreased ultrasonically in the phosphate-alkali solution before deposition. Coatings were deposited using an arc ion plating PVD technique, on π-80 Platit equipment. The parameters of the deposition process varied from coating to coating and are presented in Table 3.

Table 3. Deposition parameters

Coat-ing	Bias voltage, V	Pressure, mbar	Ti–Al/AlSi cathode arc current, A	Temper-ature, °C	Ar	N_2 flow, sccm	C_2H_2
TiN	$-75…-120$	8×10^{-3}	$(100…125)/-$	450	6	200	–
TiCN	$-60…-120$	$(5…7) \times 10^{-3}$	$(120...130)/-$	450	6	165…180	7…39
nACo	$-75…-150$	$9 \times 10^{-3}…1.2 \times 10^{-2}$	$(82…125)/(65…100)$	435…475	6	200	–
TiAlN	$-60…-150$	$8 \times 10^{-3}…1.5 \times 10^{-2}$	$(85…125)/(65…115)$	475	6	200	–
AlTiN	$-60…-150$	$4 \times 10^{-3}…1.2 \times 10^{-2}$	$(60…125)/(52...130)$	430…450	6	150…200	–

2.3. Cyclic indentation test procedure

A servo hydraulic fatigue test system INSTRON 8800 and Vickers diamond pyramid indenter were used in the indentation experiments. The total indenting load of 500 N (mean compressive load of 275 N, alternating load of 225 N), stress ratio of 0.1 with a sinusoidal loading pattern and loading frequency of 0.5…15 Hz were applied. The optical microscope Axiovert 25 (ZEISS) with 500× magnification and Buehler Omnimet Image Analysis System 5.40, including the package for crack length measurement (Palmqvist method [9]), was used. The qualitative evaluation criteria of the cracking (0…VI) from crack formation, propagation to delamination (Table 4) were considered.

Table 4. Crack types and crack evaluation criteria

	0	I	II	III	IV	V	VI
Crack type							
Crack type description	Very weak secondary radial cracks	Weak secondary radial cracks	Medium secondary radial cracks and weak radial cracks	Medium secondary radial cracks and medium radial cracks	Medium secondary radial cracks and strong radial cracks	Medium radial cracks, delamina-tion of coating and cone (ring) cracks	Strong radial cracks and delamina-tion of the coating

2.4. Comparative adhesion testing

The adhesion test on the Zwick/ZHR 8150 Rockwell hardness tester at an indentation load of 1471 N (150 kgf) was performed to asses the quality of the coatings. The test procedure followed the VDI 3198 (1992) standard [10].

3. RESULTS AND DISCUSSION

3.1. Adhesion testing

The results of the indentation test are presented by micrographs in Fig. 2. The type and the volume of a failure zone indicate to film adhesion and its brittleness, which correspond to the microstructure and the mechanical properties of the coatings. Coatings of higher E/H ratio withstand the load without nucleation of long radial and conical cracks (TiN and TiCN). However, considerable amount of long radial cracks of 10…50 μm were generated, causing the exfoliation of coating layers that is a typical behaviour of TiN and TiCN coatings under loading [11]. The longest radial cracks are present in the TiN coating and with numerous enfolds and larger exfoliations of the coating layer (Fig. 2a). It is obvious that radial cracks predispose that kind of the coating failure. The same features are seen in the case of the TiAlN coating with only difference – the conical cracks are also present (Fig. 2c). It seems that short radial cracks accelerate chipping on the bordering area of the coating–indenter contact. Emerged chips tend to make connections with the closest of the sides forming the ring or conical crack. The structural defects, presented on the surface, such as pores and non-metallic inclusions, simplify this action. Finally, the most drastically fractured case is the nACo® coating (Fig. 2e) with numerous short radial and closed conical cracks. First, the very brittle structure collapses around the indenter and then starts to take up (absorb) fracture energy by the formation of radial cracks. Eventually those are blunted by the perpendicularly formed conical cracks and do not reach the last "ring".

Among all the tested coatings, the TiCN seems to be the most endurable. The mixed failure modes are characteristic of the studied coated system. Most widely
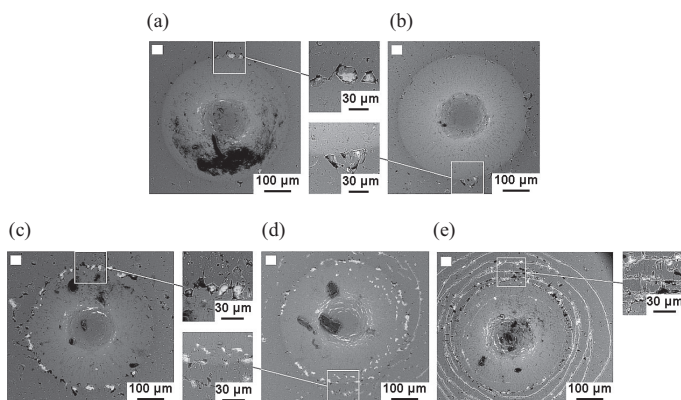

Fig. 2. SEM micrographs of the adhesion test of coatings: (a) TiN; (b) TiCN; (c) TiAlN; (d) AlTiN; (e) nACo®.

313

presented are cohesive (chipping, caused by the normal component of the stress tensor) and the delamination with buckling and fracture mode (decohesion of a coating with the formation of microcracks, caused by a combination of shear and normal stresses).

3.2. Coated system behaviour under cyclic loading

The results of cyclic indentation are given in Table 5 and in Fig. 3. The fracture analysis of the TiCN coating revealed that the "quasi-plastic" damage mode with the shortest radial cracks about 20 µm after 10 000 cycles prevailed when the Vickers diamond pyramid was used in the indentation test. In the contrast to the spherical indenters, a sharp indenter penetrates easily into the coating surface and cone cracking formation is suppressed by the radial cracks nucleation (Fig. 3). Radial cracks also become the dominant mode of the indentation fracture of the TiAlN and AlTiN coatings and lead to delamination and accelerated cracking resistance degradation (Fig. 4b). Within multilayer coatings with the "quasi-plastic" damage mode (TiCN, TiAlN, AlTiN) the cracking resistance increased with E/H ratio growth after 10 000 cycles (Fig. 5). Apart from other coatings, in nACo® with the lowest E/H ratio, "brittle" damage mode occurred with the formation of cone cracks, driven by tensile stresses in addition to "quasi-plastic" damage mode (Fig. 4c). On the other hand, the obscured sub-surface damage and the formation of radial cracks could be found below cone cracks. The multilayer coatings are preferable to the monolayer TiN coating with "quasi-plastic" damage mode, one of the lowest cracking resistance and the formation of strong radial cracks, despite the high E/H ratio of TiN (Figs. 4a, 5a).

Table 5. Crack types and crack evaluation criteria

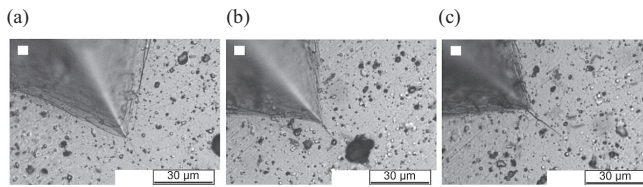|	Cycles					
	1	10	50	100	1000	10 000
TiN/Weartec™	I	I	I	I, II	II	IV
TiN/Vanadis 6	I	I	I	I	II	IV
TiCN/Weartec™	0, I	0, I	0, I	I	I	III
TiCN/Vanadis 6	0	0	0	0, I	0, I	II
nACo®/Weartec™	I	I, II Starting delamination	II Delamination	II Delamination	V Cone crack	V Cone crack
nACo®/Vanadis 6	0	I Starting delamination	V Cone crack	V Cone crack	V Cone crack	V Cone crack
TiAlN/Weartec™	0, I	I	I	I, II	II, III	VI
AlTiN/Weartec™	I	I	I	I	II	VI

Fig. 3. Impression corner of TiCN on Vanadis 6 substrate with the appearance of 0 criteria after 1 cycle (a); 0, I criteria after 1000 cycles (b); II criteria after 10 000 cycles (c).
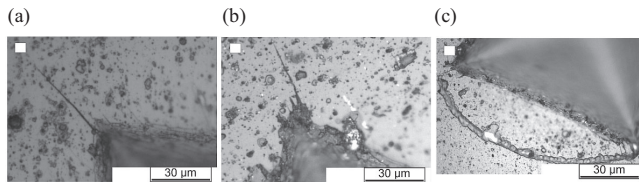

Fig. 4. Impression corner of coatings on Weartec™ after 10 000 cycles with the appearance of IV criteria, TiN (a); VI criteria, AlTiN (b); V criteria, nACo® (c).
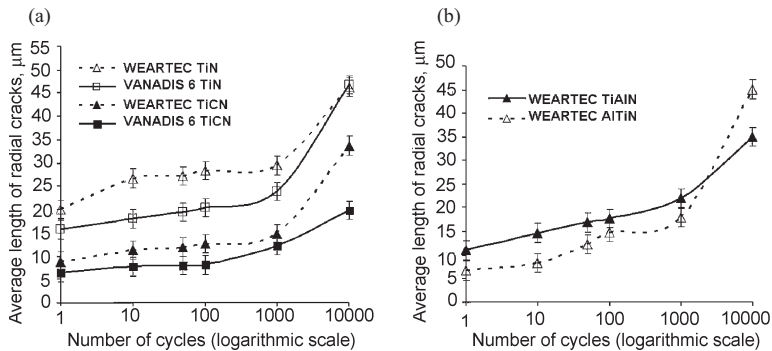

Fig. 5. An average length of radial cracks measured from the indent impression corners depending on the number of indentation cycles (standard deviation bars of 2 µm): (a) TiN and TiCN on Weartec™ and Vanadis 6; (b) TiAlN and AlTiN on Weartec™ substrate.

The observations of both substrates, coated with TiCN, exposed the advantages of PM steel Vanadis 6 over Weartec™. Vanadis 6 has higher Young's modulus, smaller carbide size and uniform carbides distribution that hampers the propagation of cracks, and crystallographic similarity with the coating, resulting in good adhesion (Fig. 5a). However, Vanadis 6 as a substrate for TiN and nACo® did not show benefits over Weartec™.

4. CONCLUSIONS

Indentation cyclic tests of coated tool steels were carried out and the following conclusions can be drawn.

1. The "quasi-plastic" damage mode with the formation of radial cracks prevailed in indentation cycling testing and is typical for high E/H values of coatings. The increase of the number of the indentation cycles leads to the radial crack growth. "Brittle" damage with the formation of cone cracks along with "quasi-plastic" damage mode is characteristic of the cyclically loaded PVD coatings with the lowest E/H ratio.
2. For multilayered coatings with the "quasi-plastic" damage mode (TiCN, TiAlN, AlTiN) the cracking resistance increases with the coating E/H ratio growth. TiCN on Vanadis 6 has the best cracking resistance (II criteria) after 10 000 cycles.
3. Multilayer coatings had higher fatigue resistance than monolayer coatings with higher E/H ratio.

ACKNOWLEDGEMENTS

REFERENCES

1. Richter, J. Application of Vickers indentation for assessment of PVD TiN coated new nonledeburitic high-speed steels. *Surf. Coat. Tech.*, 2003, **162**, 119–130.
2. Zoestbergen, E. and De Hosson, J. Th. M. Crack resistance of PVD coatings: Influence of surface treatment prior to deposition. *Surf. Eng.*, 2002, **18**, 283–288.
3. Tarrés, E., Ramirez, G., Gaillard, Y., Jiménez-Piqué, E. and Llanes, L. Contact fatigue behavior of PVD-coated hardmetals. *Int. J. Refract. Met. Hard Mater.*, 2009, **27**, 323–331.
4. Cook, R. F. and Pharr, G. M. Direct observation and analysis of indentation cracking in glasses and ceramics. *J. Am. Ceram. Soc.*, 1990, **73**, 787–817.
5. Kim, D. K., Jung, Y.-G., Peterson, I. M. and Lawn, B. R. Cyclic contact fatigue of intrinsically brittle ceramics in contact with spheres. *Acta Mater.*, 1999, **47**, 4711–4725.
6. Chiang, S. S., Marshall, D. B. and Evans, A. G. The response of solids to elastic/plastic indentation. II. Fracture initiation. *J. Appl. Phys.*, 1982, **53**, 312–317.
7. Holmberg, K., Ronkainen, H., Laukkanen, A., Wallin, K., Hogmark, S., Jacobson, S., Wiklund, U., Souza, R. M. and Ståhle, P. Residual stresses in TiN, DLC and MoS_2 coated surfaces with regard to their tribological fracture behaviour. In *Proc. 13th Nordic Symposium on Tribology NORDTRIB 2008*. Tampere, Finland, 2008, 37 p.
8. Fouvry, S., Liskiewicz, T. and Paulin, C. A global–local wear approach to quantify the contact endurance under reciprocating-fretting sliding conditions. *Wear*, 2007, **263**, 518–531.
9. Palmqvist, S. The work for the formation of a crack during Vickers indentation as a measure of the toughness of hard metals. *Arch. Eisenhüttenwes.*, 1962, **33**, 629–634.

10. VDI 3198:1992-08, *Coating (CVD, PVD) of Cold Forging Tools*. VDI-Verlag, Düsseldorf, 1991.
11. Bouzakis, K.-D., Siganos, A., Leyendecker, T. and Erkens, G. Thin hard coatings fracture propagation during the impact test. *Thin Solid Films*, 2004, **460**, 181–189.

Tööriistateraste õhukeste kõvapinnete vastupanu hindamine pragunemisele indenteerimismeetodi abil

Alina Sivitski, Andre Gregor, Mart Saarna, Priit Kulu ja Fjodor Sergejev

On hinnatud viie kõvapinde – TiN-i, TiCN-i, TiAlN-i, AlTiN-i ja nanokompo-siidi nc-AlTiN/a-Si$_3$N$_4$ (nACo®), mis on kantud pulbertööriistaterastele Weartec^{TM} ning Vanadis 6 – vastupanu pragunemisele ja väsimusele Vickersi tsüklilise indenteerimise abil. Analüütiline osa sisaldab prao arenemise hinnangut sõltuvalt kasvavate indenteerimistsüklite arvust. Lisaks on tehtud adhesiooni võrdlustest, kasutades Rockwell C tehnikat. On leitud, et pinnatud süsteemi tsük-lilisel indenteerimisel tekkivate pragude tüübid on sõltuvuses suhte Youngi moodul/kõvadus (E/H) väärtusest. Tööst saadud andmed võimaldavad võrrelda vaadeldud pinnatud süsteemi vastupanu pragunemisele ja on aluseks pinnete valikul külmvormimise (maht- ning lehtvormimise) tööriistadele.

PAPER III

Sivitski, A.; Gregor, A.; Saarna, M.; Kulu, P.; Sergejev, F. Properties and performance of hard coatings on tool steels under cyclic indentation. *Acta Mechanica Slovaca*, 2009, 13, 4, p. 84 – 94.

Properties and Performance of Hard Coatings on Tool Steels under Cyclic Indentation

ALINA SIVITSKI (EE) alina.sivitski@ttu.ee
ANDRE GREGOR (EE) andre.gregor@ttu.ee
MART SAARNA (EE) saarna@staff.ttu.ee
PRIIT KULU (EE) priit.kulu@ttu.ee
FJODOR SERGEJEV (EE) fjodor.sergejev@ttu.ee

ABSTRACT

In this paper cracking resistance and fatigue properties of five hard coatings - TiN, TiCN, TiAlN, AlTiN and nanocomposite nACo® (nc – AlTiN/a – Si_3N_4) on tool steels - Weartec™ and Vanadis 6 are evaluated by means of the cyclic Vickers indentation method. The analytical part covers an evaluation of damage evolution of the coated system versus the number of cycles. The effect of mechanical response - Young's module/Hardness ratio (E/H ratio) on the crack propagation is described in the form of a diagram with various curves, each one associated with a certain number of indentation cycles. The comparative adhesion testing was conducted with the use of the Rockwell C technique. It was found that the type of cracks formed in the coated systems under cyclic loading is dependant on the E/H ratio values. The data obtained enable the cracking and fatigue resistance of the coated system to be compared and an optimal coating for metal forming tools applications to be selected.

KEYWORDS

PVD, hard coating, multilayers, indentation method, cracking, delamination.

INTRODUCTION

Knowledge of functional properties of hard coatings has gained increasing importance as the application of PVD coatings for sheet metal cold forming and cutting tools has grown recently. Fatigue and cracking resistance are the most important properties in such long-term applications where the alternating loads are applied. Investigations of coating crack development intensity and fatigue are commonly carried out using an indentation method for its ability of measuring mechanical properties in a microscopic range [11, 14, 8].

There is a lack of generality in indentation-cracking behaviour for coated systems in publications. Most of available published works [11, 16] on the cracking resistance of hard coatings explain the morphology of a film crack under static indentation, although cyclic indentation gives more precise estimates for long-term damage mechanisms. The papers on cyclic indentation of hard films investigate contact fatigue with the use of spherical [14] or conical indenters. However, Vickers pyramid indentation has an advantage over spherical and conical ones. A far more accurate measurement of the length of radial crack propagating from square indentation imprint corners can be obtained as compared to the circle impression. As hard coatings are brittle films, there is some interest in publications which focus on indentation cracking [4, 8] and fatigue [8, 12, 6] of brittle materials.

The main elements of damage evolution and fatigue response in coated brittle systems are mechanical properties, microstructure and deposition technique. Previous research

[4, 2, 3] shows that cracking resistance and cracks types of ceramics are strongly dependant on the values of Young's module/Hardness ratio (E/H ratio). Another aspect that has an effect on coated system cracking and fatigue is the substrate material and its microstructure. Different crystal structures of the substrate and the coating can cause poor adhesion between them. Additionally, cyclic indentation tests on ceramics reveal that fine and homogeneous material structures are preferable as they are characterized by slow crack growth [8].

In single loading experiments, it is required to determine deformation models of a coated system. Three types of deformation models were observed during the single indentation cycle in previous research [11]: 1 - elastic deformation of the coating and plastic deformation of the substrate without cracking (plastic zone model), 2 - cracking of the layer directly beneath the indenter (contact region model) and 3 - cracking of the layer beneath the indenter and the uplift of the substrate near the indenter causing elastic bending of the coating (uplift model). However, under cyclic indentation, elastic brittle hard coatings do not show plastic deformation up to tensile fracture (normal stress) and may not suffer fatigue damage and the fracture criterion obeys static strength. Thus, the propagation of the crack of the coated system may be attributed to the ratcheting deformation of the substrate under cyclic indentation.

In order to determine the damage mode of a coated system, crack types are determined. Five major crack types are observed in brittle materials during single indentation tests [4, 8]: cone, radial, median, half-penny, and lateral (circumferential) cracks. Previous observations [8, 9, 13] of mechanical sectioning of brittle materials indentation tests revealed that the cracks emanating from the corners of indent impressions are mostly radials cracks (Palmqvist cracks). After the crack type determination, the contact damage models in cyclic loading for brittle materials are described [8]. The tensile-driven cone cracking ("brittle" mode) and shear-driven microdamage accumulation ("quasi-plastic" mode) were determined [8].

This paper investigates cracking resistance of hard ceramics coatings subjected to cyclic Vickers indentation. Crack types and the intensity of the dependence of crack development on the coat-ing type, deposition parameters and substrate material by analogy with Richter [8] are determined. To compare the results from different testing procedures adhesion testing is performed using Rockwell C apparatus.

EXPERIMENTAL PROCEDURE
MATERIALS

A chromium-molybdenum-vanadium alloyed spray formed (SF) cold work tool steel - Weartec^{TM} and powder metallurgical (PM) high-speed steel (HSS) - Vanadis 6 produced by Uddeholm are used as substrates for coating deposition. Chemical compositions and hardness of tool steels are listed in Table 1.

According to the manufacturer, high carbide content, size and distribution of carbides of the studied tool steels gives them an excellent friction wear (Weartec^{TM}) and chipping/cracking resistance (Vanadis 6). Powder steels, such as Vanadis 6 (Fig. 1 (b)), have smaller carbide size than spray formed steels. Smaller grain size and carbides give a more uniform structure resulting in more homogenous PM steel and better fracture and fatigue properties.

Five different PVD coatings, among them monolayer TiN and multilayer gradient TiCN, nanocomposite coating nACo® ($nc - AlTiN/a - Si_3N_4$), TiAlN and AlTiN were studied in this work. TiAlN and AlTiN coatings were deposited only on Weartec^{TM} substrate in order to reduce the number of experiments. Mechanical properties of the coatings (Table 2) were obtained by MTS Nano Indenter XP®. The nanoindentation was performed in a depth mode, a target depth of 150 nm and average indentation force of 12 mN were applied. The thickness of the coatings measured by Kalotester kaloMax® was about 2.3 μm.

The results presented in Table 2 are in good correlation with those available in the literature. In [7] the TiN coating with a thickness of 2.1 μm on HSS Bhler S790 ISOMATRIX had the nanohardness of 27 GPa and Young's modulus about 305 GPa. Fouvry et al. [5] investigated a TiCN coating with a thickness of 2.5 μm on HSS Vanadis 23 (Young's modulus of 230 GPa), which had Young's modulus of 550 GPa.

Table 1: *Chemical compositions, mechanical and surface properties of substrate materials.*

Substrate	Chemical composition, wt%						Hardness HRC / HV30	Young's modulus E (GPa)	Surface roughness Ra (μm)
	C	Si	Mn	Cr	Mo	V			
Weartec^{TM}	2.8	0.8	0.7	7.0	2.3	8.9	64 / 843	199	0.51±0.10
Vanadis 6	2.1	1.0	0.4	6.8	1.5	5.4	64 / 843	210	0.51±0.10
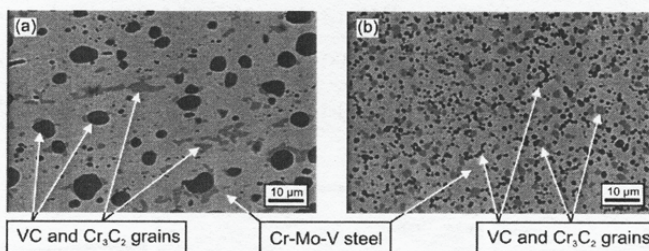
Fig. 1: *SEM micrographs of steels microstructures: (a) Weartec^{TM} (SF) and (b) Vanadis 6 (PM).*

Cross-sections of PVD coated specimens observed on the scanning electron microscope (SEM) are presented in Fig. 2.

The substrate materials and coating surface roughness were measured by a surface roughness measuring instrument of Taylor Hobson Ltd. Surtronic 3+ (using CR filter) with an accuracy of 2% (Tables1 and 2). For the substrate material, the surface roughness (R_a) was equal to 0.51 μm on the evaluation length of 4.0 mm.

COATING DEPOSITION PROCEDURE

Samples (plates) with sizes of 20x20x5 mm of two different substrate materials (Weartec^{TM} and Vanadis 6) were prepared for the deposition of PVD hard coatings and heat treated to a fixed hardness value (Table 1).

After grinding and diamond polishing (powder grain size 1 μm) all samples were degreased ultrasonically in the phosphate-alkali solution, rinsed in ethanol and dried in air. Coatings were deposited using an arc ion plating PVD technique, on π-80 Platit equipment. The parameters of the deposition process varied from coating to coating and are presented in Table 3 with reference to the coating.

CYCLIC INDENTATION TEST PROCEDURE

A servo hydraulic fatigue test system INSTRON 8800 and Vickers diamond pyramid indenter were used in the indentation experiments. The number of cycles varied from 1 up to 10 000 and a total indenting load of 500 N was applied. The application of a high indenting force is based on the results of previous studies. The application of a high indenting force is based on the results of previous study [11]. Indentation testing was carried out in the load control mode with a mean compressive load level of 275 N, alternating load of 225 N and stress ratio R = 0.1 using a sinusoidal loading pattern. The loading frequency varied from 0.5 up to 15 Hz within 1 to 1000 and 10 000 cycles, respectively.

The Palmqvist method [10] was applied for coated samples to evaluate radial cracks, based on the length measurements of the cracks emanating from the indentation impression corners. The optical microscope Axiovert 25 (ZEISS) with 500x magnification along with Buehler Omnimet Image Analysis System 5.40 with the package for image

Table 2: *Mechanical and surface properties of coatings.*

Coating/ Substrate	Type	Young's modulus E (GPa)	Nanohardness (GPa)	E/H ratio	Surface roughness R_a (μm)
TiN	Monolayer	438±80	28.5±0.6	15.4	0.08±0.01
TiCN	Multilayer	500±90	26.6±1.4	18.8	0.10±0.04
nACo®	Nanocomposite	323±13	29.0±1.5	11.1	0.10±0.04
TiAlN	Multilayer	301±90	19.9±1.2	15.2	0.10±0.04
AlTiN	Multilayer	336±13	23.8±1.0	14.1	0.05±0.01

Fig. 2: *SEM images of fractured surface of hard PVD coatings: (a) TiN; (b) TiCN; (c) nACo;(d) TiAlN; (e) AlTiN. 1- substrate; 2 - Ti adhesion layer; 3 - TiN layer; 4 - TiCN gradient coating; 5 - TiAlN gradient layer + AlTiN gradient layer; 6 - nc – AlTiN/a – Si$_3$N$_4$ gradient coating; 7 - TiAlN layer; 8 - TiAlN/AlN multilayer coating; 9 - AlTiN gradient coating.*

Table 3: *Deposition parameters.*

Coating	Bias voltage (V)	Pressure (mbar)	Ti - Al / AlSi cathode arc current (A)	Temp. (°C)	Ar flow (sccm)	N₂ flow (sccm)	C₂H₂ flow (sccm)
TiN	-75 ... -120	8×10^{-3}	100 ... 125/-	450	6	200	–
TiCN	-60 ... -120	$(5...7) \times 10^{-3}$	120 ... 130/-	450	6	165 ... 180	7...39
nACo	-75 ... -150	$9 \times 10^{-3} ... 1.2 \times 10^{-2}$	82 ... 125/ 65 ... 100	435 ... 475 475	6	200	–
TiAlN	-60 ... -150	$8 \times 10^{-3} ... 1.5 \times 10^{-2}$	85 ... 125/ 65 ... 115	430 ... 450	6	200	–
AlTiN	-90 ... -150	$4 \times 10^{-3} ... 1.2 \times 10^{-2}$	60 ... 125/ 52 ... 130		6	150 ... 200	–

capture and basic measurement functions were used to observe and evaluate the type and length of cracks. The evaluation of cyclic indentation experiments results of different coated systems was based on the following: the qualitative evaluation criteria of the cracking (0 ... VI) from crack formation, propagation to delamination of the coating was considered (Table 4).

COMPARATIVE ADHESION TESTING

The adhesion test on the Zwick/ZHR 8150 Rockwell hardness tester at an indentation load of 1471 N (150 kgf) was performed to assess the quality of the coatings. The test procedure followed the VDI 3198 (1992) standard [15].

RESULTS AND DISCUSSION
ADHESION TESTING

The results of the indentation test are presented by micrographs in Fig. 3. The micrographs of higher magnification are placed aside the main figures to indicate and specify coating cracking. The type and the volume of a failure zone indicate to film adhesion and its brittleness which correspond to the microstructure and the mechanical properties of the coatings. Coatings of higher hardness and lower

Young's modulus (higher E/H ratio) withstand the load without nucleation of long radial and conical cracks (TiN and TiCN). However, considerable amount of long radial cracks of 10 ... 50 μm were generated, causing the exfoliation of coating layers that is a typical behaviour of TiN and TiCN coatings under loading [1]. The longest radial cracks are indicated in the TiN coating and numerous enfolds and larger in size exfoliations of the coating layer are observed (Fig. 3 (a)). It is obvious that radial cracks predispose that kind of coating failure. The same features are seen in the case of TiAlN coating with only difference - the conical cracks are also present (Fig. 3 (c)). It seems that short radial cracks accelerate chipping on the bordering area of coating-indenter contact. Emerged chips tend to make connections with the closest on the sides forming the ring or conical crack. The structural defects presented on the surface, such as pores and non-metallic inclusions, simplify this action.

Finally, the most drastically fractured case - nACo® coating (Fig. 3 (e)). The worst performance of this coating was indicated by the numerous short radial and closed conical cracks. First, the very brittle structure collapses around the indenter and then starts to take up (absorb) fracture energy by the formation of radial cracks. Eventually those are blunted by the perpendicularly formed conical

Table 4: *Crack types and crack evaluation criteria.*

Criteria	0	I	II	III	IV	V	VI
Crack type							
Crack type description	Very weak secondary radial cracks, which emanate from the edge and around the corners of the imprint.	Weak secondary radial cracks.	Medium secondary radial cracks and weak radial cracks - beginning of radial cracks formation.	Medium secondary radial cracks and medium radial cracks-propagation of weak radial cracks.	Medium secondary radial cracks and strong radial cracks.	Medium radial cracks, delamination of coating in the corners of the contact impression and cone (ring) cracks at the periphery of the imprint.	Strong radial cracks and delamination of the coating around the corners of the indent impression.

cracks and are not reaching the last "ring".

Among all the tested coatings, the TiCN seems to be most endurable. The mixed failure modes are characteristic of the studied coated system. Most widely presented are cohesive (chipping caused by the normal component of a stress tensor) and the delamination with buckling and fracture mode (decohesion of a coating with the formation of microcracks, caused by a combination of shear and normal stresses).
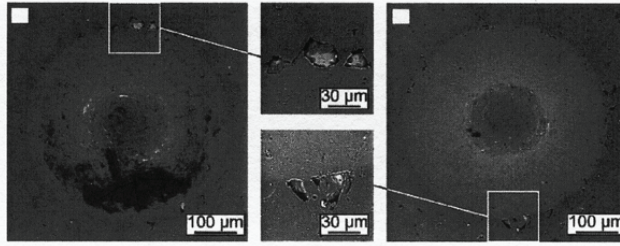
COATED SYSTEM BEHAVIOUR UNDER CYCLIC LOADING

The results of cyclic indentation are given in Table 5. After the first indentation cycle, mostly contact region model of coating deformation was presented due to the high indenting load of 500 N applied. With TiCN, no cracks at all or weak secondary ra-

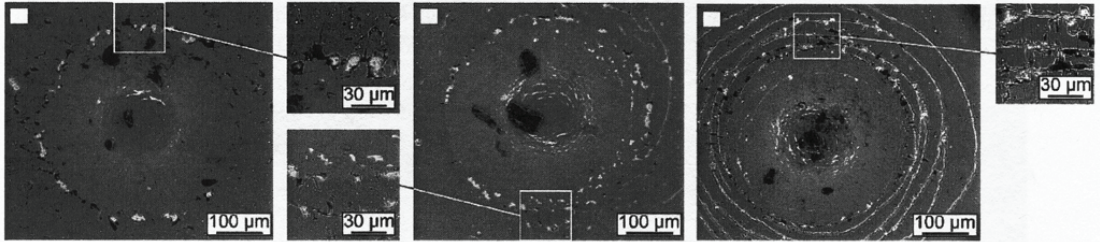dial cracks were observed in the corners of the impression (Fig. 6 (a)).

To estimate the cracking resistance of the coated system, a quantitative analysis of the samples was performed. The lengths of radial cracks from the impression corner were measured and presented on graphs (Fig. 4, 5) versus the number of indentation cycles. The error bars show the standard deviation of 2.3 μm.

Similarly to the single loading of the adhesion test, TiCN coating on both substrates had the best cracking resistance at all cycle values (Fig. 4). TiCN on Vanadis 6 showed radial cracks with a length of 20 μm and crack evaluation criteria II (Fig. 4 (a), Fig. 6 (a)). On the contrary, nACo® on both substrates had the lowest cracking resistance (Fig. 7 (c)). The cracking of this coating differed from others with the formation of cone cracks around the

Fig. 3: *SEM micrographs of the adhesion test of coatings: (a) TiN; (b) TiCN; (c) TiAlN; (d) AlTiN and (e) nACo®.*
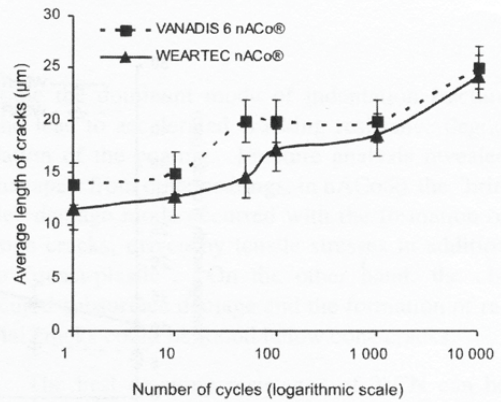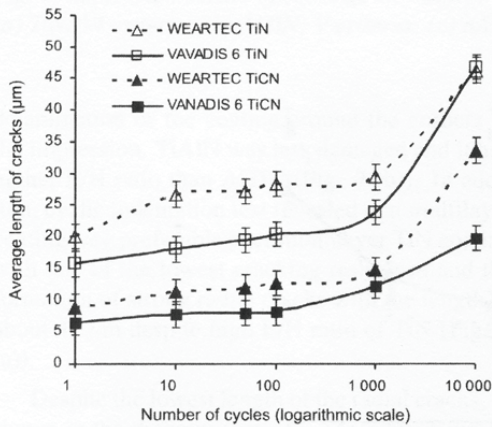

Fig. 4: *An average length of radial cracks measured from the indent impression corners depending on the number of indentation cycles, substrate material and coating combinations: (a) TiN and TiCN; (b) nACo on Weartec*^{TM} *and Vanadis 6 substrates.*

impression, in addition to radial cracks and delamination of the coating at indent impression corners validating the results of the adhesion test (Fig. 3 (e)).

The facts above allowed a hypothesis to be made that the crack type and cracking resistance of a cyclic loaded coated system is dependant on the coating E/H ratio. Radial cracking without delamination was observed in coatings with the highest E/H ratio (TiCN and TiN) and the lowest values

Table 5: *Observed crack types analysis.*

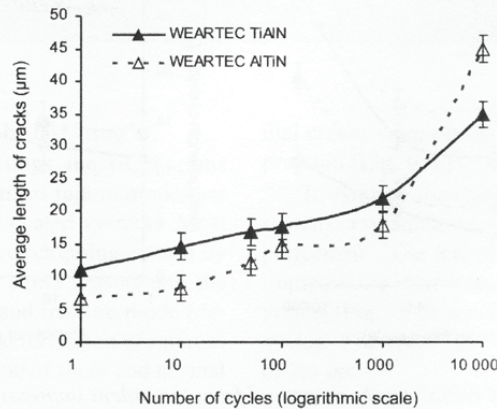| Coating / Substrate	Observed crack types analysis 1	10	50	100	1000	10000
TiN / Weartec™	I	I	I	I, II	II	IV
TiN / Vanadis 6	I	I	I	I	II	IV
TiCN / Weartec™	0, I	0, I	0, I	I	I	III
TiCN / Vanadis 6	0	0	0	0, I	0, I	II
nACo® / Weartec™	I	I, II Starting delamination	II Starting delamination	II Starting delamination	V Cone crack	V Cone crack
nACo® / Vanadis 6	O	I Starting delamination	V Cone crack	V Cone crack	V Cone crack	V Cone crack
TiAlN / Weartec™	0, I	I	I	I, II	II, III	VI
AlTiN / Weartec™	I	I	I	I	II	VI

Fig. 5: *An average length of radial cracks measured from the indent impression corner depending on the number of indentation cycles of TiAlN and AlTiN on Weartec™ substrate.*

of E/H (nACo®) showed cone cracking and delamination. The dependence between radial cracking sequence and E/H ratio values was described in the form of a diagram (Fig. 8). Each curve on the diagram is associated with a certain number of indentation cycles. According to the diagram curves, TiAlN has medium and AlTiN strong radial cracks after 10 000 cycles. Both coatings showed
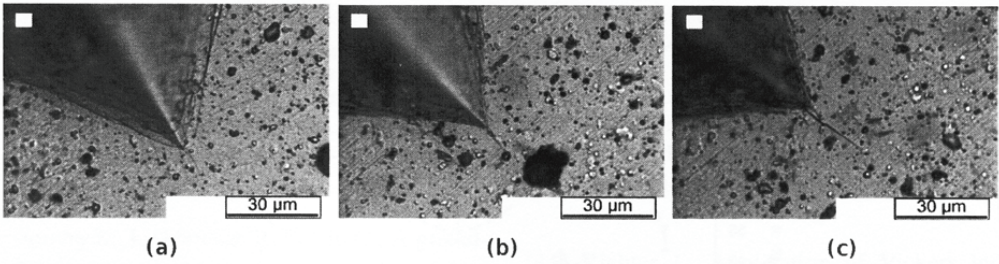
Fig. 6: *Impression corner of TiCN on Vanadis 6 substrate with the appearance of 0 criteria after: (a) 1 cycle. I criteria after: (b) 1000 cycles. II criteria after: (c) 10 000 cycles.*
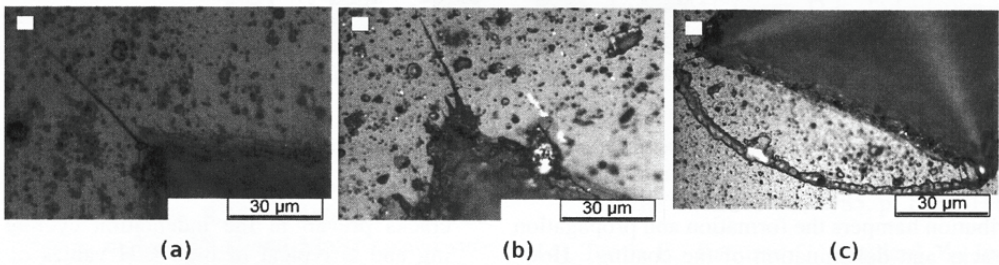

Fig. 7: *Impression corner of coatings on Weartec™ after 10 000 cycles with the appearance of IV criteria: (a) TiN; VI criteria: (b) AlTiN; V criteria: (c) nACo®.*

delamination of the coating around the corners of the impression. TiAlN was less damaged and it had higher E/H ratio than AlTiN (Fig. 7 (b)). In addition, cyclic indentation test revealed that multilayer coatings are preferable over monolayer TiN coating with one of the lowest cracking resistance and the formation of strong radial cracks with the length of about 47 μm despite high E/H ratio of TiN (Fig. 7 (a)).

Despite the lowest length of the radial cracks, as shown in the diagram (Fig. 8), nACo®coating on Weartec™ had the worst performance. The appearance of the shortest radial cracks can be explained by the formation of additional cone cracks after 1 000 and 10 000 indentation cycles what hamper the propagation of the radial cracks.

The "quasi-plastic" damage mode prevailed as the Vickers diamond pyramid was used in the indentation test. In contrast to spherical indenters, a sharp indenter penetrates easily into the coating surface and cone cracking formation is suppressed by the radial cracks nucleation. Radial cracks be-

come the dominant mode of indentation fracture and lead to accelerated cracking resistance degradation of the coating. Fracture analysis revealed that apart from other coatings, in nACo® the "brittle" damage mode occurred with the formation of cone cracks, driven by tensile stresses in addition to "quasi-plastic". On the other hand, the obscured subsurface damage and the formation of radial cracks could be found below cone cracks.

The best cracking resistance of TiCN can be also explained by good adhesion due to the presence of the carbides in both substrates. Crystallographic similarity of the substrate and the coating seem to have an effect, ensuring strong bonding between them. The observations of both substrates coated with TiCN expose the advantages of PM steel Vanadis 6 over Weartec™, as it has higher Young's module. It is assumed that Vanadis 6 works like a spring under the coating, allowing it to bend and deform (fracture) according to the contact region wear model described above. In addition, Vanadis 6 smaller carbide size and uniform carbides
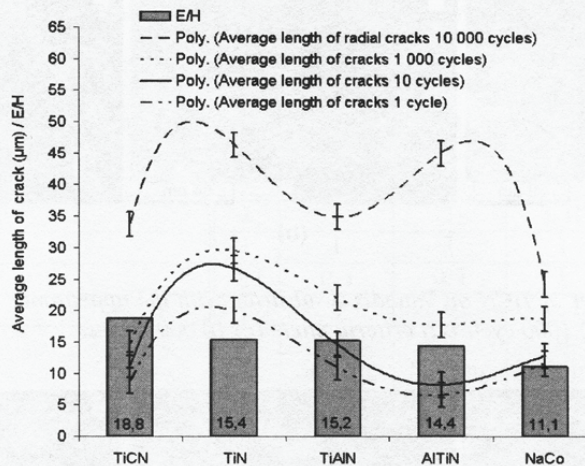
Fig. 8: *The effect of the E/H ratio on the radial crack propagation (coatings on Weartec*^{TM}*).*

distribution hampers the formation and propagation of cracks and delamination of the coating. However, Vanadis 6 as a substrate for TiN and nACo® did not show benefits over Weartec^{TM}.

CONCLUSIONS

Indentation cyclic tests of coated tool steels were carried out and the following conclusions can be drawn:

1. The increase of the number of the indentation cycles leads to the radial crack growth. It is obvious that cracking resistance and crack type is dependant on the Young's module/Hardness ratio values (E/H ratio) of the coating. Specifically, TiCN coating proved to have the best indentation cracking resistance for both substrate materials, as it had the highest E/H ratio value. Additionally, TiCN on Vanadis 6 showed less damage after 10 000 indentation cycles with (II) evaluation criteria of cracking resistance. Vanadis 6 steel has higher Young's module value and the finest microstructure also. Thus, the same conclusion can be drawn for substrate materials - their indentation cracking resistance is also dependent on the E/H ratio as well as its microstructure, carbides size and distribution.

2. Experiments revealed that the "quasi-plastic" damage mode, with the formation of radial

cracks prevail in the indentation cycling testing and is typical of high E/H values of coatings. "Brittle" damage with the formation of cone cracks is characteristic of the cyclic loaded coatings with the lowest E/H ratio values.

3. Multilayer coatings had higher fatigue resistance than monolayer coating despite higher E/H ratio.

ACKNOWLEDGEMENT

REFERENCES

[1] Bouzakis K.-D., Siganos A., Leyendecker T., Erkens G., Thin hard coatings fracture propagation during the impact test, Thin Solid Films, vol. 460, 2004, p. 181–189.

[2] Chiang S.S., Marshall D.B., Evans A.G., The response of solids to elastic/plastic indentation, I. Stresses and residual stresses, J. Appl. Phys., vol. 53, 1982, p. 298–311.

[3] Chiang S.S., Marshall D.B., Evans A.G., The response of solids to elastic/plastic indenta-

tion, II. Fracture initiation, J. Appl. Phys., vol. 53, 1982, p. 312–317.

[4] Cook R.F., Pharr G.M., Direct observation and analysis of indentation cracking in glasses and ceramics, J. Am. Ceram. Soc., vol. 73, 1990, p. 787–817.

[5] Fouvry S., Liskiewicz T., Paulin C., A global-local wear approach to quantify the contact endurance under reciprocating-fretting sliding conditions, Wear, vol. 263, 2007, p. 518–531.

[6] Guiberteau F., Padture N.P., Cai H., Lawn B.R., Simple cyclic Hertzian test for measuring damage accumulation in polycrystalline ceramics, Philos. Mag. A, vol. 68, 1993, p. 1003–1016.

[7] Holmberg K., Ronkainen H., Laukkanen A., Wallin K., Hogmark S., Jacobson S., Wiklund U., Souza R.M., Ståhle P., Residual stresses in TiN, DLC and MoS2 coated surfaces with regard to their tribological fracture behaviour, 13th Nordic Symposium on Tribology NORDTRIB 2008, Tampere, Finland, 2008, 37 p.

[8] Kim D.K., Jung Y.-G., Peterson I.M., Lawn B.R., Cyclic contact fatigue of intrinsically brittle ceramics in contact with spheres, Acta Mater., vol. 47, 1999, p. 4711–4725.

[9] Lankford J., Davidson D.L., The crack initiation threshold in ceramic materials subject to

elastic/plastic indentation, J. Mater. Sci., vol. 14, 1979, p. 1662–1668.

[10] Palmqvist S., The work for the formation of a crack during Vickers indentation as a measure of the toughness of hard metals (in Ger.), Arch. Eisenhuttenwes., vol. 33, 1962, p. 629–34.

[11] Richter J., Application of Vickers indentation for assessment of PVD TiN coated new nonledeburitic high-speed steels, Surf. Coat. Tech., vol. 162, 2003, p. 119–130.

[12] Sglavo V.M., Green D.J., Indentation determination of fatigue limits in silicate glasses, J.Am. Ceram. Soc., vol. 82, 1999, p. 1269–74.

[13] Shetty D.K., Wright I.G., Mincer P.N., Clauer A.H., Indentation fracture of WC-Co cermets = Rupture par indentation de cermets WC-Co, J. Mater. Sci., vol. 20, 1985, p. 1873–1882.

[14] Tarrés E., Ramirez G., Gaillard Y., Jimnez-Piqu E., Llanes L., Contact fatigue behavior of PVD-coated hardmetals, Int. J. Refract. Met. H. Mater., vol. 27, 2009, p. 323–331.

[15] VDI 3198:1992-08, Coating (CVD, PVD) of cold forging tools, VDI-Verlag, Dusseldorf, 1991.

[16] Zoestbergen E., De Hosson J.Th.M., Crack resistance of PVD coatings: Influence of surface treatment prior to deposition, Surf. Eng., vol. 18, 2002, p. 283–288.
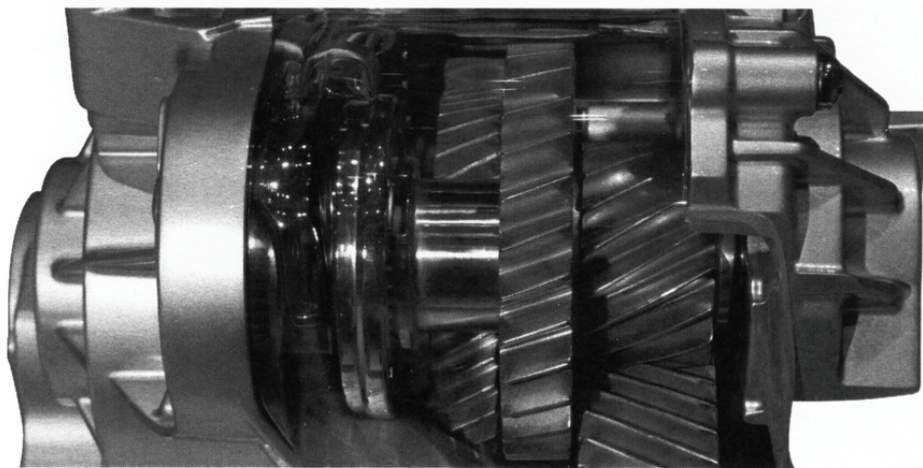
PAPER IV

Podgursky, V.; Nisumaa, R.; Adoberg, E.; Surzhenkov, A.; <u>Sivitski, A.</u>; Kulu, P. Comparative study of surface roughness and tribological behavior during running-in period of hard coatings deposited by lateral rotating cathode arc. *Wear*, 2010, 268, 5 – 6, p. 751 – 755.

Comparative study of surface roughness and tribological behavior during running-in period of hard coatings deposited by lateral rotating cathode arc

V. Podgursky [a,*], R. Nisumaa [b], E. Adoberg [a], A. Surzhenkov [a], A. Sivitski [a], P. Kulu [a]

[a] Tallinn University of Technology, Department of Materials Engineering, Ehitajate tee 5, 19086 Tallinn, Estonia
[b] Tallinn University of Technology, Centre of Materials Research, Ehitajate tee 5, 19086 Tallinn, Estonia

ARTICLE INFO

ABSTRACT

This study focuses on the influence of surface geometry of hard coatings on tribological behavior. TiN, TiAlN, AlTiN and nanocomposite (nc-Ti$_{1-x}$Al$_x$N)/(a-Si$_3$N$_4$) (nACo) coatings were deposited by means of the lateral rotating cathode arc method on high speed steel (HSS) substrates. Surface topology (area of 50 μm × 50 μm, 10 μm × 10 μm and 5 μm × 5 μm) investigations by the atomic force microscopy (AFM) revealed that for all types of coatings the non-Gaussian height distribution function (HDF) is mainly due to the macroparticles. Factors and mechanisms affecting the value of the coefficient of friction (COF) during the running-in period were discussed.

© 2009 Elsevier B.V. All rights reserved.

1. Introduction

During the last decade there has been increased interest in TiAlN, AlTiN and nACo coatings because of their success in a variety of applications [1]. nACo is formed through spontaneous self-organization [2], the resulting structure is nanocrystalline AlTiN embedded into an amorphous Si$_3$N$_4$-matrix. High hardness of (Ti,Al)N coatings ensures good resistance to abrasive wear and high chemical stability results in high resistance to solution wear.

The tribological behavior of coatings depends on a number of coating properties, including hardness, roughness, adhesion, etc. [1,3]. Previous studies [4,5] have shown that the relatively high friction during dry machining of (Ti,Al)N coatings is caused by the macroparticles on the coating surface, e.g. COF of μ-AlTiN is 0.3 in contrast to 0.7 for AlTiN [5]. The only difference between μ-AlTiN and AlTiN is that μ-AlTiN is smoother than AlTiN because of the arc process optimisation and surface post-treatment [5].

Coating surface is a fundamental aspect in the study of initial transients. Eight types of friction running-in curves were described by Blau [6,7]. It was pointed out that surface roughness and wear are crucial to the understanding of an initial frictional behavior. The first order classification of wear includes adhesive and abrasive wear, wear caused by surface fatigue, and wear due to tribochemical reactions [8]. The running-in behavior was observed in the case of self-lubricating coatings like MoS$_2$ [9] and diamond-like carbon

DLC [10] as well. Lackner et al. [11] explained the initially low COF of TiN by the roughness and chemical reactivity between the counterbodies and the increase in COF during the running-in period by abrasive wear. The influence of the defect-free coating surface on the tribological behavior could be rationalized only in the absence of macroparticles. On the other hand, it is rather difficult to separate contributions to the total roughness due to the macroparticles and the defect-free coating surface. The number of macroparticles can be reduced by polishing, however, in that case the defect-free coating surface also undergoes a structural modification. To summarize, the initial running-in period is caused by initial inconformity between the conterbodies, followed by the steady state, as conformity and smoothing occur.

Statistical analysis of the geometrical characteristics of the coating surface is the primary objective of the present preliminary study. A thorough investigation of the solid surface topology assumes surface homogeneity, randomness and isotropy to be evaluated [3]. The present study was restricted to the identification of the HDF form (either Gaussian or non-Gaussian) and the estimation of roughness parameters S_a and R_a. In addition, the influence of surface geometry on the tribological behavior was under investigation. Refs. [1,12–15] show a lack of statistical analysis concerning surface geometry and its role in relation to the friction. Finally, a comparison of the surface geometry of nACo and conventional Al-based coatings like TiAlN and AlTiN will be presented.

2. Experimental method

Coatings were deposited in the arc plating PVD-unit PLATIT-π80 using the lateral rotating ARC-cathodes (LARC) technology.

* Corresponding author. Tel.: +372 620 3358; fax: +372 620 3196.
E-mail address: vitali.podgurski@ttu.ee (V. Podgursky).

TiAlN and AlTiN correspond to 50 and 75 at.% of Al content in the $(Ti_{1-x}Al_x)N$ coating, respectively. Deposition temperature was 450 °C. Three clean HSS (X82WMoV6 5) substrates were used for the deposition of each coating. Coating thickness was 2.3 µm.

The HSS specimens were polished and cleaned with alcohol in an ultrasonic bath. Immediately after the cleaning procedure, samples were placed into the vacuum chamber and mounted on the sample holder. Finally, samples were sputter-cleaned in argon plasma and a thin metallic Ti layer was deposited on the substrates prior to the coatings.

The AFM (NT-MDT) was utilized in the contact mode with a MicroMasch triangular cantilever (force constant 2 N/m), and a set of four scans (50 µm × 50 µm, 10 µm × 10 µm, 5 µm × 5 µm and 2 × 2 µm) was used to monitor the surface. The sequential surface scanning was intentionally designed to investigate a defect-free coating surface, namely after scanning the 50 µm × 50 µm area, a place with a minimal number of defects was selected for the following scanning of the 10 µm × 10 µm area and so on. The same

procedure was repeated for each sample at five different places, i.e. in total, the sample size for every scan size was equal to 15 for each coating type.

Profilometric scans were obtained with a Mahr Perthometer (Göttingen, Germany). The scan length was 1.25 mm and the sample size was 10, i.e. 10 scans were carried out on one sample of each coating type and HSS substrate.

The fretting test (2 N, 100 µm, 10 Hz, 15% RH, 4000 cycles, Ø 10 mm Al_2O_3) at sampling rate of 333 Hz was performed on the FalexTribology NV facilities. Alumina balls were used to provide a faster response of the coatings. The tests were carried out on two different points of one sample of each coating type and HSS substrate.

3. Results and discussion

Fig. 1 shows the AFM images of the coatings and HSS substrate surfaces. The morphology of coating surfaces can be characterized
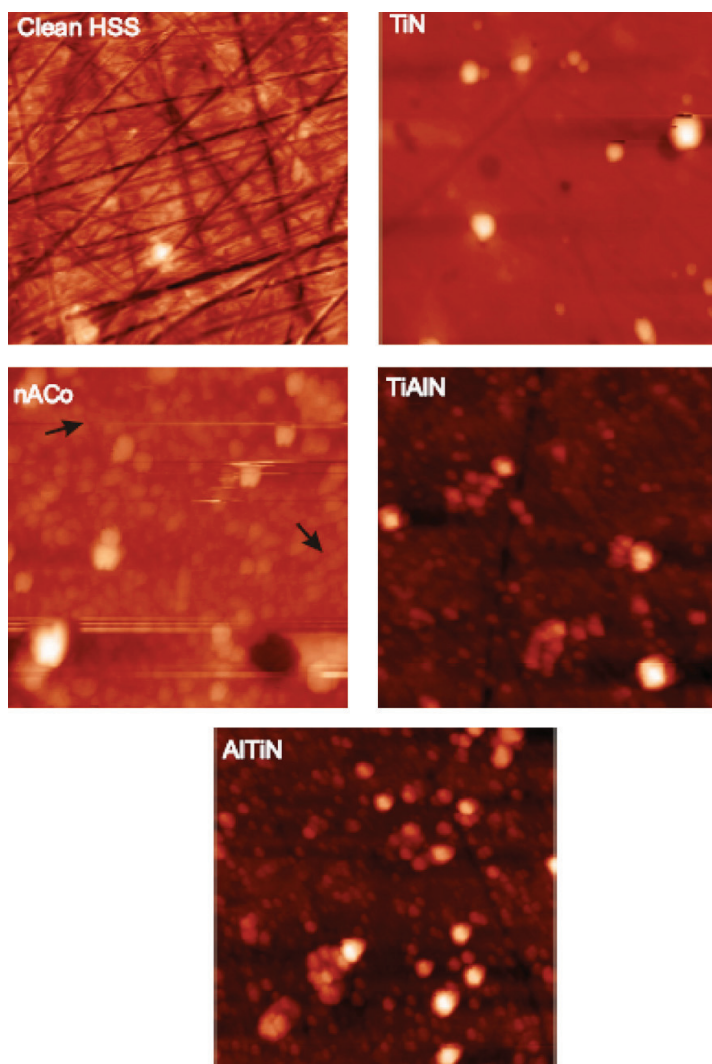

Fig. 1. AFM images (10 µm × 10 µm) of the clean HSS substrate, TiN, nACo, TiAlN and AlTiN, respectively.
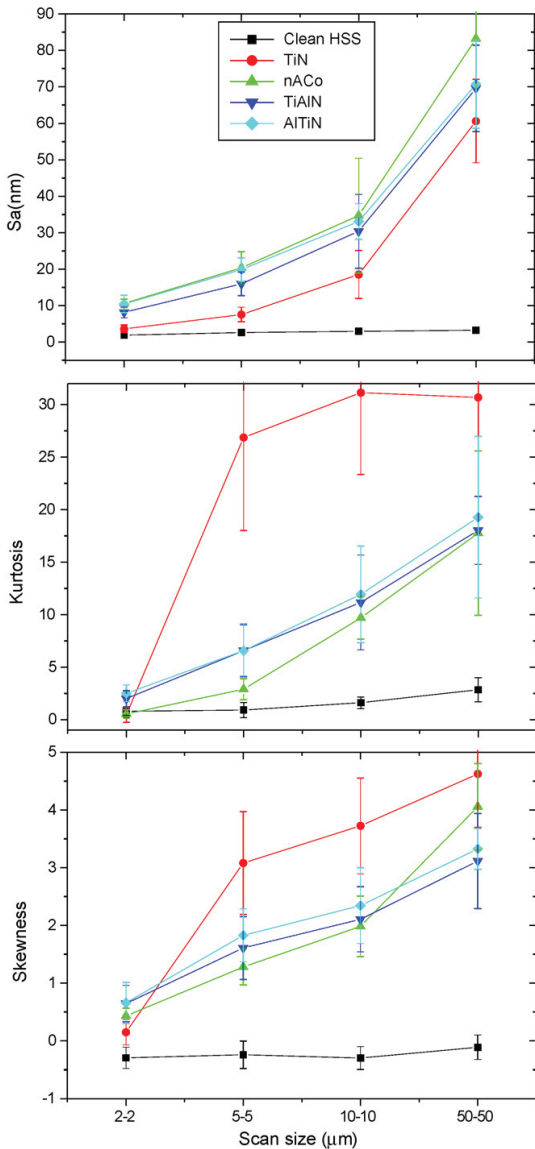
Fig. 2. The average roughness S_a, kurtosis S_{ku} and skewness S_{sk} of HSS substrate, TiN, nACo, TiAlN and AlTiN, respectively. The error bars represent the experimental standard deviation.

Table 1
Average roughness R_a of different coatings and the HSS substrate.

	Clean HSS	TiN	nACo	TiAlN	AlTiN
Roughness R_a (nm)	4 ± 0.8	70 ± 8.4	80 ± 9.6	90 ± 10.8	90 ± 10.8

structure should not be confused with the macroparticles and such structure could be an indication of the intrinsic kinetics of nACo growth on the HSS substrate.

Fig. 2a shows the average roughness S_a. S_a is the highest for AlTiN and nACo and noticeably lower for TiN. Table 1 shows the results of surface profilometry, the trend in average roughness R_a variations is in good agreement with the AFM results, i.e. TiN possesses the smallest roughness in contrast to nACo, AlTiN and TiAlN.

Average roughness S_a of the TiN surface for a 2–2 μm scan size might correspond to S_a of the defect-free TiN coating surface. This conclusion follows from the comparison with the surface roughness of coatings deposited by means of magnetron sputtering. Unlike arc evaporation, the coatings produced by sputtering show a smooth surface with a reduced number of macroparticles. S_a value of 3.6 nm for a TiN coating (2–2 μm scan size) deposited by the PLATIT π-80 (arc coating machine) is similar to the S_a value of 5.3 nm found for TiN deposited by the sputtering coating machine [5]. The roughness of the coating deposited by sputtering was estimated considering a scan area of 70–70 μm. It follows from the reasoning above that in the case of nACo for 2–2 μm scan size, the value of S_a is likely to be caused by the defect-free surface of nACo and to a smaller extent by the macroparticles. In contrast, average roughness of TiAlN and AlTiN for 2–2 μm scan size likely depends on the size and density of macroparticles, see Fig. 1.

Fig. 2 b and c shows a variation of kurtosis and skewness of HDF as a function of scan size for the coatings and the HSS substrate. Skewness and kurtosis are measures of the asymmetry and excess ("flatness") of the HDF, respectively. Symmetrical distribution functions including the Gaussian function have zero skewness. HDF parameters for larger scan sizes 50 μm × 50 μm, 10 μm × 10 μm and 5 μm × 5 μm substantially differ from the normal distribution. In the case of 2 μm × 2 μm scan size, surfaces are non-Gaussian for HSS ($S_{ku} = 0.8 \pm 0.4$, $S_{sk} = -0.3 \pm 0.2$), nACo ($S_{ku} = 0.5 \pm 0.4$, $S_{sk} = 0.4 \pm 0.1$), TiAlN ($S_{ku} = 2.0 \pm 0.8$, $S_{sk} = 0.6 \pm 0.3$) and AlTiN ($S_{ku} = 2.5 \pm 0.8$, $S_{sk} = 0.7 \pm 0.4$), with an exception of TiN ($S_{ku} = 0.5 \pm 0.6$, $S_{sk} = 0.2 \pm 0.2$), which is supposedly Gaussian for the 2.3 μm thick TiN coating. The reasons behind the variations of the HDF parameters for coatings deposited on the HSS substrate include surface roughening due to macroparticles, non-Gaussian surface of the HSS substrate and growth kinetics of the coatings on the HSS substrate. Slightly negative value of skewness for the clean HSS substrate refers to a characteristic distribution of peaks and valleys on the surface, namely deep valleys in a smoother plateau. In other words, a net of shallow scratches is localized on top of smoother plateaus formed between deeper scratches. The positive skewness means that the surface profile can be represented by high spikes protruding above a flatter average. The HDF with the positive kurtosis has a sharper "peak" and "heavier" tails, e.g. a relatively high positive value of kurtosis for larger scan sizes results from a cumulative effect of a relatively extended smooth defect-free surface and the macroparticles. It is interesting to stress that for the defect-free surface area of TiN and nACo coatings, HDF have zero and positive skewnesses despite negative skewness of the substrate resulting from coating growth kinetics on the HSS substrate. In the case of smaller scan sizes (5 μm × 5 μm and 2 μm × 2 μm), differences between TiAlN, AlTiN and nACo were revealed, namely the kurtosis is remarkably lower for nACo than for TiAlN and AlTiN. This finding gives evidence of a higher smoothness of the nACo surface. However, skewness is approximately the same for all of these coatings (TiAlN, AlTiN, nACo).

by an alternation of the defect-free surface and macroparticles. The surfaces of TiN and nACo are similar in appearance to those recently investigated by AFM [16]. It is worth noting that the different coating units PLATIT-π80 (in Denmark and Estonia) were utilized to deposit coatings in the previous [16] and the present studies. Scratches of different lengths and depths can be observed on the surface of a clean HSS substrate. Substrate scratch locations can be seen on top of the coatings as well, although there is a noticeable difference between the coatings. The relatively plane surface of the defect-free area of TiN, TiAlN and AlTiN is in contrast with a cellular-like structure covering the entire surface of the nACo coating. This structure is partially aligned, probably with the deep HSS substrate scratches depicted by arrows. Therefore, the cellular-like
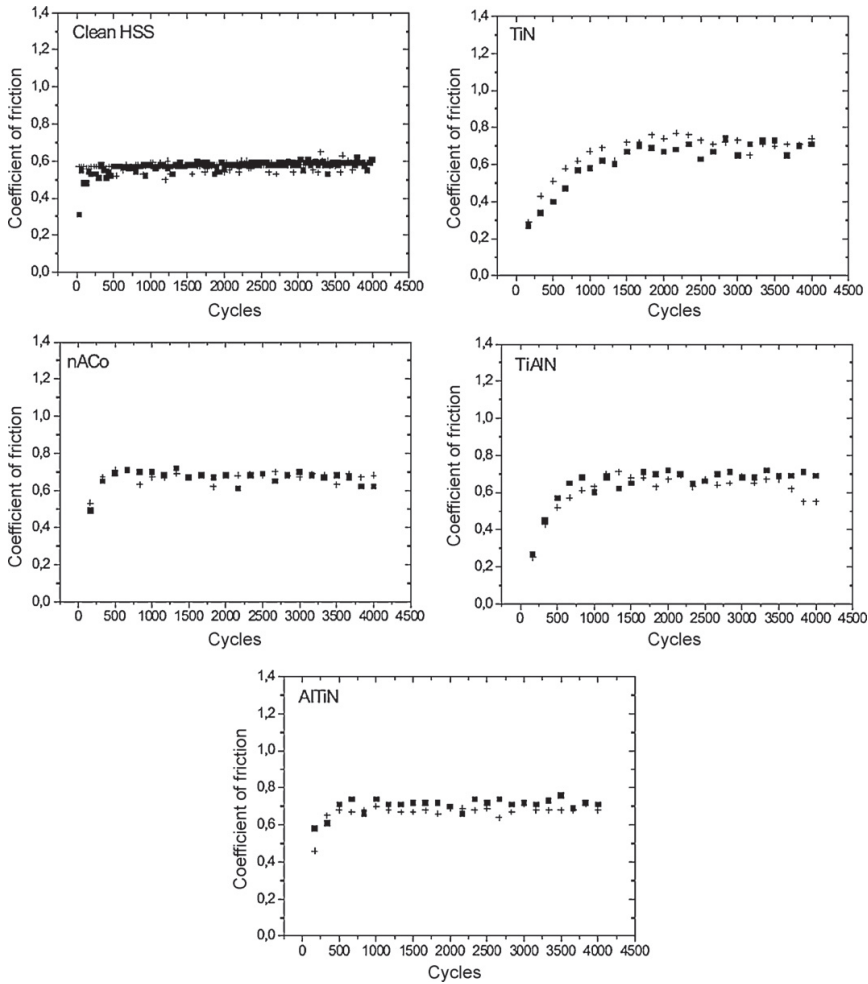
Fig. 3. Fretting tests (2 N, 10 Hz, 100 μm, 4000 cycles, RH = 15%, Ø 10 mm Al₂O₃) conducted on the HSS substrate, TiN, nACo, TiAlN and AlTiN, respectively.

It is also worth noting that the sensitivity of AFM fulfills the prerequisites for surface topography monitoring. Grinding and abrasion produce groove surfaces with negative skewness [3], in the present work, $S_{sk} = -0.3 \pm 0.2$ in the case of HSS for 50 μm × 50 μm scan size. The surface is smoother at smaller length scale, as the number of deep scratches decreases, thus the kurtosis decreases as well. However, the skewness does not change, implying that the surface profile at smaller scan sizes (or smaller scale) is similar to the surface profile at larger scan sizes, namely smoother plateaus are framed by relatively deep valleys. In other words, the HSS surface exhibits a self-similarity.

All the coatings showed an increase in COF at the beginning of the fretting test, see Fig. 3. However, the rate of increase depends on the coating, the maximal value of COF was reached after 1500–1800 cycles for TiN, 800–1200 cycles for TiAlN and 500–700 cycles for AlTiN and nACo, respectively. The initial value of COF after 166 cycles differed as well, i.e. 0.27–0.29 for TiN, 0.25–0.27 for TiAlN, 0.46–0.58 for AlTiN and 0.49–0.53 for nACo. Thus, there is a trend towards time span reduction and initial COF rise with an increase of Al content in the coating. The HDF parameters of the TiN sur-

face for larger scan sizes like 50 μm × 50 μm, 10 μm × 10 μm and 5 μm × 5 μm imply a non-Gaussian surface, suggesting a decrease in the contact area for positive skewness and higher kurtosis [17,18]. It is also apparent from an observation of large macroparticles in Fig. 1. In other words, COF is smaller at the beginning of the test, as the lower contact area minimizes static and kinetic frictions [17]. The chemical composition of macroparticles on top of TiN was investigated by Shiao and Shieu [19]. These defects possess a core-shell structure with polycrystalline Ti inside.

In view of the tribological behavior of hard coatings, the conclusions in [6–8,11] concerning the interpretation of the running-in phenomena could be expanded to include the interaction mechanisms of a counterbody with the macroparticles and asperities on the coating surface. Probably these mechanisms are particularly important in the understanding of (Ti,Al)N coating friction deposited by the arc-PVD method, as it follows from the above discussion in the Introduction. Finally, further studies are imperative to prove the assumption that the mentioned interaction mechanisms are sensitive to the conditions of the tribological test.

4. Conclusions

In this study, AFM technique was used to evaluate the geometrical characteristics of the coating surfaces. The morphology of TiN, TiAlN and AlTiN coatings depends on the morphology of the HSS substrate, although the effect of substrate roughness does not play a dominant role in the growth of nACo on HSS. In the case of relatively large scan sizes ($50\,\mu\mathrm{m} \times 50\,\mu\mathrm{m}$, $10\,\mu\mathrm{m} \times 10\,\mu\mathrm{m}$ and $5\,\mu\mathrm{m} \times 5\,\mu\mathrm{m}$), all coatings showed non-Gaussian surfaces due to the macroparticles. However, for the $2\,\mu\mathrm{m} \times 2\,\mu\mathrm{m}$ scan size, the defect-free TiN surface is likely to be Gaussian ($S_{ku} = 0.5 \pm 0.6$, $S_{sk} = 0.2 \pm 0.2$) and nACo is non-Gaussian because of relatively high skewness ($S_{sk} = 0.4 \pm 0.1$). It remains an open question whether the defect-free surfaces of TiAlN and AlTiN are Gaussian or non-Gaussian. To interpret the initial running-in period a better understanding of the interaction mechanisms between coating surface and counterbody is required.

References

[1] S. PalDey, S.C. Deevi, Single layer and multilayer wear resistant coatings of (Ti,Al)N: a review, Mater. Sci. Eng. A 342 (2003) 58–79.

[2] S. Veprek, M. Jilek, Super- and ultrahard nanocomposite coatings: generic concept for their preparation, properties and industrial applications, Vacuum 67 (2002) 443–449.

[3] B. Bhushan, Modern Tribology Handbook, CRC Press, 2001, pp. 49–80.

[4] I.J. Smith, D. Gillibrand, J.S. Brooks, W.-D. Münz, S. Harvey, R. Goodwin, Dry cutting performance of HSS twist drills coated with improved TiAlN, Surf. Coat. Technol. 90 (1997) 164–167.

[5] Dr. M. Morstein, Dr. J. Prokazka (PLATIT- http://www.platit.com), personal communication.

[6] P.J. Blau, On the nature of running-in, Tribol. Int. 38 (2005) 1007–1012.

[7] P.J. Blau, Interpretations of the friction and wear break-in behaviour of metals in sliding contact, Wear 71 (1981) 29–43.

[8] B. Bhushan, Modern Tribology Handbook, CRC Press, 2001, pp. 494–495.

[9] X. Zhu, W. Lauwerens, P. Cosemans, M. Van Stappen, J.P. Celis, L.M. Stals, J. He, Different tribological behavior of MoS_2 coatings under fretting and pin on- disk conditions, Surf. Coat. Technol. 163–164 (2003) 422–428.

[10] R. Wäsche, D. Klaffke, Tribology of DLC films under fretting condition, in: C. Donnet, A. Erdemir (Eds.), Tribology of Diamond-Like Carbon Films: Fundamentals and Applications, Springer, 2008, pp. 362–382.

[11] J.M. Lackner, W. Waldhauser, R. Berghauser, R. Ebner, B. Major, T. Schöberl, Structural, mechanical and tribological investigations of pulsed laser deposited titanium nitride coatings, Thin Solid Films 453–454 (2004) 195–202.

[12] R. Gunda, S.K. Biswas, S. Bhowmick, V. Jayaram, Mechanical properties of rough TiN coating deposited on steel by cathodic arc evaporation technique, J. Am. Ceram. Soc. 88 (2005) 1831–1837.

[13] H.C. Barshilia, K.S. Rajam, Reactive sputtering of hard nitride coatings using asymmetric-bipolar pulsed DC generator, Surf. Coat. Tehnol. 201 (2006) 1827.

[14] H.C. Barshilia, M.S. Prakasha, A. Jainb, K.S. Rajama, Structure, hardness and thermal stability of TiAlN and nanolayered TiAlN/CrN multilayer films, Vacuum 77 (2005) 169–179.

[15] M Ali, E. Hamzah, M.R. Toff, Friction coefficient and surface roughness of TiN-coated HSS deposited using cathodic arc evaporation PVD technique, Ind. Lubr. Tribol. 60 (3) (2008) 121–130.

[16] V. Podgursky, R. Nisumaa, A. Gregor, E. Adoberg, P. Kulu, Roughness of TiN and nanocomposite nc-$Ti_{1-x}Al_xN$/α-Si_3N_4 surface evaluated by means of AFM, Latvian J. Chem. 1 (2008) 62–66.

[17] C.A. Kotwal, B. Bhushan, Contact analysis of non-Gaussian surfaces for minimum static and kinetic friction and wear, Tribol. Trans. 39 (4) (1996) 890–898.

[18] S. Chandrasekaran, S. Sundararajan, Effect of microfabrication processes on surface roughness parameters of silicon surfaces, Surf. Coat. Technol. 188–189 (2004) 581–587.

[19] M.-H. Shiao, F.-S. Shieu, A formation mechanism for macroparticles in arc ion-plated TiN films, Thin Solid Films 386 (2001) 27–31.

DISSERTATIONS DEFENDED AT
TALLINN UNIVERSITY OF TECHNOLOGY ON
MECHANICAL AND INSTRUMENTAL ENGINEERING

1. **Jakob Kübarsepp**. Steel-bonded hardmetals. 1992.

2. **Jakub Kõo**. Determination of residual stresses in coatings & coated parts. 1994.

3. **Mart Tamre**. Tribocharacteristics of journal bearings unlocated axis. 1995.

4. **Paul Kallas**. Abrasive erosion of powder materials. 1996.

5. **Jüri Pirso**. Titanium and chromium carbide based cermets. 1996.

6. **Heinrich Reshetnyak**. Hard metals serviceability in sheet metal forming operations. 1996.

7. **Arvi Kruusing**. Magnetic microdevices and their fabrication methods. 1997.

8. **Roberto Carmona Davila**. Some contributions to the quality control in motor car industry. 1999.

9. **Harri Annuka**. Characterization and application of TiC-based iron alloys bonded cermets. 1999.

10. **Irina Hussainova**. Investigation of particle-wall collision and erosion prediction. 1999.

11. **Edi Kulderknup**. Reliability and uncertainty of quality measurement. 2000.

12. **Vitali Podgurski**. Laser ablation and thermal evaporation of thin films and structures. 2001.

13. **Igor Penkov**. Strength investigation of threaded joints under static and dynamic loading. 2001.

14. **Martin Eerme**. Structural modelling of engineering products and realisation of computer-based environment for product development. 2001.

15. **Toivo Tähemaa**. Assurance of synergy and competitive dependability at non-safety-critical mechatronics systems design. 2002.

16. **Jüri Resev**. Virtual differential as torque distribution control unit in automotive propulsion systems. 2002.

17. **Toomas Pihl**. Powder coatings for abrasive wear. 2002.

18. **Sergei Letunovitš**. Tribology of fine-grained cermets. 2003.

19. **Tatyana Karaulova**. Development of the modelling tool for the analysis of the production process and its entities for the SME. 2004.

20. **Grigori Nekrassov**. Development of an intelligent integrated environment for computer. 2004.

21. **Sergei Zimakov**. Novel wear resistant WC-based thermal sprayed coatings. 2004.

22. **Irina Preis**. Fatigue performance and mechanical reliability of cemented carbides. 2004.

23. **Medhat Hussainov**. Effect of solid particles on turbulence of gas in two-phase flows. 2005.

24. **Frid Kaljas**. Synergy-based approach to design of the interdisciplinary systems. 2005.

25. **Dmitri Neshumayev**. Experimental and numerical investigation of combined heat transfer enhancement technique in gas-heated channels. 2005.

26. **Renno Veinthal**. Characterization and modelling of erosion wear of powder composite materials and coatings. 2005.

27. **Sergei Tisler**. Deposition of solid particles from aerosol flow in laminar flat-plate boundary layer. 2006.

28. **Tauno Otto**. Models for monitoring of technological processes and production systems. 2006.

29. **Maksim Antonov**. Assessment of cermets performance in aggressive media. 2006.

30. **Tatjana Barashkova**. Research of the effect of correlation at the measurement of alternating voltage. 2006.

31. **Jaan Kers**. Recycling of composite plastics. 2006.

32. **Raivo Sell**. Model based mechatronic systems modeling methodology in conceptual design stage. 2007.

33. **Hans Rämmal**. Experimental methods for sound propagation studies in automotive duct systems. 2007.

34. **Meelis Pohlak**. Rapid prototyping of sheet metal components with incremental sheet forming technology. 2007.

35. **Priidu Peetsalu**. Microstructural aspects of thermal sprayed WC-Co coatings and Ni-Cr coated steels. 2007.

36. **Lauri Kollo**. Sinter/HIP technology of TiC-based cermets. 2007.

37. **Andrei Dedov**. Assessment of metal condition and remaining life of in-service power plant components operating at high temperature. 2007.

38. **Fjodor Sergejev**. Investigation of the fatigue mechanics aspects of PM hardmetals and cermets. 2007.

39. **Eduard Ševtšenko**. Intelligent decision support system for the network of collaborative SME-s. 2007.

40. **Rünno Lumiste**. Networks and innovation in machinery and electronics industry and enterprises (Estonian case studies). 2008.

41. **Kristo Karjust**. Integrated product development and production technology of large composite plastic products. 2008.

42. **Mart Saarna**. Fatigue characteristics of PM steels. 2008.

43. **Eduard Kimmari**. Exothermically synthesized B_4C-Al composites for dry sliding. 2008.

44. **Indrek Abiline**. Calibration methods of coating thickness gauges. 2008.

45. **Tiit Hindreus**. Synergy-based approach to quality assurance. 2009.

46. **Karl Raba**. Uncertainty focused product improvement models. 2009.

47. **Riho Tarbe**. Abrasive impact wear: tester, wear and grindability studies. 2009.

48. **Kristjan Juhani**. Reactive sintered chromium and titanium carbide- based cermets. 2009.

49. **Nadežda Dementjeva**. Energy planning model analysis and their adaptability for Estonian energy sector. 2009.

50. **Igor Krupenski**. Numerical simulation of two-phase turbulent flows in ash circulating fluidized bed. 2010.

51. **Aleksandr Hlebnikov**. The analysis of efficiency and optimization of district heating networks in Estonia. 2010.

52. **Andres Petritšenko**. Vibration of ladder frames. 2010.

53. **Renee Joost**. Novel methods for hardmetal production and recycling. 2010.

54. **Andre Gregor**. Hard PVD coatings for tooling. 2010.